Identification and characterization of LMX1B target genes

DISSERTATION ZUR ERLANGUNG DES DOKTORGRADES
DER NATURWISSENSCHAFTEN (DR. RER. NAT.)
DER FAKULTÄT FÜR BIOLOGIE UND VORKLINISCHE MEDIZIN
DER UNIVERSITÄT REGENSBURG

vorgelegt von

Natalya Stepanova

aus

Astana, Kasachstan

im Jahr 2015

Der Promotionsgesuch wurde eingereicht am:
18.05.2015

Die Arbeit wurde angeleitet von:
Prof. Dr. Ralph Witzgall

Unterschrift:

To my parents and my brother

Contents

Chapter 1

Introduction

1.1 Inside the nephron

The nephron represents the basic structural and functional unit of the kidney. It filters the blood, reabsorbs useful substances, and excretes waste substances with the urine. The nephron consists of the glomerulus and the tubule. The tubule is divided in three compartments: the proximal, the intermediate and the distal tubules. The glomerulus consists of three major cell types: the fenestrated endothelial cells, which build the capillary tuft located inside of Bowman's capsule, the mesangial cells, which help to maintain the three-dimensional structure of the capillary tuft, and the podocytes. The specialized form of the basement membrane called glomerular basement membrane (GBM) is located between the endothelial cells and the podocytes (Figure 1.1) (Pozzi and Zent, 2012).

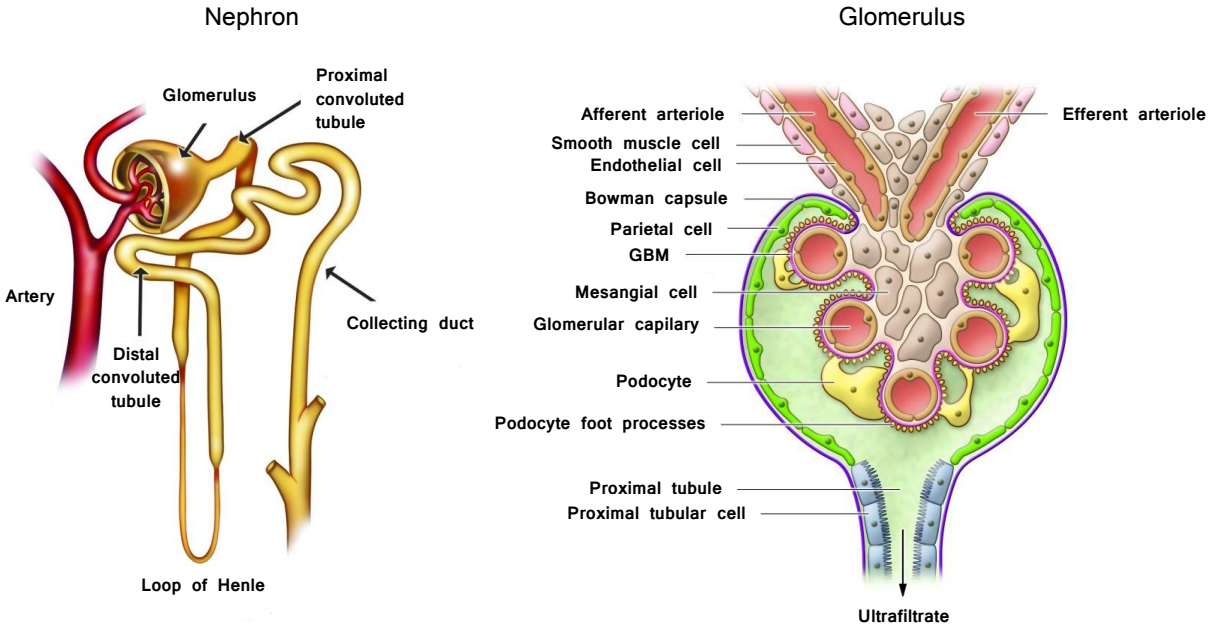

Figure 1.1: Major structural components of the nephron and the glomerulus. Figures were modified from (Albiges et al., 2012) and (Pozzi and Zent, 2012), respectively. GBM stands for glomerular basement membrane.

The podocytes are highly differentiated cells with a unique cytoarchitecture. Many large protrusions, called primary or major processes, extend directly from the podocyte

cell body. Primary processes branch and finally end in many small extensions called foot processes. The foot processes from two adjacent podocytes interdigitate with each other thus forming the slit diaphragm (Mundel and Kriz, 1995). The endothelial cells, the glomerular basement membrane, and the slit diaphragm build the glomerular filtration barrier. Dysregulation of the glomerular filtration barrier on the molecular level may lead to renal diseases. One example of such a disease is nail-patella syndrome which affects the kidneys in approximately 40% of patients (Sweeney et al., 2003). The syndrome is described in detail in Section 1.2.

1.2 Nail-Patella Syndrome

Nail-patella syndrome (NPS), also known as Österreicher syndrome (Österreicher, 1930), Turner-Kieser syndrome (Turner, 1933; Kieser, 1939), Fong disease (Fong, 1946) and hereditary osteo-onychodysplasia (Roeckerath, 1951) is a rare autosomal-dominant disorder with an incidence of ∼1:50,000. As its name indicates, the typical clinical features of nail-patella syndrome include the deformation of finger- and toenails, the hypoplasia or absence of kneecaps, and iliac horns in 95.1%, 92.7% and 70-80% of cases, respectively [reviewed by (Bongers et al., 2002)]. Approximately 40% of NPS patients suffer from renal symptoms like proteinuria, hematuria or chronic renal failure (Sweeney et al., 2003; Witzgall, 2007). Electron microscopic studies of kidney biopsies from NPS patients demonstrate morphological abnormalities such as a thickened glomerular basement membrane with both fibrillar inclusions and electron-lucent areas, and loss of podocyte foot processes (Del Pozo and Lapp, 1970; Ben-Bassat et al., 1971; Rohr et al., 2002; Witzgall, 2007).

The first report about NPS dates back to 1820 (Roeckerath, 1951). In 1955 NPS was genetically linked to the ABO blood group locus by Renwick *et al.* and in 1969 to the adenylate kinase locus by Schleutermann *et al.* (Renwick and Lawler, 1955; Schleutermann et al., 1969). Only in 1998 mutations in the *LMX1B* gene, coding for the LIM homeobox transcription factor 1 beta, were identified in patients with NPS (Dreyer et al., 1998; McIntosh et al., 1998; Vollrath et al., 1998). LMX1B and its target genes are described in Section 1.3.

1.3 LMX1B and its target genes

LIM homeobox transcription factor 1 beta (LMX1B) is a transcription factor that belongs to the family of LIM-homeodomain proteins and plays a significant role in the normal development of the dorsal limb structures, the anterior segment of the eye, dopaminergic and serotonergic neurons and the podocytes in the kidney. The *LMX1B* gene gives rise to a protein of 395 and 402 amino acids (Dunston et al., 2004). The LMX1B protein contains two N-terminal cysteine-rich zinc-binding LIM-A and LIM-B domains mediating interactions with other proteins, one central homeodomain responsible for the binding of LMX1B to specific target genes, and a C-terminal glutamine- and serine-rich transcriptional activation domain (Bongers et al., 2002). LMX1B is exclusively expressed in the brain, developing limb and eye, cranial mesenchyme, and in the podocytes.

Since the genetic linkage of nail-patella syndrome to the *LMX1B* gene, more than 140 mutations including missense, splicing, insertion/deletion and nonsense alterations have been identified in NPS patients. Roughly 82% of such mutations identified in

LMX1B are concentrated in the LIM-A and LIM-B domains, while only 18% are located in the homeodomain (Bongers et al., 2002). The binding of LMX1B to its target genes is mediated by the central homeodomain which specifically recognizes the so-called FLAT (FAR linked AT-rich) elements. These elements were characterized for the first time in the promoter sequence of the rat insulin I gene (German et al., 1992). FLAT elements can be subdivided into two types: FLAT-E (5'-TAATTA-3') and FLAT-F (5'-TTAATA-3').

To date several LMX1B target genes have been identified. Morello *et al.* have demonstrated that expression of the α3 and α4, but not of the α1, α2 and α5 chains of collagen IV in the GBM of *Lmx1b* null mice was strongly reduced. Furthermore, LMX1B showed binding to a FLAT element within the first intron of both mouse and human *COL4A4* and it upregulated reporter constructs containing this sequence (Morello et al., 2001). Moreover, LMX1B regulates expression of some genes involved in podocyte differentiation and function. Miner *et al.* have shown that Cd2ap and podocin mRNA and protein levels in *Lmx1b*$^{-/-}$ mice were significantly decreased. In cotransfection assays LMX1B showed binding to the FLAT elements within *CD2AP* and *NPHS2* (podocin) promoters *in vitro* and activated transcription of these genes through FLAT elements (Miner et al., 2002). In contrast to what has been found in the conventional *Lmx1b* knock-out mouse, podocin and the α3 and α4 chains of collagen IV were still detected in constitutive podocyte-specific *Lmx1b* knock-out mice (Suleiman et al., 2007) and in kidney biopsies from NPS patients (Heidet et al., 2003). Functional studies using chromatin immunoprecipitation and luciferase reporter assays in HeLa cells revealed that LMX1B regulates the expression of NF-κB target genes, such as *IL6* or *IL8*, by binding to the FLAT-F elements within the proximal promoter of these genes (Rascle et al., 2009).

Microarray studies of glomeruli isolated from inducible podocyte-specific *Lmx1b* knock-out mice have shown a significant increase of the mRNA levels of several actin cytoskeleton-associated proteins, including Abra and Arl4c, as well as a protein of unknown function, Crct1, in comparison to control mice. Chromatin immunoprecipitation experiments in conditionally immortalized human podocytes revealed that LMX1B binds to FLAT elements within the *ABRA* and *ARL4C* promoter regions (Burghardt et al., 2013). The aim of this PhD project was the characterization of putative target genes which have shown an upregulation in microarray studies of adult *Lmx1b* knock-out animals. Therefore, the main properties of ABRA and ARL4C are summarized in Subsections 1.3.1 and 1.3.2, respectively. Currently there is no biological information available regarding CRCT1 (Cysteine-rich C-terminal 1), making it attractive as a research object.

1.3.1 ABRA – Actin Binding Rho Activating

The actin binding Rho activating protein ABRA was identified in 2002 by two different laboratories and is also named STARS (for Striated Muscle Activator of Rho Signaling) and ms1 (for myocyte stress factor 1) (Arai et al., 2002; Mahadeva et al., 2002). Initially, ABRA transcripts were discovered in human and murine cardiac and skeletal muscles (Arai et al., 2002; Mahadeva et al., 2002), and most recently in smooth muscles (Troidl et al., 2009). In rat primary cardiomyocytes ABRA showed localization to the I-band and was partially seen between Z-lines of the sarcomere. Binding of ABRA to F-actin and activation of Rho-signaling events was demonstrated in transfected COS-7 cells (Arai et al., 2002). Recently, Fogl *et al.* characterized two independent F-actin binding domains at the C-terminus of the protein – actin binding domains 1 and 2 (ABD1 and ABD2) located between amino acids 193-296 and 294-375, respectively. Moreover,

ABD1 showed higher affinity to F-actin in comparison to ABD2 (Fogl et al., 2012).

Two members of the actin-binding LIM (ABLIM) protein family, ABLIM-2 and ABLIM-3 were recently reported as interaction partners of ABRA. Upon ABLIM-2 and ABLIM-3 association with ABRA, the activation of downstream targets of the serum response factor (SRF) is initiated (Barrientos et al., 2007). Another pathway of ABRA-mediated SRF signaling includes depletion of G-actin and release of myocardin-related transcription factors (MTRFs) which after transport into the nucleus stimulate SRF targets (Kuwahara et al., 2005). Finally, ABRA stimulates the SRF-dependent transcription via RhoA activation (Arai et al., 2002). A scheme of the ABRA-mediated regulation of actin dynamics and SRF signaling is shown in Figure 1.2.

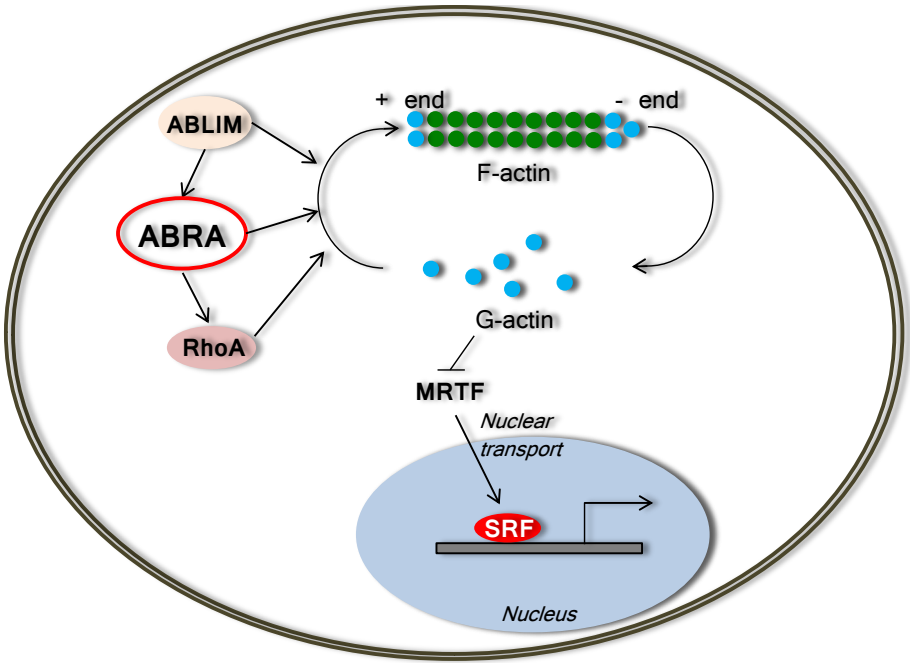

Figure 1.2: A scheme of the ABRA-mediated regulation of actin dynamics and SRF signaling. ABRA stimulates F-actin polymerization directly or through activation of RhoA. ABLIM proteins associate with ABRA and stimulate the ABRA-dependent activation of the downstream targets of SRF. Upon the ABRA-dependent polymerization of F-actin, MTRFs are released from the inhibitory influence of G-actin and imported into the nucleus, where they stimulate SRF transcriptional activity. Abbreviations: ABLIM – actin binding LIM domain protein, MTRF – myocardin-related transcription factor, RhoA – Ras homolog gene family, member A, SRF – serum response factor. Modified from (Kuwahara et al., 2005; Barrientos et al., 2007).

1.3.2 ARL4C – ADP-Ribosylation Factor-Like 4C

The ADP-Ribosylation Factor-Like 4C (ARL4C), also known as ARL7, belongs to the ARF-related family of small GTP-binding proteins (Jacobs et al., 1999). As reported by Jacobs *et al.* transcripts of human ARL4C are highly enriched in the brain, and lower levels of ARL4C were detected in the spleen, thymus, esophagus, stomach, intestine and uterus (Jacobs et al., 1999). A few years after the work of Jacobs *et al.*, Wei *et al.* demonstrated mRNA expression of ARL4C in human lung, brain, leukocytes and

placenta (Wei et al., 2009). Recent immunohistochemical analysis of mouse embryos on day 15 revealed that Arl4c was expressed in the brain, in some epithelial rudiments, and in the kidney, where Arl4c was detected in ureteric buds, pretubular aggregates, renal vesicles, and the comma-shaped body (Matsumoto et al., 2014).

The subcellular localization of ARL4C depends on the binding to GTP or GDP. In overexpression studies the wild-type form of ARL4C and the active GTP-bound mutant of ARL4C were detected within the cytoplasm and at the plasma membrane of filopodia. On the other hand, the inactive GDP-bound ARL4C mutant was detected in the perinuclear region of the cell and was not associated with filopodia (Engel et al., 2004). A ARL4C mutant which lacked the myristoylation site lost its ability to bind to the plasma membrane (Engel et al., 2004).

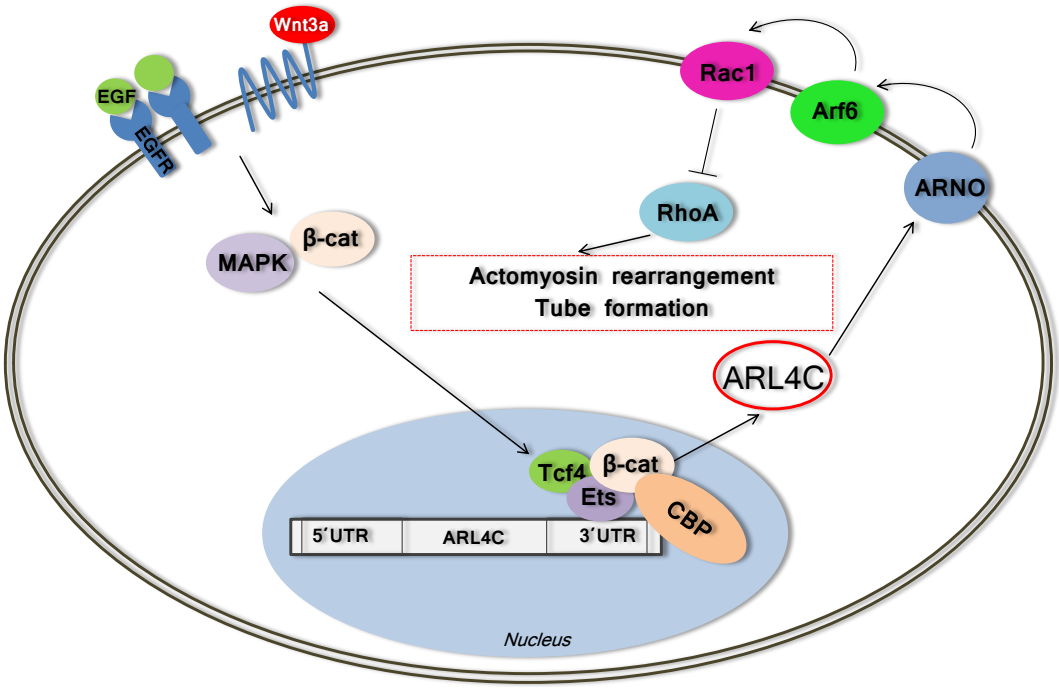

Figure 1.3: Scheme of the Arl4c-mediated regulation of actomyosin rearrangement and epithelial tube formation after combinatorial induction of Wnt3a/EGF signaling based on the data from Matsumoto *et al.* (Matsumoto et al., 2014). The induction of Wnt3a/EGF activates the MAPK and β-catenin pathways, then a complex consisting of Ets/Tcf4/CBP forms at the Ets-binding site in the 3' non-coding region of the *Arl4c* gene. Arl4c induces ARNO and Arf6, resulting in Rac1 activation. Rac1 induction leads to the inhibition of RhoA, rearrangement of the cytoskeleton and tubular structure formation. Abbreviations: β-cat – β-catenin, ARF6 – ADP-ribosylation factor 6, ARNO – Arf nucleotide-binding site opener, CBP – cyclic AMP-responsive element binding protein [(CREB)-binding protein], EGF – epidermal growth factor, EGFR – epidermal growth factor receptor, MAPK – mitogen activated kinase-like protein, Rac1 – ras-related C3 botulinum toxin substrate 1, RhoA – Ras homolog gene family, member A, Tcf4 –T-cell factor 4, UTR – untranslated region, Wnt3a – wingless-type MMTV integration site family, member 3A.

The first reported interaction partner of ARL4C was α-tubulin. Wei *et al.* have shown that the association of both proteins leads to microtubule-dependent vesicular transport (Wei et al., 2009). Hofmann *et al.* demonstrated that Arl4c was able to recruit ARNO (Arf nucleotide-binding site opener) and Arf6 (ADP-ribosylation factor 6) to the

plasma membrane (Hofmann et al., 2007). Recent findings of Matsumoto *et al.* shed light on the interaction of Arl4c with other proteins (Matsumoto et al., 2014). It was demonstrated that the expression of Arl4c was induced by the combined action of Wnt3a and epidermal growth factor (Wnt3a/EGF). The Wnt3a/EGF signaling activated the MAPK and β-catenin pathways, then a complex of Ets/Tcf4/CBP formed at the Ets-binding site in the 3' non-coding region of the *Arl4c* gene (Matsumoto et al., 2014). Arl4c induced ARNO and Arf6, resulting in Rac1 activation. Finally, Rac1 activation led to RhoA inhibition, rearrangement of the cytoskeleton and tubular structure formation as shown in Figure 1.3 (Matsumoto et al., 2014).

1.4 The podocyte actin cytoskeleton

The cytoskeleton is a dynamic network of filaments with a large number of functions, including cell shape maintenance, cell migration, intracellular transport, cell division, etc. It consists of three main components: microfilaments, intermediate filaments, and microtubules. Microfilaments, or actin filaments, are polymeric structures with a diameter of 5-9 nm, formed by actin. Intermediate filaments, as its name indicates, are the fibers of the cytoskeleton with an intermediate size of about 10 nm. They are composed of intermediate filament proteins. The largest component of the cytoskeleton are the microtubules, which have a diameter of around 25 nm and are formed by a protein called tubulin (Alberts et al., 2008).

As mentioned previously, the following segments can be distinguished in podocytes: the cell body, the large processes, and the foot processes (FPs). The cell body and the large processes contain all components of cell cytoskeleton, while the FPs are exclusively composed of actin filaments and actin-associated proteins (Drenckhahn and Franke, 1988). The membrane of FPs is functionally divided into three domains: the apical membrane domain (AMD), the basal membrane domain (BMD), and the slit diaphragm (SD), as shown in Figure 1.4 (Kerjaschki, 2001).

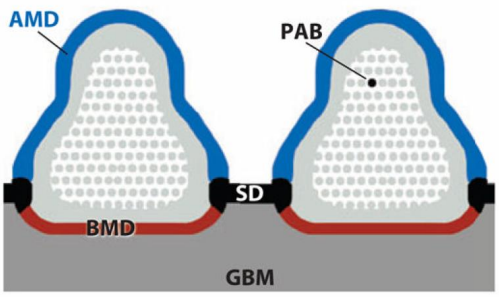

Figure 1.4: Scheme of three membrane domains of FPs: the apical membrane domain (AMD) (blue), the basal membrane domain (BMD) (red), and the SD (black). PAB stands for parallel actin bundles. The figure was taken from Greka and Mundel, 2012.

The disruption of any of the three FP domains leads to the reorganization of the actin cytoskeleton: parallel bundles of actin cytoskeleton change into a disordered structure (Shirato et al., 1996; Kerjaschki, 2001), which is followed by the retraction of FPs and the loss of the slit diaphragm. This process is known as foot process effacement. Foot process effacement leads to proteinuria (Farquhar et al., 1957; Murphy et al., 1979) which is typical of numerous glomerular disorders, such as focal segmental glomerulosclerosis

(FSGS) (Grishman and Churg, 1975), minimal change disease (Farquhar et al., 1957), and diabetic nephropathy (Kerjaschki, 2001). The described morphological changes in the FP actin cytoskeleton were also observed in some NPS patients (Del Pozo and Lapp, 1970). Therefore, the purpose of Subsection 1.4.1 is to present the current knowledge in the (re)organization of the actin cytoskeleton during podocyte injury.

1.4.1 (Re)organization of the actin cytoskeleton after podocyte injury

It is now commonly accepted that podocytes play a key role in the maintenance of the glomerular filtration barrier. Injury of podocytes leads to proteinuria and development of glomerular diseases. During podocyte injury, changes in their shape are observed, which is called foot process effacement. The FPs of each podocytes are retracted, moreover the amount of filtration slits is reduced, so that FPs appears as a continuous cytoplasmic sheet along the GBM as shown in Figure 1.5 (Shirato, 2002).

To date many causes of podocyte injury have been described, including changes in the SD structure (Simons et al., 2001; Verma et al., 2003), interference with the GBM or the podocyte-GBM interaction (Noakes et al., 1995; Kreidberg et al., 1996; Raats et al., 1997; Regele et al., 2000; Kretzler et al., 2001), modulations of the negatively charged podocyte membrane (Orlando et al., 2001; Takeda et al., 2001; Galeano et al., 2007), alterations of the transcriptional regulation of podocytes (Quaggin, 2002; Rascle et al., 2007), and reorganization of the podocyte actin cytoskeleton (Smoyer and Mundel, 1998; Kos et al., 2003; Jones et al., 2006; Verma et al., 2006).

Despite the increasing number of studies on actin-associated proteins in podocytes, the molecular mechanisms of the reorganization of the podocyte cytoskeleton remain unclear. Upon podocyte injury the coordinated parallel bundles of actin filaments change into an interwoven network (Shirato et al., 1996; Kerjaschki, 2001). The expression of actin and the actin-filament cross-linking protein α-actinin is increased (Shirato et al., 1996). Studies by Smoyer *et al.* consider α-actinin-4 as initiator of FP effacement (Smoyer et al., 1997). Subsequently glomerular α3-integrin is induced (Smoyer et al., 1997). The importance of α-actinin-4 in podocyte injury was demonstrated by the fact that mutations in the *ACTN4* gene coding for α-actinin-4 lead to an autosomal dominant form of FSGS (Kaplan et al., 2000; Pollak, 2002). Miao *et al.* discovered further cytoskeletal proteins involved in the dynamic changes of foot processes. Transgelin, survivin, Arp2, cytokeratin7, and vinculin mRNA and protein levels were significantly increased in puromycin aminonucleoside nephropathy in rats and in patients with proteinuric renal diseases (Miao et al., 2009). Mutations in the *MYH9* gene, which encodes another component of the FP cytoskeleton (non-muscle myosin heavy chain IIA), are associated with Epstein, Fechtner, and Sebastian syndromes, and May-Hegglin anomaly (Arrondel et al., 2002; Seri et al., 2003).

The Rho family of small GTPases takes part in many cellular aspects including regulation of actin cytoskeleton (Hall, 1998). Recent studies in podocytes indicate that signaling pathways regulated by the most studied members of Rho-GTPases (RhoA, Rac1 and Cdc42) are crucial for maintenance of structural and functional podocyte integrity. Activation of RhoA in podocytes leads to albuminuria accompanied by FP effacement (Zhu et al., 2011; Wang et al., 2012). Podocyte-specific deletion of Cdc42 causes proteinuria, FP effacement, and glomerulosclerosis, while deletion of Rac1 in podocytes prevents FP effacement (Blattner et al., 2013).

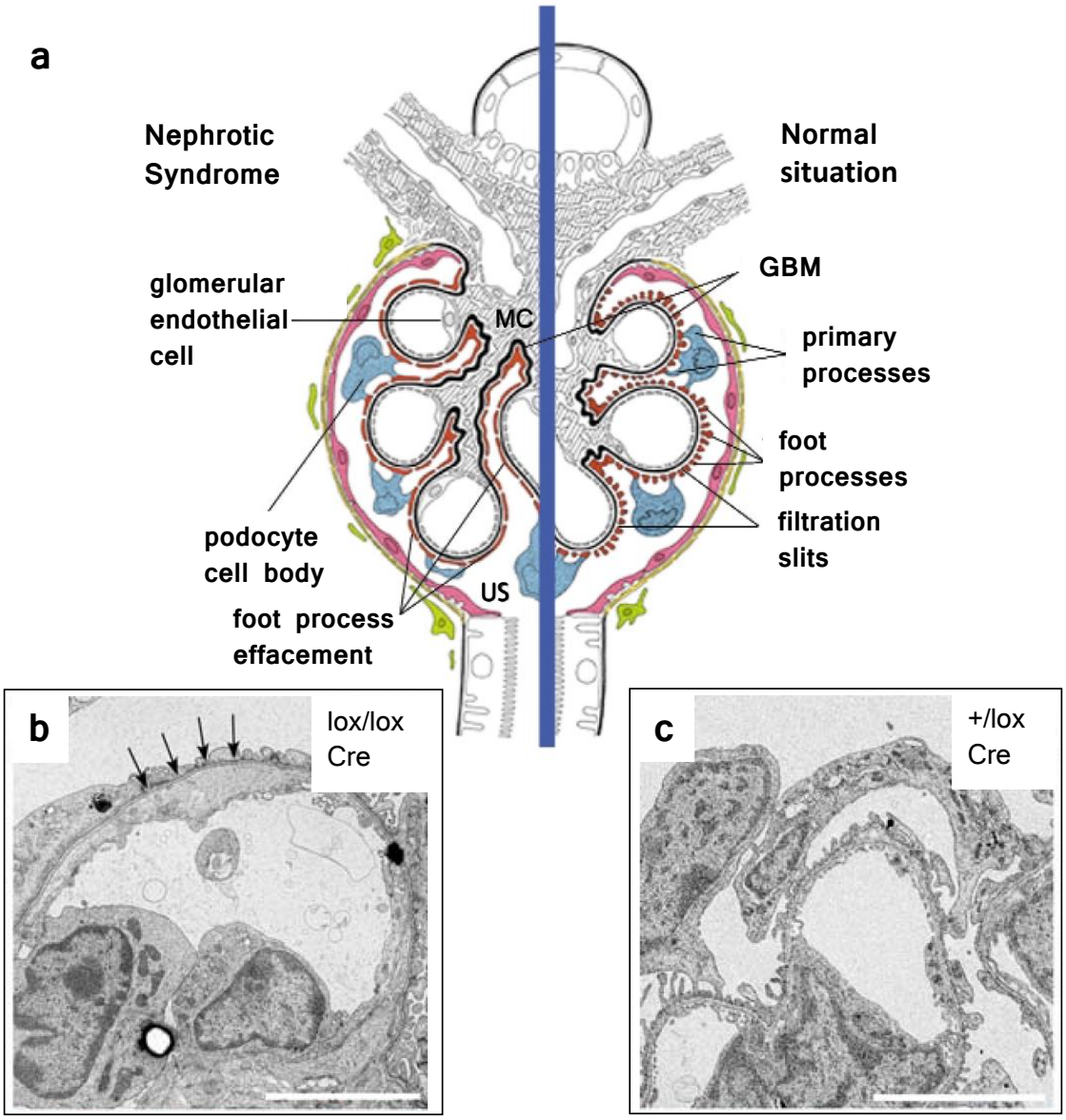

Figure 1.5: (a) The structure of the affected (left) and of the normal (right) glomerulus. Nephrotic syndrome leads to FP effacement. (b-c) Ultrastructural imaging taken from kidneys of mice with podocyte-specific inactivation of *Lmx1b*, where FP effacement and a thickened GBM are observed (arrows in b). Scale bars, 5 µm. Abbreviations: GBM, glomerular basement membrane; MC, mesangial cells; US, urine space; *+/lox* control mice with one wild-type and one floxed *Lmx1b* allele; *lox/lox*, mice with two floxed *Lmx1b* alleles; *Cre*, Cre transgene under control of the human *NPHS2* promoter. Modified from (Somlo and Mundel, 2000; Suleiman et al., 2007).

1.5 Actin and actin-associated proteins

One of the objectives of this study was to unveil the role of LMX1B for the maintenance of the podocyte actin cytoskeleton. Because of the fact that to date about 150 proteins involved in the formation of the actin cytoskeleton are known (Zaidel-Bar et al., 2007), only several proteins, including actin, α-actinin-1, α-actinin-4, focal adhesion kinase, non-muscle myosin heavy chain IIA, paxillin, talin, utrophin, vasodilator stimulated

phosphoprotein, vinculin, and zyxin were chosen for these studies. The essential information about the selected proteins will be presented in the following subsections. The interactions between the actin-associated proteins in the podocyte FPs are shown in Figure 1.6.

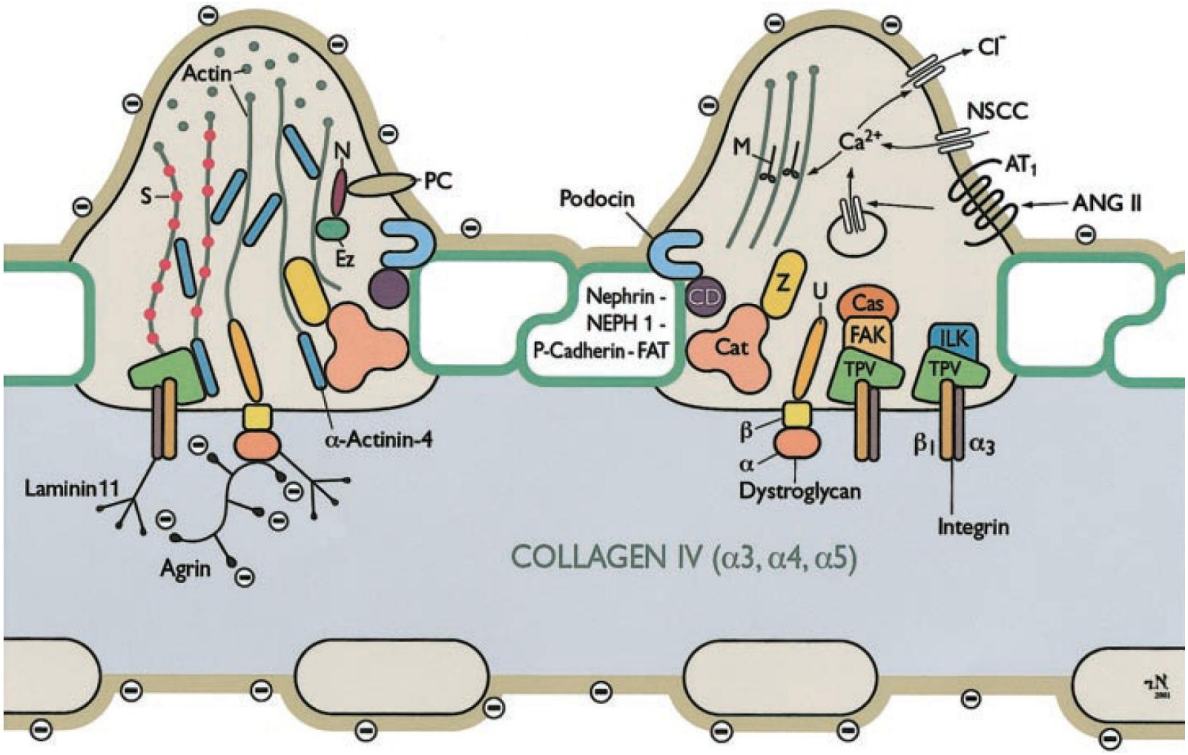

Figure 1.6: Scheme of the molecular composition of podocyte FPs. Abbreviations: Cas, p130Cas; Cat, catenins; CD, CD2-associated protein; Ez, ezrin; FAK, focal adhesion kinase; ILK, integrin-linked kinase; M, myosin; N, NHERF2; NSCC, nonselective cation channel; PC, podocalyxin; S, synaptopodin; TPV, talin, paxillin, vinculin; U, utrophin; z, ZO-1. The figure was taken from Pavenstädt *et al.*, 2003.

1.5.1 Actin

Actin is the most abundant protein in many eukaryotic cells. It builds microfilaments, one of the major components of the actin cytoskeleton. Actin exists in two forms, monomeric G-actin (globular) and polymeric F-actin (filamentous). A multitude of actin-associated proteins is engaged in the maintenance of the actin cytoskeleton. Thus, the actin-binding protein formin promotes elongation of actin filaments, while actin-related protein 2/3 (Arp2/3) induces branched actin filaments. Profilin increases the elongation of actin filaments, and cofilin accelerates its disassembly. Another actin-associated protein, α-actinin, cross-links microfilaments into loose bundles (Alberts et al., 2008). As previously mentioned, actin filaments in healthy podocytes are organized in parallel bundles. Podocyte injury causes the reorganization of actin filaments into a dense network (Shirato et al., 1996; Kerjaschki, 2001). Moreover, the expression of actin is increased (Shirato et al., 1996).

1.5.2 α-Actinins

α-Actinin was originally isolated from striated muscles (Ebashi and Ebashi, 1965). To date, four α-actinins have been reported, which are named α-actinin-1, -2, -3 and -4. α-Actinins are dimeric proteins with an essential role in cross-linking actin filaments. In vertebrates, α-actinin-1 and α-actinin-4 are expressed in most tissues and cell types, while expression of α-actinin-2 and α-actinin-3 is restricted to muscles (Foley and Young, 2014). Despite the great sequence similarity between α-actinin-1 and α-actinin-4, mutations in these genes lead to different abnormalities. Thus, mutations in the α-actinin-1 gene can lead to congenital macrothrombocytopenia characterized by decreased numbers of thrombocytes (Guéguen et al., 2013). On the other hand, mutations in the α-actinin-4 gene are associated with different tumors, including breast cancer (Honda et al., 1998), ovarian cancer (Yamamoto et al., 2007), neuroendocrine lung cancer (Miyanaga et al., 2013), and many others. Additionally, mutations in the α-actinin-4 gene result in focal segmental glomerulosclerosis characterized by proteinuria and kidney failure (Kaplan et al., 2000).

1.5.3 Focal Adhesion Kinase

Focal adhesion kinase (FAK), also known as protein tyrosine kinase 2 (PTK2), is a cytoplasmic tyrosine kinase localized to focal adhesions (Schaller et al., 1992). It interacts with the integrin-binding proteins paxillin (Hildebrand et al., 1995), talin (Chen et al., 1995), and vinculin (Stevens et al., 1996). Fibroblast-like cells derived from $fak^{-/-}$ murine embryos at day 8 showed decreased mobility (Ilić et al., 1995). The importance of FAK in cell-matrix adhesion of podocytes during glomerular injury was demonstrated by Ma *et al.* As a consequence of glomerular injury FAK is activated in murine podocytes, which then leads to proteinuria and FP effacement. Inhibition of FAK with specific pharmacological agent protects against glomerular damage (Ma et al., 2010).

1.5.4 Non-muscle myosin heavy chain IIA

The non-muscle myosin heavy chain IIA (NMMHC-IIA) is a cytoskeletal protein encoded by the *MYH9* gene. It plays a role in cell contractility, motility, morphology, cytokinesis, and polarity (Müller et al., 2011). Mutations in the *MYH9* gene are associated with various autosomal-dominant diseases such as Epstein, Fechtner, and Sebastian syndromes, and May-Hegglin anomaly. All of them are characterized by macrothrombocytopenia, hearing defects, cataracts, Döhle-like bodies in neutrophils, and glomerular injury (Seri et al., 2003). In adult human kidney *MYH9* mRNA and protein are predominantly expressed in podocytes (Arrondel et al., 2002). Recent studies by Johnstone *et al.* revealed that the podocyte-specific deletion of *Myh9* predisposes mice to glomerulopathy. Mice with the podocyte-specific deletion of *Myh9* showed no renal insufficiency or proteinuria compared to control. However, mutant mice treated with doxorubicin hydrochloride developed proteinuria and glomerulosclerosis, while control mice were resistant (Johnstone et al., 2011).

1.5.5 Paxillin

The cytoskeleton-associated protein paxillin was initially localized to the focal adhesions at the ends of actin stress fibers in chicken embryo fibroblasts (Turner et al., 1990). To

date the binding of paxillin to various focal adhesion proteins including vinculin (Turner et al., 1990), focal adhesion kinase (Hildebrand et al., 1995), and β_1 integrin (Schaller et al., 1995) has been reported. Hagel *et al.* have demonstrated the necessity of paxillin for normal development of mice: no paxillin-deficient embryos were detected after embryonic day 9.5 (Hagel et al., 2002). During maturation of a healthy rat kidney the expression of paxillin is reduced and restricted to distal tubular cells (Matsuura et al., 2011).

1.5.6 Talin

The cytoskeletal protein talin identified in focal adhesions (Burridge and Connell, 1983a; Burridge and Connell, 1983b) plays an essential role in linking the actin cytoskeleton to integrins (Horwitz et al., 1986; Critchley et al., 1999). Besides actin and integrin, talin is able to interact with other focal adhesion proteins such as vinculin (Critchley and Gingras, 2008). Recent studies of talin1 in murine podocytes revealed that talin1 is important for development of the glomerular filtration barrier and its maintenance (Tian et al., 2014). The podocyte-specific loss of talin1 in mice leads to severe proteinuria, foot process effacement, and kidney failure. The activation of β_1 integrin as well as cell spreading and adhesion in the *talin1*-deficient podocytes were moderately reduced. Nevertheless, significant changes in the actin cytoskeleton of podocytes without *talin1* were observed (Tian et al., 2014).

1.5.7 Utrophin

Utrophin, also known as dystrophin-related protein (DRP), is a component of the dystrophin-glycoprotein complex. Utrophin participates in linking the actin cytoskeleton to agrin, a major heparan sulfate proteoglycan in the glomerular basement membrane, through its interaction with β-dystroglycan. In the normal human and rat kidney utrophin was localized within glomerulus outlining the peripheral capillary loops (Raats et al., 2000; Regele et al., 2000). Detailed immunoelectron microscopy studies of the rat kidney demonstrated that utrophin was localized at the cytoplasm of some podocyte foot processes with the strongest intensity in the regions near the GBM (Raats et al., 2000).

1.5.8 Vasodilator stimulated phosphoprotein

Vasodilator stimulated phosphoprotein (VASP) was initially described in human platelets as a major protein phosphorylated in response to stimulation with vasodilators (Halbrügge and Walter, 1989). VASP is known to interact with multiple actin-associated proteins. It is able to bind profilin, which as a consequence leads to actin polymerization (Reinhard et al., 1995). Its interaction with other cytoskeletal proteins, such as vinculin (Brindle et al., 1996), talin, α-actinin, and F-actin stabilizes focal adhesion and the connection with actin filaments (Hemmings et al., 1995). Recent studies by Harris *et al.* on conditionally immortalized podocytes revealed that proteases present in the plasma of focal segmental glomerulosclerosis (FSGS) patients after transplatation lead to a podocin-dependent phosphorylation of VASP via protease-activated receptor-1. Additionally, FSGS plasma induced VASP phosphorylation-dependent motility of podocytes (Harris et al., 2013).

1.5.9 Vinculin

Vinculin was originally described as an intracellular protein localized at specialized sites where microfilaments terminate at cell membranes (Geiger et al., 1980). This cytoskeletal protein consists of head and tail domains separated by a proline-rich region (Price et al., 1989). The head domain of vinculin is able to bind talin, which then leads to the recruitment of vinculin to focal adhesions, while the tail domain binds F-actin and paxillin (Ziegler et al., 2008). Vinculin plays an essential role during embryonic development: vinculin-deficient embryos die due to heart and brain defects (Xu et al., 1998). Moreover, vinculin-deficient mouse embryonic fibroblasts show reduced adhesion and migration rates (Xu et al., 1998).

1.5.10 Zyxin

The integrin-associated linker protein zyxin was discovered at both cell-matrix and cell-cell junctions (Crawford and Beckerle, 1991). The interaction of zyxin with several focal adhesion proteins including α-actinin (Crawford et al., 1992) and VASP (Grange et al., 2013) was demonstrated. Zyxin is not absolutely essential for development: zyxin null mice showed no defects, they are viable and fertile (Hoffman et al., 2003).

1.6 Research goals

The main purpose of this study was to clarify the molecular pathway(s) regulated by LMX1B by focusing on the characterization of the putative LMX1B target genes which are upregulated after the inactivation of *Lmx1b*, and on the importance of LMX1B for the maintenance of the podocyte actin cytoskeleton. The specific goals of the studies were:

1) Identification of LMX1B binding elements (FLAT elements) within the promoter regions of its putative target genes.

2) Determination of the role of LMX1B in the transcriptional regulation of its putative target genes.

3) Demonstration of the subcellular localization of the corresponding proteins and their interaction with the actin cytoskeleton.

4) Determination of the effect of Abra, Arl4c and Crct1 on F-actin and paxillin.

5) Demonstration of the localization of Abra, Arl4c and Crct1 in the kidney and determination of their role in nail-patella syndrome.

6) Investigation of the role of LMX1B in the dynamics of the podocyte actin cytoskeleton.

Chapter 2

Materials and methods

2.1 Materials

2.1.1 Chemicals and reagents

Chemicals/reagents	Producer
0.25% Trypsin-EDTA solution	Sigma-Aldrich
4-(2-hydroxyethyl)-1-piperazineethanesulfonic acid (HEPES)	Roth
5x Phusion® HF Reaction Buffer	NEB
Acetic acid	Merck
Acrylamid/bis solution 37.5:1	Serva
Agarose	Roth
Albumin fraction V	Roth
Amido black 10B	Merck
Ammonium persulfate (APS)	Fluka
Ampicillin sodium salt	Roth
Aprotinin	Roth
Bacto agar	Becton Dickinson
Bacto tryptone	Becton Dickinson
Bacto yeast extract	Becton Dickinson
β-mercaptoethanol	Merck
Bovine serum albumine (BSA)	Sigma
Bromophenol blue	Serva
Calcium chloride	Roth
Cyanogen bromide-activated-Sepharose® 4B	Sigma-Aldrich
DEAE-Dextran	Sigma-Aldrich
Deoxynucleotide triphosphates (dNTPs)	Fermentas
Dimethyl sulfoxide (DMSO)	Sigma
Dipotassium phosphate	Merck
Dithiothreitol (DTT)	Roth
DMEM/Ham's F12	PAA
Doxycycline hyclate	Applichem
Dulbecco's modified Eagle's Medium (DMEM) - high glucose	Sigma-Aldrich
Ethanol	Sigma
Ethidium bromide	Sigma
Ethylene glycol tetraacetic acid (EGTA)	Serva

Ethylenediaminetetraacetic acid (EDTA)	Roth
Fetal bovine serum (FBS)	Gibco
Ficoll® 400	Serva
Formaldehyde solution, 37%	Sigma
G-418-sulfate	Invitrogen
Glucose	Merck
Glycerine/glycerol	Roth
Glycine	Merck
Hydrochloric acid	Merck
Hygromycin B liquid	PAA
Imidazole	Merck
Immersol 518F for Microscope	Carl Zeiss
Isopropanol (2-propanol)	Merck
Isopropyl β-D-1-thiogalactopyranoside (IPTG)	Fermentas
ITS supplement	PAA
Kanamycin sulfate	Roth
λ DNA/Hind III Marker, 2	Fermentas
Leupeptin	Serva
Light cycler®480 SYBR Green I master mix	Roche
Magnesium chloride	Sigma
Magnesium sulfate	Merck
Methanol	Merck
Monopotassium phosphate	Merck
Nickel sulfate	Merck
PageRuler prestained protein ladder	ThermoScientific
Paraformaldehyde	Merck
Penicillin-streptomycin	Sigma-Aldrich
Phenylmethanesulfonylfluoride (PMSF)	Sigma-Aldrich
ϕX174 DNA/BsuRI (HaeIII) Marker, 9	Fermentas
Polyethylen glycol (PEG 3350)	Sigma-Aldrich
Potassium acetate	Merck
Potassium chloride	Merck
Powdered milk	Sucofin
Puromycine	PAA
Roti®-Phenol (Phenol/chlorophorm/isoamylalcohol 25:24:1)	Roth
Roti®-Quant	Roth
RPMI-1640 with L-glutamine	Sigma
Sodium acetate	Roth
Sodium azide	Merck
Sodium cacodylate trihydrate	Fluka
Sodium chloride	VWR
Sodium dodecyl sulfate (SDS)	Serva
Sodium fluoride	Merck
Sodium hydrogen carbonate	Merck
Sodium hydroxide	Merck
Tetramethylenediamine (TEMED)	Serva
Thimerosal	Sigma-Aldrich
Tris	Affymetrix

Trisodium phosphate	Merck
Triton X-100	Roth
Tween® 20	Roth
Urea	Merck
Western Lightning-ECL Enhanced Luminol Reagent	Perkin Elmer
Western Lightning-ECL Oxidizing Reagent	Perkin Elmer

2.1.2 Consumables

Consumable	**Producer**
15 ml tube	Sarstedt
50 ml tube	Sarstedt
96-well white non-binding plate for luciferase assay	Greiner bio-one
Autoclave tape	VWR
Cell scraper	Sarstedt
Centrifuge tubes for centrifuge (20 ml)	Beckman coulter GmbH
Chromotography paper "3MM Chr"	Whatman
Cover glasses 24 x 40 mm	Roth
Cover glasses 24 x 60 mm	Roth
CryoPure tube 1.8 ml	Sarstedt
Culture flasks	Schott duran
Filter tips	Sarstedt
Folded filters ⌀ 90 mm	Schleicher & Schull
Gene Pulser® Cuvette for electroporation	Bio-Rad
Glass coverslips 12 mm	R.Langenbrinck
Glass coverslips 22 mm	R.Langenbrinck
Glass Pasteur pipettes	VWR
Glassware (media bottles, beakers with scale, Erlenmeyer flasks etc.)	VWR
Light cycler 96-well plate	Sarstedt
Membrane filters VSWP (0.025 µm)	Millipore
Micro tube 0.2 ml	Sarstedt
Micro tube 1.5 ml	Sarstedt
Microscope slides	Roth
Neubauer counting chamber depth 0.1 mm	Marienfeld
Nitrile gloves	Kimtech
Parafilm	Pechiney Plastic Packaging
Pipette tips	Sarstedt
Polystyrene cuvettes for spectrophotometer U-2000	Sarstedt
PVDF transfer membrane (0.45 µm)	Millipore
Scalpel	Swann-Morton
Serological pipettes	Sarstedt
Sterile filter 0.20 µm	VWR
SuperFrost® Plus Microscope Slides	R.Langenbrinck
Syringes	Brown

Task wipes	Kimtech
Tissue culture dishes	Sarstedt
Tissue culture flasks	Sarstedt
Tissue culture plates	Sarstedt

2.1.3 Enzymes

A. Restriction enzymes

Enzyme	Producer
*Bam*HI-HF: 20 U/µl	NEB
*Eco*RI-HF: 20 U/µl	NEB
*Kpn*I-HF: 20 U/µl	NEB
*Mlu*I: 10 U/µl	Fermentas
*Nhe*I-HF: 20 U/µl	NEB
*Xho*I: 20 U/µl	NEB

B. DNA and RNA modifying enzymes

Enzyme	Producer
BAP (Bacterial alkaline phosphatase): 150 U/µl	Invitrogen
T4 DNA ligase: 400 U/µl	NEB
Phusion® DNA Polymerase: 2 U/µl	Finnzymes
RNase A: 1µg/µl	Serva

2.1.4 Equipment and instruments

Equipment/ Instrument	Producer
Agarose gel documentation system "Gel Max"	Intas
Agarose gel electrophoresis apparatus "Horizon 58"	Gibco BRL™
Autoclave "Systec 5050 ELV"	Tuttnauer
Battery powered pipette filler for all pipetting from 0.1 ml to 200 ml Pipetus®-akku	Hitschmann Laborgerte
Bunsen burner	Usbeck
Centrifuge "Heraeus Pico 17" with Ch.500005 PP rotor	Thermo Scientific
Chemiluminescence system "Fusion Fx7"	Vilber Lourmat Deutschland GmbH

CO2 incubator "APT.line™CB"	Binder
Confocal microscope "LSM 510 Meta"	Zeiss
Cryostat "Leica CM3050s"	Leica
Electrophoresis power supply "PS 608"	Gibco BRL™
Electrophoresis power supply "Standard Power Pack P25"	Biometra
Electroporator "Gene Pulser Xcell™Electroporation System"	Bio-Rad
Filter catridge set "Seralpur PRO 90 CN"	Seral
Fluorescence microscope "Axiovert 200"	Zeiss
Flow cytometry system "CyFlow Space"	Partec
Freezers -20°C	Privileg
Freezers -80°C "Herafreeze"	Heraeus
Gel electrophoresis chamber "Owl™EasyCast™B2 Mini Gel Electrophoresis Systems"	Thermo Scientific
Heating block "VLM LS 1"	VLM
Hot plate with a magnetic stirrer "MR 2002" and "MR 3001"	Heidolph
Ice machine "AF-10"	Scotsman
Incubator "Kelvitron t"	Heraeus
Incubator "Unitron"	Infors
Laboratory balance "KERN 770"	KERN & Sohn GmbH
Laboratory pH Meter "CG 842"	SCHOTT Gerte GmbH
Laminar flow bench "Lamin Air HA 2448 GS"	Heraeus
LightCycler® 480 II	Roche
Liquid nitrogen container "ARPEGE TP 170"	Air Liquide Medical GmbH
Microplate luminometer "MicroLumat Plus LB96V"	Berthold Technologies
Microtome "Leica RM2255"	Leica
Microscope "Nikon Eclipse TS 100"	Nikon
Microwave "Privileg 8016 G"	Privileg
pH electrode "SenTix60"	WTW
Pipette 2-20, 20-200	Labmate
Pipette P2, P10N, P1000	Gilson
Refrigerated centrifuge "Avanti® J-26 XP" with rotor Ja-10 and Ja-25.50	Beckman Coulter
Refrigerated centrifuge "Multifuge 3 L-R" with rotor Ch. 2454	Heraeus
Refrigerated centrifuge "Sigma 3K20" with rotor Nr. 12158	B.Braun, Laboratory Centrifuges GmbH
Refrigerators	Privileg
Rocking platform shaker "Duomax 1030"	Heidolph
Rotating wheel for Eppendorf-tubes	Workshop of University of Regensburg NWF III
Spectrophotometer "U-2000"	Hitachi

Tabletop high-speed micro centrifuge"HITACHI himac CT15RE" with rotor T15A61-1041	VWR
Thermal cycler "MyCycler"	Bio-Rad
Thermomixer "5436" for Eppendorf tubes	Eppendorf
Trans-Blot® SD Semi-Dry ElectrophoreticTransfer Cell	Bio-Rad
Transmission electron microscope "EM Zeiss 902"	Zeiss
Ultramicrotome "Ultracut E"	Reichert Jung
UV-visible spectrophotometer "Evolution 201"	Thermo Scientific
Vacuum gas pump	VWR
Vertical gel electrophoresis cell "Mini Protean Tetra cell"	Bio-Rad
Vortexer "Vortex-Genie 2"	Scientific Industries
Weighing scale "BL 1500 S"	Sartorius

2.1.5 Software

A. Programs

Program	Purpose	Company
Adobe Photoshop	Digital image processing	Adobe Systems Incorporated
Bio1D	Optical density	Vilber Lourmat
FCS express version 3	FACS data analysis	De Novo Software
FileMaker Pro 6	Institute databases	FileMaker, Inc.
Fusion version 15.18	WB imaging	Vilber Lourmat
ImageJ 1.46r		National Institutes of Health
LightCycler®480 1.5.0	Real-time PCR	Roche
Microsoft Excel	Data calculations, diagrams and tables	Microsoft
Microsoft Word	Word processing	Microsoft
SPOT Advanced 4.0.9	Image processing	Diagnostic instruments, Inc.
Thermo Insight 1.4.40	DNA/RNA concentration measurement	Thermo Scientific
ZEN (blue edition)	LSM images visualization	Carl Zeiss MicroImaging GmbH

B. Internet databases and software

Name of the database/software	Purpose	Internet address

EMBOSS: stretcher	Needleman-Wunsch alignment of two sequences	www.emboss.bioinformatics.nl/cgi-bin/emboss/stretcher
Nucleotide	Gene and transcript source	www.ncbi.nlm.nih.gov/nuccore
Primer3	Primer design	www.bioinfo.ut.ee/primer3-0.4.0/primer3
Protein	Protein sequence source	www.ncbi.nlm.nih.gov/protein
PubMed	Biomedical literature search	www.ncbi.nlm.nih.gov/pubmed
RestrictionMapper	Mapping sites for restriction enzymes in DNA sequences	www.restrictionmapper.org
UCSC Genome Browser	Promoter studies	www.genome.ucsc.edu
Universal ProbeLibrary Assay Design Center	Primer design for RT-qPCR	www.lifescience.roche.com

2.1.6 Kits

Kit name	**Producer**
E.Z.N.A.® Gel Extraction Kit	VWR
iScript™cDNA Synthesis Kit	Bio-Rad
NucleoSpin® RNA II	Macherey-Nagel
Western Lightning Chemiluminescence Reagent	Perkin Elmer
Wizard® *Plus* Midipreps DNA Purification System	Promega

2.1.7 Antibodies

A. Primary antibodies, peptides

Name	**Immunogen/Epitope**	**Species**	**Dilution**	**Source**
12CA5	HA-epitope	Mouse mAb	1:30 WB, IF	J. Kyriakis
Acti-stain-555 Fluorescent Phalloidin	F-actin	-	1:500 IF	Cytoskeleton

Acti-stain-488 Fluorescent Phalloidin	F-actin	-	1:500 IF	Cytoskeleton
Anti-Abra	mouse Abra	Rabbit, polyclonal	1:100 WB 1:1 IF	this work
Anti-Actin	C-terminal actin fragment (C11 peptide attached to MAP backbone)	Rabbit, polyclonal	1:2500 WB	Sigma-Aldrich
Anti-Arl4c	aa of mouse Arl4c	Rabbit, polyclonal	1:30 WB undiluted IF	this work
Anti-Crct1	Peptide mapping near N-terminus of NICE-1 of human origin	Goat, polyclonal	1:500 WB 1:2500 IF	Santa Cruz Biotechnology
Anti-GAPDH	314-333 aa of mouse GAPDH	Rabbit polyclonal	1:10000 WB	Sigma-Adrich
Anti-His6	Histidine-Tagged Proteins	Mouse mAb	1:100 WB	Calbiochem
Anti-LMX1B	322-395 aa of human LMX1B, clone 193-67	Mouse mAb	1:10 WB	D. Heudobler
Anti-Paxillin	1-557 aa of chicken paxillin	Mouse mAb	1:10000 WB	BD Transduction Laboratories

B. Secondary antibodies

Name	**Immunogen/Epitope**	**Species**	**Dilution**	**Source**
Anti-goat IgG FITC-conjugated	Goat IgG	Donkey, polyclonal	1:100 IF	Santa Cruz Biotechnology
Anti-mouse IgG (Fab specific) peroxidase conjugate	Mouse IgG, Fab specific	Goat, polyclonal	1:10000 WB	Sigma-Aldrich

Anti-mouse IgG Cy^{TM}3-conjugated	Mouse IgG (H&L)	Goat, polyclonal	1:400 IF	Dianova
Anti-mouse IgG (whole molecule) FITC-conjugated	Mouse IgG	Goat, polyclonal	1:150 IF	Cappel
Anti-rabbit IgG (whole molecule) peroxidase conjugate	Rabbit IgG	Goat, polyclonal	1:20000 WB	Sigma-Aldrich
Anti-rabbit IgG Cy^{TM}3-conjugated	Rabbit IgG (H&L)	Goat, polyclonal	1:300 IF	Dianova
Anti-rabbit IgG DyLight^{TM}405 conjugated	Rabbit IgG (H&L)	Donkey, polyclonal	1:600 IF	Rockland

2.1.8 Oligonucleotides

A. Oligonucleotides for PCR

Oligonucleotides for PCR were synthesized by Metabion (Planegg). "F" and "R" stands for "Forward" and "Reverse" primers, respectively. T_m is the melting temperature of oligonucleotides calculated with OligoAnalyzer 3.1.

Name	**Sequence [5'-3']**	**T_m [°C]**
	Cloning to pGL4.10	
*Nhe*I-hABRA.wt F	ATT TGC GCT AGC TCA GAT GCC GTT GAA CTC TG	64.7
*Xho*I-hABRA.wt R	GCA AAT CTC GAG GAG GCT GGA GTG CAG TGG	66.8
*Nhe*I-hARL4C.wt F	ATT TGC GCT AGC AGC ATC TCC ATC CCA AAC AG	65.0

*Xho*I-hARL4C.wt R	GCA AAT CTC GAG ACC CAG CTG AGA CCA GAG AA	65.1
*Nhe*I-hIL6.wt F	ATT TGC GCT AGC TGA GAC CAA GGA TCC TCC TG	65.4
*Xho*I-hIL6.wt R	GCA AAT CTC GAG AGT TCA TAG CTG GGC TCC TG	64.3
	Cloning to pcDNA3.1	
*Bam*HI-Kozak-HA-mAbra F	ATT TGC GGA TCC GCC ACC ATG TAC CCA TAC GAC GTC CCA GAC TAC GCT ATG GCT CCA GGA GAA AGG GA	73.5
*Xho*I-mAbra R	ATT TGC CTC GAG TTA CTC AAG GAG AGT AAT C	59.3
*Bam*HI-Kozak-HA-mArl4c F	ATT TGC GGA TCC GCC ACC ATG TAC CCA TAC GAC GTC CCA GAC TAC GCT ATG GGC AAC ATC TCC TCC AAC	72.9
*Xho*I-mArl4c R	ATT TGC CTC GAG TTA CCG CTT CTT CTT CTG C	63.3
*Bam*HI-Kozak-HA-mCrct1 F	ATT TGC GGA TCC GCC ACC ATG TAC CCA TAC GAC GTC CCA GAC TAC GCT ATG TCT CAA CAG GGC GCC A	73.9
*Xho*I-mCrct1 R	ATT TGC CTC GAG TCA GCA GCC ACC GGA GCA G	69.3
	Cloning to pET21a	
*Bam*HI-mAbra F	ATT TGC GGA TCC ATG GCT CCA GGA GAA AGG GA	66.9
*Xho*I-mAbra R	ATT TGC CTC GAG CTC AAG GAG AGT AAT CAC	61.4
*Bam*HI-mArl4c F	ATT TGC GGA TCC AAG TCG CTG CCG GTG GCC G	71.4
*Xho*I-mArl4c R	ATT TGC CTC GAG CCG CTT CTT CTT CTG CTT G	65.2
*Bam*HI-mCrct1 F	ATT TGC GGA TCC ATG TCT CAA CAG GGC GCC A	67.9

*Xho*I-mCrct1 R	ATT TGC CTC GCA GCC ACC GGA GCA GCA G	71.1
	Cloning to pminiSOG-C1-mCherry	
*Xho*I-mAbra F	ATT TGC CTC GAG TAA TGG CTC CAG GAG AAA GGG A	65.9
*Kpn*I-mAbra R	ATT TGC GGT ACC TTA CTC AAG GAG AGT AAT CAC	60.7
*Xho*I-mArl4c F	ATT TGC CTC GAG TAA TGG GCA ACA TCT CCT CCA AC	65.2
*Kpn*I-mArl4c R	ATT TGC GGT ACC TTA CCG CTT CTT CTT CTG CTT G	64.2
*Xho*I-mCrct1 F	ATT TGC CTC GAG TAA TGT CTC AAC AGG GCG CCA	66.8
*Kpn*I-mCrct1 R	ATT TGC GGT ACC TCA GCA GCC ACC GGA GCA GCA GCA G	72.2
	Cloning to pLVPT-rtTR-KRAB-2SM2	
*Bam*HI-mAbra F	ATT TGC GGA TCC ATG GCT CCA GGA GAA AGG G	66.3
*Mlu*I-mAbra R	ATT TGC ACG CGT GGC TCA AGG AGA GTA ATC AC	64.7
*Bam*HI-mArl4c F	ATT TGC GGA TCC ATG GGC AAC ATC TCC TCC AAC	66.1
*Mlu*I-mArl4c R	ATT TGC ACG CGT GGC CGC TTC TTC TTC TGC TTG	68.1
*Bam*HI-mCrct1 F	ATT TGC GGC TCC ATG TCT CAA CAG GGC GCC	67.2
*Mlu*I-mCrct1 R	ATT TGC ACG CGT GGG CAG CCA CCG GAG CAG CAG	73.5
	Oligonucleotides for PCR from genomic DNA	
rtTA F	CCC ACT TCT GAG ACA ACG	52.8
rtTA R	GGT CAA AGT CGT CAA GGG	53.2

Tomato F	CTC TGC TGC CTC CTG GCT TCT	61.6
Tomato R1	CGA GGC GGA TCA CAA GCA ATA	57.5
Tomato R2	TCA ATG GGC GGG GGT CGT T	62.3
Cre F	TGG ACA TGT TCA GGG ATC GC	57.4
Cre R	TCA GCT ACA CCA GAG ACG GA	57.4
Floxed *Lmx1b* F	AGG CTC CAT CCA TTC TTC TC	54.1
Floxed *Lmx1b* R	CCA CAA TAA GCA AGA GGC AC	54.1
	Oligonucleotides for qPCR	
luc2 F	CAT GAC CGA GAA GGA GAT CG	54.8
luc2 R	CAG CTT CTT GGC GGT TGT A	55.4

B. Oligonucleotides for site-specific mutagenesis

Oligonucleotides for PCR were synthesized by Metabion (Planegg). "F" and "R" stands for "Forward" and "Reverse" primers, respectively. T_m is the melting temperature of oligonucleotides calculated with OligoAnalyzer 3.1.

Name	**Sequence [5'-3']**	**T_m [°C]**
Abra-mut F	CTG TAG ATT AAG TCT AGA ATC ACT TCC C	54.4
Abra-mut R	GGG AAG TGA TTC TAG ACT TAA TCT ACA G	54.4
Arl4c-mut F	GTC CAG CCA AGT AAG CTT GAT GAA ATG AAA ATA ATA G	59.3
Arl4c-mut R	CTA TTA TTT TCA TTT CAT CAA GCT TAC TTG GCT GGA C	59.3

C. Oligonucleotides for cloning of shRNAs into pInducer10 vector

The shRNAs were designed using the miR RNAi design option of the Block-iT RNAi Designer program. "T" and "B" stands for "Top" and "Bottom" strands, respectively.

Name	Sequence [5'-3']
*Xho*I-Arl4c-shRNA # 559 T	TCG AGT AAC GAT GTG CAG AGA CTG GAG TTT TGG CCA CTG ACT GAC TCC AGT CTG CAC ATC GTT AG
*Eco*RI-Arl4c–shRNA # 559 B	AAT TCT AAC GAT GTG CAG ACT GGA GTC AGT CAG TGG CCA AAA CTC CAG TCT CTG CAC ATC GTT AC
*Xho*I-Arl4c-shRNA # 850 T	TCG AGC AAA CTT GGT CAC CTT GTG CAG TTT TGG CCA CTG ACT GAC TGC ACA AGG ACC AAG TTT GG
*Eco*RI-Arl4c–shRNA # 850 B	AAT TCC AAA CTT GGT CCT TGT GCA GTC AGT CAG TGG CCA AAA CTG CAC AAG GTG ACC AAG TTT GC
*Xho*I-Arl4c-shRNA # 1037 T	TCG AGT CAT AGA GCT TGT CCA TGC CCG TTT TGG CCA CTG ACT GAC GGG CAT GGA AGC TCT ATG AG
*Eco*RI-Arl4c–shRNA # 1037 B	AAT TCT CAT AGA GCT TCC ATG CCC GTC AGT CAG TGG CCA AAA CGG GCA TGG ACA AGC TCT ATG AC

2.1.9 Vectors

A. Outside plasmids

Vector	Selection marker	Source
mEmerald-FAK	kan	M. W. Davidson (National High Magnetic Field Laboratory, Florida State University)
mEmerald-Talin	kan	M. W. Davidson (National High Magnetic Field Laboratory, Florida State University)
mEmerald-VASP	kan	M. W. Davidson (National High Magnetic Field Laboratory, Florida State University)
Lifeact-GFP	kan	R. Faessler, S. Wickstroem (Max Plank Institute of Biochemistry)
pcDNA3.1	amp	Invitrogen
pcDNA6.2/N-EmGFP-MYH9	amp	T. Vallenius (University of Helsinki)

pCMV delta R8.2	amp	Addgene
pCMV-SPORT6.1/Crct1	amp	Source BioScience
pCR4-TOPO/Abra	kan	Source BioScience
pCS2+/GFP-UtrCH	amp	E. Kerkhoff (The Molecular Cell Biology Laboratory, University of Regensburg)
pDEST/Lifeact-mCherry-N1	kan	Addgene
pEGFP-α-actinin1	kan	C.A. Otey (Department of Cell Biology and Physiology, UNC, Chapel Hill, USA)
pEGFP-α-actinin4	kan	C.A. Otey (Department of Cell Biology and Physiology, UNC, Chapel Hill, USA)
pET21a	amp	Novagen
pEYFP/Arl4c-wt	kan	Th. Engel (Leibniz Institute for Arteriosclerosis Research, University Muenster)
pEYFP/Arl4c-T27N	kan	Th. Engel (Leibniz Institute for Arteriosclerosis Research, University Muenster)
pEYFP/Arl4c-Q71L	kan	Th. Engel (Leibniz Institute for Arteriosclerosis Research, University Muenster)
pGL3-Enhancer	amp	Promega
pInducer10	amp	S.Elledge (Brigham and Women's Hospital, Boston)
pLVPT-rtTR-KRAB-2SM2	amp	Addgene
pmCherry/Paxillin-C3	kan	E. Kerkhoff (The Molecular Cell Biology Laboratory, University of Regensburg)

pmCherry-C1/Zyxin	kan	E. Kerkhoff (The Molecular Cell Biology Laboratory, University of Regensburg)
pMD2.G	amp	Addgene
pminiSOG-C1	kan	M. W. Davidson (National High Magnetic Field Laboratory, Florida State University)
pYX-Asc/Arl4c	amp	Source BioScience
Vinculin-Venus	amp	Addgene

B. Own constructs

Name of construct	**Size of insert [kbp]**	**5' cloning site**	**3' cloning site**	**Resistance**
pcDNA3.1/HA-mAbra	1.1	*Bam*HI	*Xho*I	amp
pcDNA3.1/HA-mArl4c	0.6	*Bam*HI	*Xho*I	amp
pcDNA3.1/HA-mCrct1	0.3	*Bam*HI	*Xho*I	amp
pET21a/mAbra-His	1.1	*Bam*HI	*Xho*I	amp
pET21a/mArl4c-His	0.4	*Bam*HI	*Xho*I	amp
pET21a/mCrct1-His	0.3	*Bam*HI	*Xho*I	amp
pGL4.10/hAbra.wt	0.4	*Nhe*I	*Xho*I	amp
pGL4.10/hArl4c.wt	1.9	*Nhe*I	*Xho*I	amp
pGL4.10/hIL6.wt	1.3	*Nhe*I	*Xho*I	amp
pInducer10/shRNA-Arl4c #559	0.065	*Xho*I	*Eco*RI	amp
pInducer10/shRNA-Arl4c #850	0.065	*Xho*I	*Eco*RI	amp
pInducer10/shRNA-Arl4c #1037	0.065	*Xho*I	*Eco*RI	amp

pLVPT-rtTR-KRAB-2SM2/mAbra-GFP	1.1	*Bam*HI	*Mlu*I	amp
pLVPT-rtTR-KRAB-2SM2/mArl4c-GFP	0.6	*Bam*HI	*Mlu*I	amp
pLVPT-rtTR-KRAB-2SM2/mCrct1-GFP	0.3	*Bam*HI	*Mlu*I	amp
pminiSOG-C1-mCherry/mAbra	1.1	*Xho*I	*Kpn*I	kan
pminiSOG-C1-mCherry/mArl4c	0.6	*Xho*I	*Kpn*I	kan
pminiSOG-C1-mCherry/mCrct1	0.3	*Xho*I	*Kpn*I	kan

2.1.10 Cells

A. Bacterial strains

Strain	Antibiotic resistance
DH5α	none
BL21(DE3)	none
BL21(DE3)pLysS	chloramphenicol
Rosetta(DE3)pLysS	chloramphenicol
TOP 10	none

B. Cell lines

Name	Description	Source
COS-7	African green monkey kidney fibroblast-like cell line	B. Royer-Pokora (Institute of Human Genetics, Heidelberg)
HEK293T	Human Embrionic Kidney 293 cells, which constitutively express the simian virus 40 (SV40) large T antigen	W. Nickel (University of Heidelberg, Biochemistry Center)

Murine podocyte cell line	Podocytes isolated from H-2kb-tsA58 mice, which carried temperature-sensitive SV40 large T antigen under control of the IFN-γ-inducible H-2kb promoter	K. Endlich (University of Heidelberg, Institute of Anatomy and Cell Biology I)
Human podocyte cell line	conditionally immortalized human podocyte cell line transfected with the temperature-sensitive SV40-7 gene	M.A. Saleem (University of Bristol)
HtTA-1/myc-LMX1B clone #34	HtTA-1 transfected with pUHD10-3/myc-LMX1B	A. Rascle (University of Regensburg)

C. Mouse strains

Name	Description	Source
Lmx1b^{2loxP}	LoxP sites are above and below of exons 4 and 6 respectively	R. Johnson (MD Anderson Cancer Center, Houston, USA)
P2.5-rtTA	Gene for reverse tetracycline-dependent transactivator (rtTA) under the control of 2.5 kbp of human NPHS2 promoter	J.Kopp (NIH, Bethesda, USA)
LC-1	Expression of the luciferase and *cre* gene is regulated by the Tet system	H. Bujard (ZMBH, Heidelberg)
mT/mG	Expression of membrane-targeted tandem dimer Tomato (mT) prior to Cre-mediated excision and membrane-targeted green fluorescent protein (mG) after excision	T.Huber (Nephrology, University Medical Center, University of Freiburg)

2.1.11 Media, solutions, buffers

A. Media and solutions for work with bacteria

Medium/solution	Components
LB Broth	Amount per 1 liter: 10 g Bacto-Tryptone 5 g Yeast Extract 10 g NaCl
LB Broth with agar (Agar plates)	Amount per 1 liter: 10 g Bacto-Tryptone 5 g Yeast Extract 10 g NaCl 15 g Bacto Agar After autoclaving medium was cooled to about 50°C and appropriate antibiotics were added. Approximately 25 ml were poured into each plate. Inverted plates were stored at 4°C.
Transformation and storage solution (TSS)	10% PEG 3350 5% DMSO 25 mM $MgSO_4$ LB medium

B. Solutions and buffers for DNA isolation, cloning and electrophoresis

Solution/buffer	Components
Cell lysis solution (Alkaline SDS solution)	0.2 M NaOH/1% SDS
Cell resuspension solution (GTE buffer)	50 mM glucose 25 mM Tris, pH 8.0 10 mM EDTA pH 8.0
CutSmart buffer, 1×	50 mM Potassium acetate 20 mM Tris acetate 10 mM Magnesium acetate 100 µg/ml BSA pH 7.9 at 25°C
DNA loading buffer, 5×	0.125% bromophenol blue 15% Ficoll type 400 50 mM EDTA, pH 8.0 0.5% SDS

dNTP, 10 mM	10 mM dATP, 10 mM dTTP, 10 mM dCTP, 10 mM dGTP
NEBuffer 1.1, 1×	10 mM Bis Tris Propane-HCl 10 mM $MgCl_2$ 100 µg/ml BSA pH 7.0 at 25°C
NEBuffer 2.1, 1×	50 mM NaCl 10 mM Tris-HCl 10 mM $MgCl_2$ 100 µg/ml BSA pH 7.9 at 25°C
NEBuffer 3.1, 1×	100 mM NaCl 50 mM Tris-HCl 10 mM $MgCl_2$ 100 µg/ml BSA pH 7.9 at 25°C
Potassium acetate solution	5 M potassium acetate pH 4.8 was adjusted with 5 M acetic acid
Sodium acetate, 3 M	3 M sodium acetate pH 5.2 was adjusted with glacial acetic acid
Solution 1 for genomic DNA isolation from blood	10 mM Tris, pH 7.6 10 mM KCl 10 mM $MgCl_2$ 2.4% NP-40
Solution 2 for genomic DNA isolation from blood	10 mM Tris pH 7.6 10 mM KCl 10 mM $MgCl_2$ 0.5 M NaCl 2 mM EDTA 0.5% SDS
T4 DNA ligase buffer	50 mM Tris-HCl 10 mM $MgCl_2$ 1 mM ATP 10 mM DTT pH 7.5 at 25°C
TAE, 50×	2 M Tris 0.1 M EDTA pH 8.0 was adjusted with acetic acid

C. Buffers for protein isolation

Buffer	Components
G actin buffer	1% Triton X-100 20 mM Tris, pH 7.4 5 mM EGTA, pH 7.4 20 mM NaF 25 mM sodium pyrophosphate 10 mM DTT 0.5 mM PMSF 2 μg/ml leupeptin 2 μg/ml aprotinin prepared each time fresh
Protein lysis buffer	1× PBS 1% Triton X-100 6 M urea stored at 4°C

D. Buffers for protein electrophoresis

Buffer	Components
Laemmlie buffer, 5× **(SDS-PAGE loading buffer)**	2% SDS 5% β-mercaptoethanol or 200 mM DTT 20% glycerol 0.1% bromophenol blue 62.5 mM Tris-HCl, pH 6.8
Lower gel buffer, 4×	1.5 M Tris, pH 8.8 0.4% SDS
SDS-PAGE Running buffer, 10×	0.25 M Tris base 1.92 M glycine 1% SDS
Upper gel buffer, 4×	0.5 M Tris, pH 6.8 0.4% SDS

Resolving gel components	10%	12%	15%
30% acrylamide/ 0.8% bisacrylamide	1.66 ml	1.98 ml	2.46 ml
4× lower gel buffer, pH 8.8	1.25 ml	1.25 ml	1.25 ml
deionized water	2.07 ml	1.75 ml	1.27 ml
TEMED	2.9 µl	2.9 µl	2.9 µl
10% APS	13.9 µl	13.9 µl	13.9 µl

Stacking gel components	4%
30% acrylamide/ 0.8% bisacrylamide	0.39 ml
4× upper gel buffer, pH 6.8	0.75 ml
deionized water	1.84 ml
TEMED	3 µl
10% APS	15 µl

E. Solutions and buffers for protein detection

Solution/buffer	Components
Amido black destaining solution	50% methanol 10% acetic acid
Amido black staining solution	1.5 mM amido black 10 B 50% methanol 10% acetic acid
Blocking buffer	5% low-fat milk in PBST buffer
PBST	0.02% Tween® 20 1× PBS
Semi-dry transfer buffer, 1×	25 mM Tris base 192 mM glycine 20% methanol 0.02% SDS

F. Buffers for recombinant protein purification

Buffer	Components
Binding buffer, 8×	40 mM imidazole 4 M NaCl 160 mM Tris-HCl, pH 7.9
Charge buffer, 8×	400 mM $NiSO_4 \cdot H_2O$
Elute buffer, 4×	4 M imidazole 2 M NaCl 80 mM Tris-HCl, pH 7.9
SDS-sample buffer	125 mM Tris, pH 6.7 2.5% SDS 10% glycerol 2.5% β-mercaptoethanol 0.01% bromophenol blue
Strip buffer, 2×	200 mM EDTA 1 M NaCl 40 mM Tris-HCl, pH 7.9
Wash buffer, 4×	240 mM imidazole 2 M NaCl 80 mM Tris-HCl, pH 7.9

G. Buffers for coupling of proteins

Buffer	Components
Coupling buffer	100 mM $NaHCO_3$, pH 8.3 500 mM NaCl
Wash buffer 1	100 mM NaAc, pH 4.0 500 mM NaCl
Wash buffer 2	100 mM $NaHCO_3$, pH 8.0 500 mM NaCl

H. Buffers for affinity purification of antibodies

Buffer	Components
Wash buffer A	10 mM Tris-HCl, pH 7.5 170 mM NaCl
Wash buffer B	10 mM Tris-HCl, pH 7.5 170 mM NaCl 0.02% Tween® 20
Wash buffer C	10 mM Tris-HCl, pH 7.5 500 mM NaCl 0.02% Tween® 20

I. Media, solutions and buffers for work with cells

Medium/solution/buffer	Components
Ca^{2+}-buffer (Krebs-Henseleit Buffer)	150 mM NaCl 5 mM KCl 2.2 mM $CaCl_2 \cdot 2H_2O$ 1 mM $MgCl_2 \cdot 6H_2O$ 5 mM glucose ($C_6H_{12}O_6 \cdot H_2O$) 10 mM HEPES
DEAE-dextran/chloroquine solution	1× PBS 10 mg/ml DEAE-dextrane 2.5 mM chloroquine Solution was stored at 4°C
Freezing medium	10% DMSO in FCS
PBS, 10×, pH 7.5	Solution A: 1.4 M NaCl 100 mM $K_2HPO_4 \cdot 3H_2O$ Solution B: 100 mM KH_2PO_4 Solution A was adjusted to pH 7.5 with solution B

2.2 Working with bacteria

2.2.1 Storage and inoculation of bacteria

The work with bacteria was carried out under sterile conditions near the flame. All solutions were autoclaved at 121°C and 1 bar for 20 min. Solutions containing heat-sensitive components (e.g. antibiotics, IPTG) were filter-sterilized through an 0.20 μm filter. Bacterial cultures were shortly (days/weeks) stored at 4°C on antibiotic plates or in 15 ml tubes with LB medium containing suitable antibiotic. For long-term storage 600 μl of freshly saturated bacterial cultures were frozen at -80°C in CryoTube vial containing 300 μl of 100% glycerol.

Bacterial cultures were inoculated with overnight cultures diluted 1:100 or with splinter of solid ice from frozen bacterial stock and were grown in Erlenmeyer flask in LB medium with appropriate antibiotic. All bacterial cultures were grown overnight (∼16 h) at 37°C with constant agitation (250 rpm, "Unitron"). Working concentrations of antibiotics used in this work are shown in Table 2.1. All antibiotics were stored at -20°C.

Antibiotic	Working concentration [μg/ml]
Ampicillin	Plates: 50 Liquid cultures: 500
Chloramphenicol	34
Kanamycin	30

Table 2.1: Working concentration of antibiotics

2.2.2 Transformation of chemically competent bacteria

A. Cell preparation

The fresh overnight bacterial culture of DH5α strain was diluted 1:100 in LB medium and was incubated at 37°C with constant agitation (250 rpm, "Unitron") until cells reached an OD_{600} of 0.4 to 0.5. Cells were pelleted by centrifugation (10 min, 2500 rpm, 4°C, "Multifuge 3 L-R", rotor Ch.2454). The supernatant was removed and the pellet was resuspended in 1/10 of the initial volume of bacterial culture in TSS buffer. 200-μl aliquots were immediately frozen at -80°C.

B. Cell transformation

10 μl of plasmid DNA were added to 200 μl of chemically competent cells and incubated for 30 min on ice. Cells were placed at 42°C for 90 s and then again on ice for 2 min. Cells containing DNA were transferred into a 15 ml tube containing 800 μl of LB medium and were grown at 37°C for 1 h with constant agitation (250 rpm, "Unitron"). 30 μl, 100 μl, 300 μl and the remaining bacterial culture was plated on LB plates containing an appropriate antibiotic. Plates were incubated overnight at 37°C in the "Kelvitron t" incubator.

2.2.3 Bacteria transformation by electroporation

A. Cell preparation

The fresh overnight bacterial cultures of DH5α and TOP10 strains were diluted 1:100 in LB medium without antibiotics and were incubated at 37°C with constant agitation (250 rpm, "Unitron") until cells reached an OD_{600} of 0.4 to 0.5. 50 ml of cell aliquots were incubated on ice for 30 min and afterwards centrifuged (15 min, 4000 rpm, 4°C, "Multifuge 3 L-R", rotor Ch.2454). The supernatant was discharged, the cell pellet was resuspended in 50 ml of ice-cold autoclaved water and incubated on ice for 15 min. The cells were centrifuged (15 min, 4000 rpm, 4°C, "Multifuge 3 L-R", rotor Ch.2454) and the supernatant was discarded. The cell pellet was resuspended in 20 ml of ice-cold water and after 15 min incubation on ice, the cells were centrifuged (15 min, 4000 rpm, 4°C, "Multifuge 3 L-R", rotor Ch.2454). The supernatant was poured off and the cell pellet was resuspended in 10 ml of ice-cold water. After 15 min of incubation on ice, the cells were centrifuged (15 min, 4000 rpm, 4°C, "Multifuge 3 L-R", rotor Ch.2454). The supernatant was discarded and finally the pellet was resuspended in 10% ice-cold glycerol. 100 µl of aliquots were directly frozen at -80°C.

B. Cell transformation

The electroporation device ("Gene Pulser Xcell^{TM}Electroporation System") was set to 2.5 kV, 25 µF. 10 µl of dialyzed ligation mixture were added to 100 µl of electro competent cells and left on ice for 30 s. The cells were transferred into an electroporation cuvette, which was wiped with a Kimtech wipe and placed in the sample chamber. Immediately after applying an electric pulse, 200 µl of LB medium were added. Then bacteria were transferred with a pipette in the 15 ml tube containing 800 µl of LB medium and were grown at 37°C for 1 h with constant agitation (250 rpm, "Unitron"). 30 µl, 100 µl, 300 µl and the remaining bacterial culture was plated on LB plates containing an appropriate antibiotic. Plates were incubated overnight at 37°C in the "Kelvitron t" incubator.

2.2.4 Preparation of plasmid DNA by alkaline lysis with sodium dodecyl sulfate: Minipreparation

Principle of the method

In this work plasmid DNA for colony screening was extracted using alkaline lysis minipreparation. This method is based on bacterial protein denaturation by sodium dodecyl sulfate (SDS) treatment and chromosomal and plasmid DNA denaturation by NaOH. Potassium acetate treatment precipitates chromosomal DNA and proteins which are removed from solution by centrifugation. Moreover, potassium acetate reanneals covalently closed plasmid DNA. During the last step ethanol precipitates plasmid DNA from the supernatant (Birnboim and Doly, 1979).

Course of the experiment

A single bacterial colony was inoculated in 5 ml of LB medium and was grown overnight at 37°C with constant agitation (250 rpm, "Unitron"). On the next day 1.5 ml of cells were centrifuged (1 min, 13000 rpm, room temperature, centrifuge "Heraeus Pico 17", Ch.500005 PP rotor). After that the supernatant was discarded. The cell pellet was

resuspended in 100 µl of GTE buffer containing 5 µg/ml of RNase A and left for 5 min at room temperature. 200 µl of alkaline SDS solution were added, mixed and incubated on ice for 5 min. Afterwards 150 µl of potassium acetate solution were added and the sample was vortexed for 2 s and incubated on ice for 5 min. The sample was centrifuged twice (3 min, 13000 rpm, room temperature, "Heraeus Pico 17"), each time transferring the supernatant into a fresh 1.5 ml tube. 900 µl of 100% ethanol were added to the supernatant and plasmid DNA was pelleted by centrifugation (30 min, 13000 rpm, 4°C, "HITACHI himac CT15RE", rotor T15A61-1041). The pellet was washed once with 600 µl of 70% ethanol and air-dried. Finally the pellet was dissolved with 50 µl of water and analyzed for the presence of positive colonies by digestion with suitable restriction enzymes.

2.2.5 Preparation of plasmid DNA with Wizard® Plus Midipreps DNA Purification System

Principle of the method

Purification of plasmid DNA with Wizard® Plus Midipreps DNA Purification System is based on the ability of DNA to bind Wizard® Midipreps DNA Purification Resin. Bacterial lysate is cleared before the binding of DNA to the resin. Finally DNA is washed with Column Wash Solution and eluted with water.

Course of the experiment

1 ml of fresh bacterial culture or splinter of solid ice of frozen bacterial stock was inoculated in 100 ml of LB medium containing appropriate antibiotic. Bacteria were grown in Erlenmeyer flask overnight (∼16 h) at 37°C with constant agitation (250 rpm, "Unitron"). Cells were collected by centrifugation (20 min, 3500 rpm, 4°C, "Multifuge 3 L-R", rotor Ch.2425) and the pellet was dissolved in 3 ml of Cell Resuspension Solution (50 mM Tris-HCl pH 7.5, 10 mM EDTA, 100 µg/ml RNase A). Cells were lysed with 3 ml of Cell Lysis Solution (0.2 M NaOH, 1% SDS) and neutralized with 3 ml of Neutralization Solution (1.32 M potassium acetate, pH 4.8). The lysate was centrifuged (30 min, 13000 rpm, 4°C, "Sigma 3K20", rotor nr. 12158) and then the supernatant was filtered through a filter paper. 10 ml of DNA Purification Resin were added to the DNA solution. The resin/DNA mixture was transferred into the Midicolumn and the sample was passed through a column. The Midicolumn was washed twice with 15 ml of Column Wash Solution (80 mM potassium acetate, 8.3 mM Tris-HCl, pH 7.5, 40 µM EDTA). The reservoir was separated from the Midicolumn and placed in a 1.5 ml tube. The resin was dried by centrifugation (2 min, 13000 rpm, room temperature, "Heraeus Pico 17", rotor Ch.500005 PP). Afterwards 300 µl of autoclaved preheated (65°C) water was added to the resin and incubated for 1 min. Finally DNA was eluted by centrifugation (20 s, 13000 rpm, room temperature, "Heraeus Pico 17", rotor Ch.500005 PP). The reservoir was removed and discarded. Purified DNA was stored at -20°C.

2.3 Working with DNA

2.3.1 Isolation and purification of DNA

A. Genomic DNA extraction from blood

Principle of the method

Genomic DNA from blood was extracted using a method described by John et al. (John et al., 1991). Hypotonic solution 1 separates white blood cells from the other blood constituents. During centrifugation white blood cells form a pellet in the bottom of the tube. NaCl in solution 2 disperses white blood cells and SDS lyses them thereby releasing DNA. Afterwards DNA is extracted with phenol:chlorofrom:isoamyl and finally precipitated with ethanol.

Course of the experiment

Equal volumes of blood and solution 1 for genomic DNA extraction from blood were combined and inverted several times. Then the mixture was centrifuged (15 min, 2000 rpm, room temperature, "Multifuge 3 L-R", rotor Ch.2425). The supernatant was removed and the pellet was resuspended in 1/5 volume of solution 2. The mixture was phenolized until the interphase was clear. After every addition of phenol:chlorophorm:isoamyl, the mixture was centrifuged (10 min, 4000 rpm, room temperature,"Multifuge 3 L-R", rotor Ch.2425). The upper phase was transferred to a new tube and DNA was precipitated with 2 vol of 100% ethanol. Genomic DNA was recovered with a heat-sealed Pasteur pipette and washed twice with 70% ethanol. DNA was air-dried and dissolved in water.

B. Phenol extraction and ethanol precipitation of DNA

Principle of the method

This method was used for the purification of PCR products. Addition of equal volumes of phenol:chlorophorm:isoamyl to an aqueous solution of DNA leads to a phase separation between an upper aqueous phase containing DNA and a lower organic phase. DNA precipitates in 70% ethanol in the presence of monovalent cations. Salts and small organic molecules are removed by washing the DNA pellet with 70% ethanol.

Course of the experiment

Equal volumes of phenol:chlorophorm:isoamyl (25:24:1) were added to the PCR product and vortexed. The mixture was then centrifuged (10 min, 14000 rpm, room temperature, "Heraeus Pico 17", rotor Ch.500005 PP). The upper aqueous phase containing DNA was transferred into a new 1.5 ml tube. 1/10 vol of 3 M sodium acetate, pH 5.2, and 3 vol of ice-cold absolute ethanol were added to the DNA solution and then centrifuged (1 h, 14000 rpm, 4°C, "HITACHI himac CT15RE", rotor T15A61-1041). The supernatant was removed and the pelleted DNA was washed once with 70% ice-cold ethanol (10 min, 14000 rpm, 4°C, "HITACHI himac CT15RE", rotor T15A61-1041). The pellet was air-dried and then dissolved in autoclaved water.

C. DNA restriction fragment extraction from agarose gel with E.Z.N.A.® Gel Extraction Kit

Principle of the method

The E.Z.N.A.® Gel Extraction Kit was used during this work for the extraction and purification of restriction fragments from agarose gel. The method is based on the reversible DNA binding to the HiBind DNA Mini Column. Contaminations, such as restriction enzymes or salts, are removed from the column during the washing step and purified DNA fragments are eluted with a low salt buffer.

Course of the experiment

DNA was separated on agarose gel and a fragment of interest was excised with a scalpel. The weight of the gel fragment containing DNA was estimated and the appropriate volume of Binding Buffer (XP2) was added [1 ml of Binding Buffer (XP2) per 1 g of a gel]. The mixture was incubated at 60°C for 7 min on "Thermomixer 5436 for Eppendorf tubes". The HiBind DNA Mini Column was placed in a 2 ml collection tube and the DNA/agarose solution was added to the HiBind DNA Mini Column. The column was centrifuged (1 min, 10000× g, room temperature, "Heraeus Pico 17", rotor Ch.500005 PP) and the flow-through was discarded. When the volume of the DNA/agarose mixture was more than 700 µl, loading and centrifugation steps were repeated. Subsequently 300 µl of Binding Buffer (XP2) were added into the HiBind DNA Mini Column and the column was centrifuged (1 min, 13000× g, room temperature, "Heraeus Pico 17", rotor Ch.500005 PP). The flow-through was discarded and the column was placed in the same collection tube. The column was washed twice with 700 µl of SPW Wash Buffer, after each SPW Wash Buffer application the column was centrifuged (1 min, 13000× g, room temperature, "Heraeus Pico 17", rotor Ch.500005 PP). The flow-through was discarded. After the last washing step, the empty column was centrifuged (2 min, 13000× g, room temperature, "Heraeus Pico 17", rotor Ch.500005 PP) and the column was placed in a fresh 1.5 ml tube. 30 µl of Elution Buffer (10 mM Tris-HCl, pH 8.5) was added to the column and incubated for 2 min at room temperature. Finally the column was centrifuged to elute the DNA (1 min, 13000× g, room temperature, "Heraeus Pico 17", rotor Ch.500005 PP). The eluted DNA was stored at -20°C.

2.3.2 Estimation of DNA concentration

A. Concentration via OD measurement

The DNA concentration was measured spectrophotometrically at a wavelength of λ = 260 nm against water (UV-Visible spectrophotometer "Evolution 201"). Assuming that 1 A_{260} U of dsDNA equals 0.05 µg/µl H_2O, the concentration of DNA was calculated using the following formula:

$$\mathcal{C}_{\mathrm{DNA}}\,[\mu\mathrm{g}/\mu\mathrm{l}] = A_{260} \times 0.05 \times \mathrm{DF}, \tag{2.1}$$

where *DF* is the dilution factor. The purity of the isolated DNA was assessed by measuring the absorbance at a wavelength λ = 280 nm (maximum absorption of proteins) and determining the A_{260}/A_{280} ratio. The ratio of well-purified DNA should be $\geq$ 1.8.

B. Estimation the amount of DNA in agarose gels

In order to estimate the amount of DNA in agarose gels, 1 µl of DNA was mixed with 21 µl of 1× DNA sample buffer. 2 and 20 µl of diluted DNA and 100 ng of molecular weight size marker were separated on agarose gel. 2 µl of diluted DNA corresponded to the concentration in 0.1 µl, while 20 µl to the concentration in 1 µl. DNA concentration was estimated by comparing the analyzed bands with the molecular weight size marker.

2.3.3 Agarose gel electrophoresis

The required amount of agarose was mixed with 1× TAE buffer (for 1% agarose gel 1 g of agarose was mixed with 100 ml of 1× TAE buffer). The concentration of agarose gel depends on the size of DNA fragments. The mixture was heated in a microwave oven to melt the agarose, then ethidium bromide was added in order to reach a final concentration of 0.5 µg/ml. The gel was poured into a tray with a comb where it solidified. DNA samples were mixed with 5× DNA loading buffer. Samples and 100 ng of molecular weight size marker were loaded into the wells. Electrophoresis was performed in 1× TAE buffer at a voltage of 130 V for 30 min (minigel), 130 V for 40 min (midigel) or 15 V overnight (preparative gel). The electrophoretically separated DNA fragments were visualized by placing an agarose gel on UV light and photographed by the agarose gel documentation system "Gel Max".

2.3.4 The Polymerase Chain Reaction

Principle of the method

The Polymerase Chain Reaction (PCR) is a rapid method for the amplification of selected sequences of double-stranded DNA. PCR consists of three steps: denaturation of DNA (separation of two DNA strands), primer annealing to the target sequence and DNA synthesis (extension).

Course of the experiment

PCR was performed by making use of Phusion High Fidelity DNA Polymerase. Each reaction mixture contained 10 µl of 5× Phusion HF Buffer, 1 µl of 10 mM dNTPs, 2.5 µl of 10 µM forward primer, 2.5 µl of 10 µM reverse primer, DNA template (10 ng of plasmid DNA or 150 ng of genomic DNA), 0.5 µl of Phusion DNA Polymerase. Finally water was added in order to obtain a total volume of 50 µl. Table 2.2 shows a typical cycling protocol for PCR.

2.3.5 Site-directed mutagenesis

Site-directed mutagenesis was performed by making use of *Pfu* DNA Polymerase. Each reaction mixture contained 50 ng of the plasmid targeted for mutagenesis, 125 ng of each primer, 10 mM dNTP, 2.5 U of *Pfu* DNA Polymerase and 5 µl of 10× reaction buffer. Finally water was added to obtain a total volume of 50 µl. Table 2.3 shows a cycling protocol for site-directed mutagenesis.

Following the cycling protocol, the mixture was placed on ice for 2 min to cool the reaction to $\leq$ 37°C. To digest the parental (i.e., the nonmutated) dsDNA, 1 µl of the restriction enzyme *Dpn*I (20 U/µl) was added to the reaction mixture and incubated at

Cycle step	Temperature [°C]	Time	Cycles
Initial denaturation	98	30 s	1
Denaturation	98	5 s	
Annealing	X	20 s	35
Extension	72	30 s/kb	
Final extension	72	10 min	1
	4	hold	

Table 2.2: Cycling protocol for PCR. Notice that if the primer is ≥20 nt the annealing temperature X equals T_m+3°C, if the primer is ≤20 nt the annealing temperature X equals to the lower T_m primer.

Cycle step	Temperature [°C]	Time	Cycles
Initial denaturation	95	30 s	1
Denaturation	95	30 s	
Annealing	55	60 s	12
Extension	68	1 min/kb	

Table 2.3: Cycling protocol for site-directed mutagenesis.

37°C for 1 hour. Following incubation, DH5α cells were transformed with the mutated plasmid.

2.3.6 Generating double-stranded oligonucleotides

Complementary oligonucleotides were mixed at 1:1 molar ratio in a test tube and diluted to a final concentration of 100 ng/µl in water. The annealing reaction was performed in a thermal cycler using the program listed in Table 2.4. Annealed oligonucleotides were used for cloning into pInducer10 system.

Cycle step	Temperature	Time	Cycles
Step 1	95°C	5 min	1
Step 2	95°C (−1°C/cycle)	1 min	70
Step 3	4°C	hold	1

Table 2.4: Protocol for double-stranded oligonucleotide generation

2.3.7 DNA digestion with restriction endonucleases

Digestion of both vectors and insert fragments was performed with several restriction enzymes, which were used according to the manufacturer's instructions. The reaction mixture contained 1/10 of the final volume of 10× supplied reaction buffer and 2 U of the appropriate enzyme per 1 µg of plasmid. Additives such as BSA were added when recommended by the manufacture. The mixture was filled up with water to the

required final volume. Digestion was performed for a few hours at the enzyme's optimum incubation temperature. Digested DNA fragments were separated on an agarose gel.

2.3.8 Ligation of DNA fragments

150 ng of vector were combined with a 5-fold molar excess of insert (cloning of cDNA) or 100-fold molar excess of oligonucleotides (shRNA cloning). The volume was adjusted to 8 µl with distilled water (dH_2O). 1 µl of 10× T4 DNA ligase buffer and 1 µl of T4 DNA ligase were added to the ligation mixture. The mixture was briefly centrifuged and incubated overnight at 4°C. After incubation 10 µl of dH_2O were added to the ligation mixture and dialyzed against water on 0.025 µm cellulose membrane filter for 1 h at room temperature. Electro- or chemically competent bacteria were transformed with 10 µl of ligation mixture.

2.3.9 DNA sequencing

DNA sequencing is the determination of the exact order of nucleotide sequence in a DNA molecule. The sequencing of constructs was carried out by the company Seqlab-Microsynth (Goettingen). For one sequencing reaction 1.2 µg of plasmid DNA were mixed with 3 µl of 50 pmol sequencing primer and filled up with water up to a final volume of 15 µl in a 1.5 ml tube. The sequenced DNA was compared with the original sequence using EMBOSS stretcher software.

2.3.10 The real-time polymerase chain reaction

Principle of the method

The real-time polymerase chain reaction (real-time PCR), also known as quantitative PCR (qPCR), is a method which enables amplification and monitoring of PCR products in real time. Complementary DNA transcribed from total RNA was analyzed using SYBR Green I fluorescent dye. After SYBR Green I binds to double-stranded DNA molecules, a fluorescent signal at 521 nm wavelength is emitted. The emitted fluorescence intensity, which is proportional to the amount of amplified PCR product, was measured during each cycle.

Course of the experiment

Primers for real-time PCR were designed using the Universal ProbeLibrary Assay Design Center (Roche). The Light cycler 96-well plate was loaded with 50 ng of cDNA, 5 µl of forward and reverse primer mix at 21.3 µM final concentration, 10 µl of 2× Light cycler®480 SYBR Green I master mix and filled with PCR-grade water to 20 µl of final volume. For standard curve preparation 0.15, 0.31, 0.62, 1.25 and 5 ng of cDNA were mixed with primer mix and master mix. The real-time PCR was performed on LightCycler® 480 II (Roche). Data were monitored and analyzed with LightCycler®480 1.5.0 software (Roche). Table 2.5 shows the cycling protocol for real-time PCR.

Cycle step	Temperature [°C]	Time	Cycles
Pre-incubation	95	7 min	1
Amplification	95	10 s	45
	60	10 s	
	72	10 s	
Melting curve	95	5 s	1
	65	1 min	
Cooling	40	30 s	1

Table 2.5: Cycling protocol for real-time PCR.

2.4 Working with proteins

2.4.1 Protein isolation from cell culture

Proteins were isolated from cells, which were grown on 60 mm dishes (approximately 80% confluency). The medium was aspirated and cells were washed twice with 1× ice-cold PBS. Then cells were collected by scraping, transferred to a 1.5 ml tube and centrifuged (5 min, 600× g , 4°C, "HITACHI himac CT15RE", rotor T15A61-1041). After centrifugation the supernatant was decanted and the cell pellet was resuspended in 50 µl of 1× protein lysis buffer and incubated on ice for 15 min. The lysate was then centrifuged (5 min, 14000 rpm, 4°C, "HITACHI himac CT15RE", rotor T15A61-1041) and the supernatant was collected in a fresh tube. The protein lysates were stored at -80°C.

2.4.2 Determination of protein concentration

Principle of the method

The Bradford protein assay is a spectroscopic method for the determination of protein concentrations. The method is based on the fact that the absorption maximum of Coomassie Brillant Blue-G250 shifts from 470 nm to 595 nm when bound to a protein. This absorption change is proportional to the protein concentration (Bradford, 1976).

Course of the experiment

In order to prepare a calibration curve 0 µg, 1 µg, 2.5 µg, 5 µg, 15 µg and 50 µg of BSA in 10 µl of water were diluted in 1 ml Roti-Quant solution in a plastic cuvette. 5 µl of protein lysate with unknown concentration were mixed with 1 ml of Roti-Quant solution in a plastic cuvette. Next samples and standards were incubated for 5 min at room temperature and the absorbance ratio at 590 nm to 450 nm was measured against water. Unknown sample concentrations were calculated from the standard curve.

2.4.3 Sodium dodecyl sulfate polyacrylamide gel electrophoresis (SDS-PAGE)

Principle of the method

SDS is an anionic detergent which unfolds polypeptide chains and strongly binds to them by interacting with polar and non-polar amino acids. Since proteins bind SDS they have a negative charge and migrate in an electric field through the gel towards the anode. Using SDS-PAGE technique proteins are separated primarily by size.

Course of the experiment

In this work the vertical mini-PROTEAN II Electrophoresis Cell SDS-polyacrylamide gel electrophoresis system was used. Depending on the molecular mass of the studied proteins 10, 12 or 15% polyacrylamide gels were used. The resolving gel was poured into the apparatus and covered with a thin 100% isopropanol layer in order to achieve a resolving gel surface as uniform as possible. After the resolving gel was polymerized, isopropanol was removed and the stacking gel was poured onto the separating gel and a comb was inserted in the stacking gel. Finally, the gel was placed into the gel chamber and filled with 1× running buffer. Samples were mixed with 5× Laemmli sample buffer and heated to 100°C for 5 min. For the experiments 10-30 µg of proteins per lane were separated. To estimate the protein size, 1-3 µl of prestained protein size marker was used. While running in the stacking gel, a voltage of 100 V was applied and then the voltage was increased to 150-200 V. The gel was either stained with amido black or proteins were transferred to a polyvinylidene difluoride (PVDF) membrane and Western blot was performed.

Separation range [kDa]	Acrylamide concentration [%]
20-100	10
10-70	12
8-50	15

Table 2.6: Polyacrylamide gel resolution as a function of the concentration of polyacrylamide in SDS-PAGE

2.4.4 Protein detection

A. Amido black staining

After protein separation the gel was stained with 1× amido black staining solution for 10 min. The gel was then destained twice with 1× amido black destaining solution for 30 min before overnight incubation with destaining solution. Photographs of the gels were saved for documentation.

B. Western Blot

After being separated on a polyacrylamide gel proteins were transferred to a 0.45 µm PVDF membrane using the semi-dry blotting technique. Transfer was performed for

1 h at 22 V using the Trans-Blot SD Semi-Dry ElectrophoreticTransfer Cell. First, the membrane was soaked with 100% methanol for 1 min and then in transfer buffer for 5 min. Gel and Whatman 3MM papers were soaked in transfer buffer as well. Then, on the anode plate of the semi-dry blotting apparatus three Whatman Papers, the PVDF membrane, the separating gel and another three Whatman Papers were arranged on top of each other. Finally, the gel/blotting paper/filter paper sandwich was covered with the cathode plate. After transfer, the membrane was placed in the blocking solution for 30 min at room temperature on a rotating platform shaker "Duomax 1030". All other steps were performed on a rotating platform as well in order to assure equal distribution of solutions on the membrane. After blocking, the blot was incubated with the diluted primary antibody at 4°C overnight. Primary and secondary antibodies were diluted in blocking buffer. On the next day the membrane was washed 2× 5 minutes and 2× 10 minutes with PBST. Then diluted HRP-conjugated secondary antibody was added and the incubation was continued for 1 h at room temperature. Finally, the membrane was washed 5× 5 min with PBST and 1× 5 min with PBS. The measurement of chemiluminescence was performed using the Western Lightning Chemoluminiscence Reagent from Perkin Elmer. The membrane was incubated with pre-mixed 1:1 luminol and oxidation reagents for 1 min and the excess of reagents was removed on a Kimtech tissue. The signal from the membrane was collected with the chemiluminiscence system "Fusion Fx7". Densitometric data analysis was performed on Bio1D software.

2.4.5 Affinity purification of His-tag fusion proteins

Principle of the method

In this work six histidines (His-Tag) were fused to the proteins of interest at the carboxy-terminus. The expression of recombinant proteins was induced by IPTG in different strains of *Escherichia coli*. Histidines have affinity to immobilized Ni^{2+} ions. Fusion proteins were purified on the Ni^{2+}-charged His-Bind resins.

Course of the experiment

a) Induction of protein expression and purification

The small-scale bacterial culture was grown overnight at 37°C in LB medium with an appropriate antibiotic. On the next day a large-scale culture was inoculated and grown at 37°C until the OD_{550} reached 0.5. Bacteria were then induced with 1 mM IPTG for the appropriate time and temperature. A 1 ml of aliquot was taken before and after induction, centrifuged for 1 min at maximum speed and resuspended in 1× SDS-sample buffer in a volume of 200 µl of SDS-sample buffer per 1 OD_{550} and boiled for 5 min. 20 µl of induced and non-induced bacterial lysate were separated on a polyacrylamide gel. After induction, bacteria were harvested and resuspended in 2 ml per 100 OD_{550} of 1× binding buffer/0.1% Triton X-100. Bacteria were sonicated 5-6 times (1× 30 s) using "Vibra-Cell" ultrasonic processor with a 30 s interval. Then bacteria were centrifuged (10 min, 10000× g, 4°C, "Avanti J-26 XP", rotor Ja-10). The pellet was washed three times with 1× binding buffer/0.1% Triton X-100. Afterwards the pellet was resuspended in 1 ml per 100 OD_{550} of 1× binding buffer/0.1% Triton X-100/6 M urea and rotated overnight at 4°C on rotating wheel. The lysate was then centrifuged (30 min, 12000 rpm, 4°C, "Avanti J-26 XP", rotor Ja-10). The supernatant containing the protein of interest was

purified with His-Bind resin. After protein binding, the column was washed with 10 bed volumes of 1× binding buffer/0.1% Triton X-100/6 M urea. The protein was eluted with 0.5 bed volume of 1× elute buffer/0.1% Triton X-100/6 M urea. 3-4 protein fractions were collected. The protein concentration was determined using Bradford protein assay. The proteins were finally separated on a SDS-PAGE gel.

b) Column preparation and regeneration

The column was washed with 3 bed volumes of H_2O, 5 bed volumes of 1× charge buffer, 3 bed volumes of 1× binding buffer/0.1% Triton X-100/6 M urea. After protein elution, the column was washed with 5 bed volumes of H_2O, 3 bed volumes of 1× strip buffer. The column was stored in 1× strip buffer at 4°C.

2.4.6 Generation of antisera

Purified recombinant proteins for the generation of polyclonal antibodies were dialyzed against 1× PBS. Approximately 6 mg of proteins were sent to Davids Biotechnologie GmbH (Regensburg) where rabbits were immunized with each protein 5 times with 2 weeks interval between immunizations (total time of immunization protocol is 63 days). On the day of immunization, 1 ml of serum was collected (preimmune serum). On the 63rd day, 40-90 ml of antisera were collected from rabbits.

2.4.7 Coupling of proteins to cyanogen bromide-activated sepharose beads

Principle of the method

In the reaction of cyanogen bromide (CNBr) with hydroxyl groups on agarose beads cyanate esters and imidocarbonates are formed. These groups react with amino-group of proteins allowing the protein coupling to the beads. Recombinant Crct1, Abra and Arl4c were coupled to cyanogen bromide-activated beads in order to affinity-purify rabbit antisera.

Course of the experiment

Recombinant proteins were dialyzed at 4°C against 3× 100 volumes of coupling buffer. 5 to 10 mg of proteins were used per 1 ml of bed volume of beads. CNBr-Sepharose beads were swollen in 10 ml of cold 1 mM HCl for 30 min at room temperature. Then beads were washed 6 times with 10 ml of 1 mM HCl and with 2 ml coupling buffer. Proteins were then immediately combined with activated sepharose beads and incubated overnight at 4°C under constant agitation on the rotating wheel. On the next day, the flow-through was collected in order to determine the coupling efficiency. Beads were washed with 10 ml of coupling buffer. Remaining active groups were blocked by incubating them 2 hours at room temperature with 5 ml of 0.2 M glycine pH 8.0. The column was washed first with 10 ml of wash buffer 1 and then with 10 ml of wash buffer 2. The two washing steps were repeated twice. The column was then washed with 10 ml of coupling buffer and finally with 10 ml of 1× PBS. Ready-to-use column was either used for affinity purification of antibodies or stored at 4°C in 1× PBS/0.04% thimerosal.

2.4.8 Affinity purification of antibodies

The column with CNBr-coupled recombinant protein was washed with 10 bed volumes of 1× PBS. Beads were subsequently resuspended in antibody solution and incubated overnight under constant agitation at 4°C on a rotating wheel. The next morning beads were washed with buffer A, buffer B, buffer C and buffer A (10 bed volumes each). Antibodies were eluted with 1 bed volume of 0.2 M glycine HCl pH 2.0/0.2 M NaCl. Three fractions were collected and immediately neutralized with 0.2 bed volumes of 1 M Tris pH 8.8. Purified antibodies were stored at -20°C with 0.04% thimerosal. After antibody purification the column was washed with 20 bed volumes of 1× PBS. The column was stored at 4°C in 1× PBS/0.04% thimerosal.

2.4.9 G-actin / F-actin ratio determination

Principle of the method

There are two forms of actin – filamentous (F-actin) and globular (G-actin) actin. In the first step of the assay cells are lysed with G-actin buffer, which solubilizes G-actin, but not F-actin. During the following centrifugation step, G-actin remains in the supernatant and F-actin in the pellet. After washing the pellet with G-actin buffer, the pellet is resuspended in protein lysis buffer. A final centrifugation step leaves F-actin in the supernatant.

Course of the experiment

The day before the experiment 0.4×10^6 cells were plated into a 35-mm dish. On the next day the cells were washed twice with ice-cold 1× PBS and collected by scraping into a 1.5-ml tube. Cells were centrifuged (5 min, 1000× g, 4°C, "HITACHI himac CT15RE", rotor T15A61-1041). The cell pellet was resuspended in 100 µl of ice-cold G-actin buffer and left on ice for 5 min. Afterwards the cell suspension was centrifuged (10 min, 16000× g, 4°C, "HITACHI himac CT15RE", rotor T15A61-1041). The supernatant containing the G-actin fraction was transferred into a fresh 1.5 ml tube. The pellet was washed once with G-actin buffer, resuspended in 100 µl of protein lysis buffer and left on ice for 5 min. Insoluble material was removed by centrifugation (10 min, 16000× g, 4°C, "HITACHI himac CT15RE", rotor T15A61-1041) and the supernatant containing the F-actin fraction was transferred into a fresh 1.5 ml tube. For Western blot analysis 20 µl of F- and G-actin were separated on a polyacrylamide gel.

2.5 Working with mammalian cells

2.5.1 Mammalian cell culture

Work with mammalian cells was performed under sterile conditions in a laminar flow bench "Lamin Air HA 2448 GS". In order to prevent bacterial or fungal contaminations all used materials were either sterile packed or autoclaved before use at 121°C. Cell lines used in this work and complete growth medium are listed in Table 2.7.

Cell name	Medium	Additives
COS-7	DMEM	10% FCS
HEK293T	DMEM	10% FCS
Human podocyte cell line	RPMI 1640	10% FCS
HtTA-1/LMX1B	DMEM	10% FCS
		30 ng/ml doxycycline
		300 µg/ml hygromycin B
		200 µg/ml geneticin
Mouse podocyte cell line	RPMI 1640	10% FCS
Primary podocytes	DMEM/F-12	10% FCS
		100 U/ml penicillin
		100 µg/ml streptomycin
		1× insulin/transferrin/selenium

Table 2.7: Cell lines and growth medium

A. Subculturing

Cell cultures were maintained in a CO_2-incubator at 95% relative humidity. HEK293T, COS-7, HtTA-1/LMX1B and primary podocytes isolated from mice were grown at 37°C, while mouse and human podocyte cell lines were grown at 33°C. The human and murine podocyte cell lines contain a temperature-sensitive promoter which allows cells to proliferate at 33°C and differentiate at 37°C (Saleem et al., 2002). The growth medium for each cell line was changed every 2 or 3 days. Cells were grown until 80-90% of confluence. Before splitting, the medium was aspirated and cells were washed once with 1× PBS. Trypsin was then added (e.g. 2 ml per 75 cm^2 flask) and cells were incubated for 5 min at 33°C or 37°C. Then complete growth medium was added and the appropriate volume of cells was transferred to a fresh flask filled with complete growth medium. Growth medium, 1× PBS and 1× trypsin were stored at 4°C. Before subculturing they were warmed to a room temperature. Antibiotics were added to the medium directly before use.

B. Freezing cells

Cells were grown in a 75 cm^2 flask until 90% confluence. The medium was then aspirated from the cells and cells were washed once with 1× PBS. 2 ml of trypsin were added and the cells were incubated 5 min at 37°C. 10 ml of growth medium were added and cells were centrifuged (5 min, 100× g, 4°C, "Multifuge 3 L-R", rotor Ch.2425). The medium was aspirated and the cell pellet was resuspended in 3 ml of freezing medium and separated into 3 cryovials. Cells were kept at -80°C overnight and then stored in liquid nitrogen.

C. Thawing cells

The cryovials were removed from liquid nitrogen and thawed at room temperature. The fresh medium was added to the vial and cells were transferred drop-wise to a 15 ml tube containing 10 ml of medium. Afterwards cells were centrifuged (5 min, 160× g, 4°C, "Multifuge 3 L-R", rotor Ch.2425). The medium containing DMSO was aspirated and

cells were resuspended carefully with 5 ml of complete growth medium and placed in a 25 cm^2 flask.

D. Cell counting with Neubauer Chamber

Ten µl of a cell suspension was applied to a Neubauer Chamber for cell counting. Cells were counted in the big squares. Because the surface area of a big square is 0.01 cm^2 and the depth of the chamber is 0.01 cm, the cell chamber volume equals 0.000,1 ml. The cell concentration is $C = N/V = N \times 10,000$ cells/ml, where N is the number of cells counted in a big square and V is the volume of the chamber.

2.5.2 Expression of proteins in mammalian cells

A. Transient transfection of COS-7 cells

Principle of the method

In this work COS-7 cells were transiently transfected with DEAE-dextran/chloroquine. The DEAE-dextran is a positively charged molecule which binds the negatively charged DNA. After binding the complex is able to cross the negatively charged cell membrane. The chloroquine reduces lysosomal degradation of DNA. The DMSO shock results in an increase of the transfection efficiency.

Course of the experiment

The day before the transfection 4.2×10^5 COS-7 cells were plated into a 60-mm dish. The next day cells were approximately 50% confluent. Immediately before transfection 200 µl of the DEAE-dextran/chloroquine solution and 20 µg of recombinant DNA were added to 5 ml of DMEM/10% FCS and mixed. The medium was removed from the cells and the DNA/DEAE-dextran/chloroquine solution was added. After 4 h of incubation, the medium was removed and 3 ml of 10% DMSO/1× PBS were added. The cells were incubated for 2 min at room temperature. Then the DMSO was removed and the cells were washed once with 1× PBS. Fresh DMEM/10% FCS was added and the cells were incubated for 48 h. Subsequently the proteins were isolated and used for Western blot (e.g. during antibody titration).

B. Transient transfection of HtTA-1/LMX1B, human and mouse podocyte cell lines with polyethylenimine

Principle of the method

Polyethylenimine (PEI) is a polymer which is used for transfection of mammalian cell lines. PEI is able to package the negatively charged DNA molecules into positively charged particles which can enter the anionic cell membrane.

Course of the experiment

The cells were plated on the required plate or dish the day before transfection. The appropriate amount of DNA was diluted in the medium without FCS and polyethylenimine was added. The transfection mixture was vortexed, shortly centrifuged and incubated for 20 min at room temperature. During incubation the complete medium from the cells

was changed to a FCS-free medium. The transfection mixture was added to the cells drop-wise and cells were incubated for 6 h. After incubation the medium was changed to complete medium and cells were incubated for 24 to 48 h. Number of the cells (N_{cells}), amount of DNA (m_{DNA}) and volume of PEI reagent (V_{PEI}) are listed in Table 2.8.

Culture vessel	N_{cells}	m_{DNA} [µg]	V_{PEI} [µl]
24-well plate	2×10^4	1	3
6-well plate	1×10^5	1-3	3
35-mm dish	1×10^5	1-3	3

Table 2.8: Transfection complex preparation for different cell culture formats

C. Transient transfection of primary podocytes

The day before transfection 2×10^4 primary podocytes were plated into a 24-well plate with a 10-mm coverslip. The cells were then transfected with 1 µg of plasmid and 2 µl Lipofectamine 2000 in a total volume of 100 µl. After 4 h of incubation the medium containing the transfection mixture was removed, and fresh medium was added. The cells were incubated for another 48 h.

2.5.3 Induction of HtTA-1/LMX1B

The tet-off human HeLa cell line HtTA-1 expressing the human LMX1B protein was grown in DMEM containing 10% FCS, 200 µg/ml geneticin, 30 ng/ml doxycycline and 300 µg/ml hygromycin B. For the induction of LMX1B expression the cells were incubated in doxycycline-free medium for a minimum of 4 days.

2.5.4 Generation of stable cell lines

Lentivirus production

The day before the lentivirus production 8×10^6 HEK293T cells were seeded into a 15 cm plate in 25 ml DMEM/10% FCS. On the next day the medium was substituted with 20 ml of FCS-free DMEM. 15 µg of pLVPT-rtTR-KRAB-2SM2 containing the cDNA of interest, 3.75 µg of VSV-G envelope expressing plasmid pMD2.G, 11.25 µg of the packaging plasmid pCMVΔR8.2 were mixed in DMEM to a final volume of 1,380 µl. Then 120 µl of PEI (1 µg/µl) was added to the mixture and incubated for 10 min at room temperature. Afterwards the mixture was added drop-wise to the cells, which were then incubated for 6 h at 37°C in a CO_2-incubator. After incubation the medium was substituted with 30 ml of complete DMEM medium and the cells were incubated for another 48 h. Then the medium was transferred to a 30 ml tube and centrifuged (10 min, 4°C, 6000× g, "Avanti J-26 XP", rotor Ja-25.50). The supenatant was transferred to a fresh tube and centrifuged (2 h, 4°C, 75600× g, "Avanti J-26 XP", rotor Ja-25.50). Then the supernatant was removed and the pellet was resuspended in 300 µl of DMEM/10% FCS. The pellet was incubated on ice. The next day 100 µl aliquots were frozen at -80°C.

Virus titer estimation by flow cytometry

Coding sequences of Crct1, Abra or Arl4c were cloned into pLVPT-rtTR-KRAB-2SM2. The virus titer was determined by counting the percentage of GFP-positive cells by flow cytometry. 1×10^5 of the mouse podocyte cell line per well were plated into a 24-well plate using RPMI/10% FCS medium. After attachment of the cells to the plate (4 h after plating) 1 µl of polybrene (8 µg/ml) and 50 µl and 10 µl of undiluted virus and 10 µl of 1:10 diluted virus were added to the cells. The next day the medium was changed to fresh medium and cells were incubated for another 48 h in a CO_2-incubator. After incubation the cells were trypsinized, washed in 1× PBS and finally resuspended in 1 ml of 1× PBS for flow cytometry analysis. Flow cytometry was performed at the Department of Genetics (Prof. Dr. Frank Sprenger, University of Regensburg) on CyFlow Space flow cytometry system. 100,000 events were collected with Flow Max Software. Data were analyzed with Flowing Software. Virus concentration was calculated from multiplicity of infection (MOI) equation 2.2:

$$MOI = -\ln(1-a) = \frac{N_v}{N_c} \tag{2.2}$$

where a is the GFP positive fraction, N_v – number of viral particles and N_c – number of cells.

Transduction of target cells

On the day of transduction the cells were plated at the desired density. Four hours after plating viral particles at a MOI of 7 and polybrene at final concentration of 8 µg/ml were added to the cells. The cells were incubated overnight and on the next day the medium was replaced by fresh culture medium. The cells were incubated for another 2 to 4 days.

2.5.5 Measuring promoter activity by luciferase assay

HtTA-1/LMX1B cells were induced for LMX1B expression. On the 3rd day of induction 10^5 cells were plated into a 24-well plate. The next day cells were transfected with 0.5 µg of *Firefly*-luciferase reporter vectors pGL3-Enhancer containing promoter fragments of Abra. 24 h after transfection the growth medium was removed from the cells. Then the cells were washed twice with 1× PBS and lysed with 200 µl of 1% Triton X-100/1× PBS for 15 min. The cells were then collected and centrifuged (5 min, 15000 rpm, 4°C, "HITACHI himac CT15RE", rotor T15A61-1041). The supernatant was transferred to a fresh 1.5 ml tube. Cell lysates were stored at -80°C.

Measurement of luciferase activity

Measurement of luciferase activity was performed on the microplate luminometer "Microlumat Plus LB86V µp-version 2.0". 20 µl of lysate was transferred to 96-well white polystyrene plate. Measurements were performed automatically by addition of 100 µl of Luciferase Assay Reagent I. The obtained data were normalized to the protein amount.

2.5.6 Immunofluorescence staining

Cells for immunofluorescence staining were grown on a 10 mm glass coverslip in a 24-well plate. On the day the staining the cells were washed twice with ice cold 1× PBS and

then fixed with 4% paraformaldehyde/1× PBS pH 7.4 for 20 min at room temperature. Afterwards the cells were washed twice with ice cold 1× PBS and permeabilized and blocked with 0.2% Triton X-100/2% BSA/1× PBS. The cells were incubated with the primary antibody diluted in 1× PBS/2% BSA overnight at 4°C. On the next day the cells were washed three times with 1× PBS and incubated with the secondary antibody diluted in 1× PBS/2% BSA for 1 h at room temperature in the dark. The cells were then washed three times with 1× PBS. The coverslip was mounted with a drop of mounting solution on a microscope slide and covered with a cover slip. Specimens were stored in the dark at 4°C.

2.5.7 Transmission electron microscopy studies

Photoconversion

10^5 conditionally immortalized human podocytes were plated into a 35 mm glass bottom culture dish (MatTek Corporation). The next morning cells were transfected with 1 μg of pminiSOG-C1/mCherry encoding Abra, Arl4c and Crct1. 48 h after transfection the cells were washed with 1× PBS and fixed with 2% glutaraldehyde in 0.1 M sodium cacodylate buffer, pH 7.4 for 5 min at room temperature, and then incubated for 15 min on ice. All of the next steps were performed on ice. Cells were washed twice with 0.1 M sodium cacodylate buffer. Then the cells were incubated with blocking buffer (50 mM glycine, 10 mM KCN, 10 mM aminotriazole, 0.002% hydrogen peroxide in 0.1 M sodium cacodylate buffer) for 45 min. In the next step the cells were washed with 0.1 M sodium cacodylate buffer. Diaminobenzidine tetrahydrochloride (DAB) was freshly diluted to 1 mg/ml in 0.1 M sodium cacodylate buffer, pH 7.4 and filtered through a 0.22 μm filter. For photooxidation DAB solution was added to the cells placed on ice. Cells transfected with pminiSOG-C1/mCherry were identified in the fluorescence microscope. A stream of oxygen was continuously administered over the top the culture dish. The samples were then illuminated by an intense light from a HBO 103W/2 mercury lamp for 10 min, using a standard fluorescein isothiocyanate (FITC) filter.

Cell fixation for transmission electron microscopy

All the steps described in this paragraph were performed on ice. After photoconversion, cells were removed from the microscope and washed five times with 0.1 M sodium cacodylate buffer (each time 1 min). Then the cells were post-fixed with 1% OsO_4 for 30 min, washed three times with 0.1 M sodium cacodylate buffer and left overnight in 0.1 M sodium cacodylate buffer. The next morning the cells were washed three times with distilled water (each time 1 min). Then the cells were stained with 2% uranyl acetate for 30 min and washed five times with distilled water. Finally the cells were dehydrated in an ethanol gradient: 20% (2 min), 50% (2 min), 70% (2× 2 min), 90% (2× 2 min), 100% (2 min) of ethanol on ice and finally 100% ethanol (2× 2 min) at room temperature. The glass coverslip was separated from culture dish, washed twice with pure acetone (2 min). In the last step the glass coverslip was embedded with 100% epoxy resin (epon) and polymerized in an oven at 30°C for three days and then at 60°C for another 2 days. After embedding the glass coverslip was removed and the plastic block was cut into thin sections by a diamond knife in the ultramicrotome "Ultracut E". Each section was 70 nm thick. The electron microscopic pictures were taken in the transmission electron microscope "EM Zeiss 902".

2.5.8 Fluorescence recovery after photobleaching

Principle of the method

The turnover rate of proteins involved in the regulation of the actin cytoskeleton was analyzed by Fluorescence Recovery After Photobleaching (FRAP). The proteins under investigation were fused to fluorescent tags such as GFP, Emerald or mCherry. Using a strong excitation laser, the fluorescence of a tagged protein was bleached in the region of interest (ROI). The fluorescence recovers when unbleached fluorescently-tagged proteins from outside of the bleached region enter the ROI.

Course of the experiment

FRAP studies were performed on induced and non-induced HtTA-1/LMX1B cells and on primary podocytes. On the 4th day after induction 10^5 HtTA-1/LMX1B cells and 2×10^4 primary podocytes were plated into a 6-well plate with a 22 mm glass coverslip. On the next day cells were transfected with 1 µg of expression plasmids. On the subsequent day the cells were washed twice with 1× PBS and measurements were performed in Ca^{2+}-buffer at 37°C. The fluorescence intensity of a region of interest (ROI) was monitored, then the ROI was bleached and recovery of fluorescence over time was tracked. Pictures were taken every 0.369 s. Every FRAP curve was normalized by setting the pre-bleach intensity to 1. Approximately 60 curves were averaged and fitted using the function:

$$y(t) = A(1 - e^{-\frac{t}{\tau}}), \tag{2.3}$$

where A is the final value of the recovered fluorescence intensity, the time constant τ is the fitting parameter and t is the time after bleaching. The recovery half-time $t_{1/2}$ was obtained from τ by using the equation 2.4:

$$t_{1/2} = \tau \ln 0.5 \tag{2.4}$$

2.6 Working with kidneys

2.6.1 Isolation of primary podocytes

After anesthetization of mice, the abdominal cavity and thorax were opened. A syringe with 40 ml of magnetic bead suspension at a concentration of 2×10^6 beads/ml was inserted into the left ventricle, the abdominal aorta was cut open below the renal arteries, and the suspension was administered at a constant pressure of 60 mm Hg. The kidneys were isolated, decapsulated and cut into small pieces which were digested with 1 mg/ml collagenase A for 30 min at 37°C. Digested kidney pieces were pushed through a 500 µm cell strainer and the filtrate was washed extensively with 1× PBS using a magnet. Finally, isolated glomeruli were plated in a cell culture flask containing complete growth medium for primary podocytes.

2.6.2 Immunofluorescence

A. Immunofluorescence of frozen kidney sections

Kidney tissue in Tissue-Tek O.C.T. embedding compound was cut to 7 µm thick sections using the cryostat “Leica CM3050s”. Sections were mounted on SuperFrost Plus

microscope slides and dried at room temperature for 30 min. Slides were stored at -80°C. Before proceeding sections were washed three times with 1× PBS and then blocked with 10% horse serum/1% BSA/1× PBS for 30 min. The primary antibody was diluted in 10% horse serum/1% BSA/1× PBS, added to the sections and incubated overnight at 4°C. The next morning sections were washed three times 15 min with 1% BSA/1× PBS. The secondary antibody was diluted in 1% BSA/1× PBS applied to the section and incubated for 90 min at room temperature. Finally, sections were washed three times with 1× PBS (15 min each washing), mounted in Mowiol and covered with a 22 mm cover slip.

B. Immunofluorescence of paraffin-embedded kidneys

Kidney tissue embedded in paraffin was cut on the microtome "Leica RM2255" at a thickness of 7 µm and mounted onto microscope slides. The sections were dried at 37°C for 2 days and then stored at room temperature. Kidney sections were deparaffinized and rehydrated using the protocol presented in Table 2.9. As a next step the heat-mediated epitope retrieval protocol was performed. Kidney sections were placed in 10 mM trisodium citrate (dihydrate) buffer, pH 6.0 and autoclaved (120°C). Subsequently sections were cooled to room temperature and the immunostaining was performed as described previously in 2.6.2, A.

Solution	**Time of incubation**
Xylene	10 min
Xylene (fresh)	10 min
100% isopropanol	2 min
100% isopropanol (fresh)	2 min
96% isopropanol	2 min
80% isopropanol	2 min
70% isopropanol	2 min
50% isopropanol	2 min
Distilled water	2 min

Table 2.9: Rehydration protocol

Chapter 3

Results

3.1 State of the art

3.1.1 Inducible podocyte-specific *Lmx1b* knock-out mice

In order to identify LMX1B-target genes studies were performed on inducible podocyte-specific *Lmx1b* knock-out mice. These triple-transgenic mice carry three constructs. Figure 3.1 (A, B) shows a schematic diagram of this knock-out mouse. The P2.5-rtTA cassette is only active in podocytes, it contains a reverse transcriptional transactivator (rtTA) under control of a 2.5 kbp *NPHS2* promoter fragment. Through the addition of doxycycline as a structural analog of tetracycline, rtTA activates the transcription of Cre recombinase, which is controlled by a specific Tet promoter. The expressed Cre recombinase finally mediates the deletion of a loxP-flanked segment of *Lmx1b* which encodes the homeodomain of *Lmx1b* (Gossen and Bujard, 1992).

3.1.2 Quadruple transgenic mice and "green podocytes"

The glomerulus contains three cell types: endothelial cells, mesangial cells, and podocytes. The separation of podocytes with from other cells of the glomerulus was achieved by crossing inducible podocyte-specific *Lmx1b* knock-out mice with a double-fluorescent Cre reporter mouse containing the mT/mG cassette (Boerries et al., 2013) (Muzumdar et al., 2007). Mice from this cross are called quadruple transgenic mice from here on. Figure 3.1 (C) shows Cre-mediated recombination of the mT/mG cassette. Podocytes from quadruple trangenic mice, where Cre recombination took place, express membrane-targeted enhanced green fluorescent protein (mG) – "green podocytes". On the other side, podocytes from quadruple transgenic mice without Cre recombination, endothelial and mesangial cells, express membrane-targeted tandem dimer Tomato (mT) – "red cells". The use of quadruple transgenic mice enabled to determine the filamentous actin content described in Subsections 3.3.2 and 3.3.4, as well as to perform FRAP measurements presented in Subsection 3.9.2, only in the recombined "green podocytes".

The presence of the loxP-flanked *Lmx1b* allele, the rtTA cassette, the Cre cassette and the mT/mG cassette were determined by PCR with primers presented in Subsection 2.1.8. Results from genotyping analysis are demonstrated in Figure 3.2.

Inducible podocyte-specific *Lmx1b* knock-out mice as well as quadriple transgenic animals are healthy and have a normal lifespan without induction of Cre-mediated inactivation of *Lmx1b* homeobox. Mice are viable up to two years. However, already after one

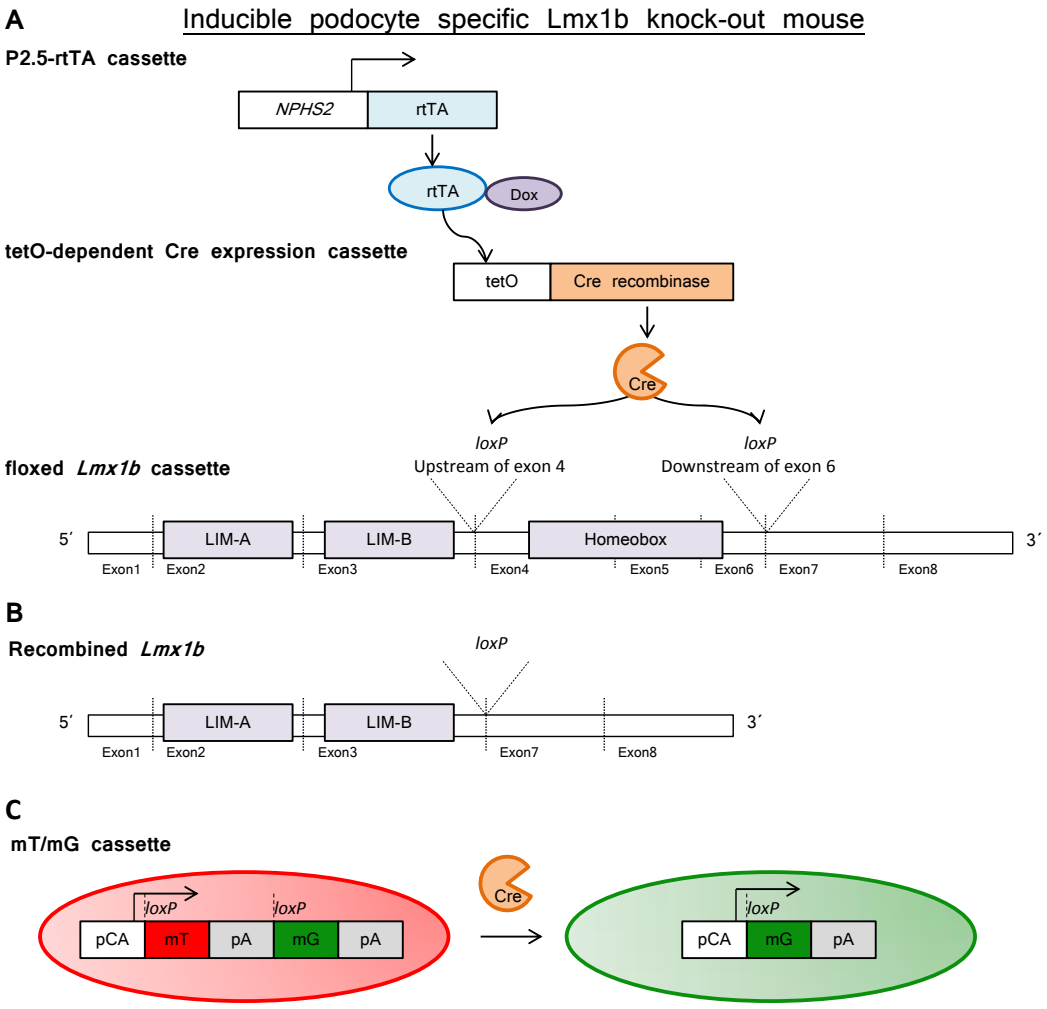

Figure 3.1: Generation of inducible podocyte-specific *Lmx1b* knock-out mice. (A) The *NPHS2*-regulated reverse transcriptional transactivator (rtTA) protein is expressed exclusively in podocytes. rtTA activates transcription of tetO-dependent Cre recombinase after doxycycline binding. Finally, Cre recombinase mediates the removal of the *loxP*-flanked homeobox of *Lmx1b*. (B) Scheme of the *Lmx1b* gene after recombination. (C) Before Cre-mediated recombination cells containing the mT/mG construct express membrane-targeted tandem dimer Tomato (mT). Membrane-targeted green fluorescent protein (mG) is expressed in the cells only after Cre recombination [modified from (Muzumdar et al., 2007)]. pA, *loxP*, and Cre stands for polyadenylation sequences, sequences recognized and excised by Cre recombinase, and Cre recombinase, respectively.

week of induction of *Lmx1b* inactivation mice develop proteinuria as shown in Figure 3.3.

3.1.3 Microarray studies of glomeruli isolated from inducible podocyte-specific *Lmx1b* knock-out mice

Fourteen-week-old female inducible podocyte-specific *Lmx1b* knock-out ($Lmx1b^{lox/lox}$, rtTA, Cre) and control ($Lmx1b^{lox/lox}$, rtTA) mice were administered 2 mg/ml of doxycycline for 0, 1, 3, 5 and 7 days (three animals per group). *In vivo* microarray stud-

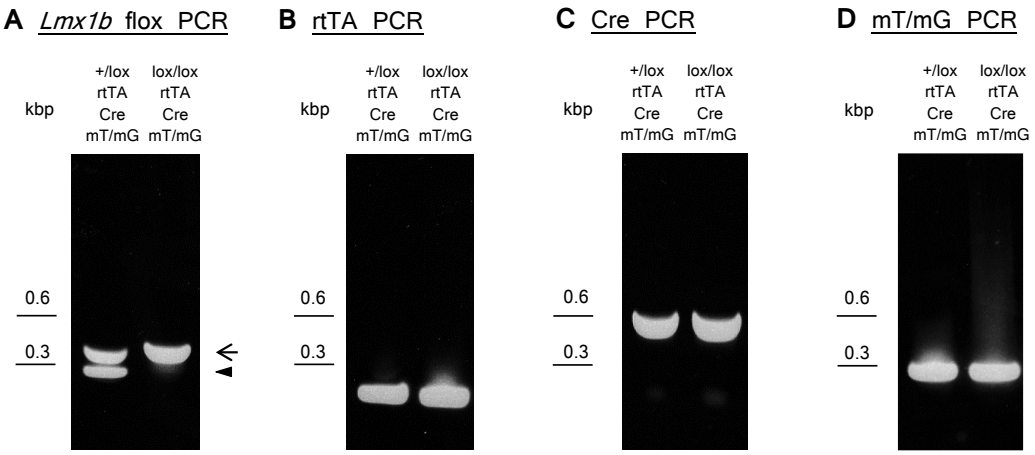

Figure 3.2: Results from genotyping of the quadriple transgenic heterozygous (*Lmx1b*$^{+/lox}$) control and homozygous (*Lmx1b*$^{lox/lox}$) *Lmx1b* knock-out mice. PCR analysis of total genomic DNA for the presence of (A) the loxP-flanked *Lmx1b* allele, (B) the rtTA cassette (188 bp), (C) the Cre cassette (613 bp) and (D) the mT/mG cassette (330 bp). The *Lmx1b* wild-type allele is indicated by an arrowhead (220 bp) and the floxed allele is indicated by an arrow (330 bp).

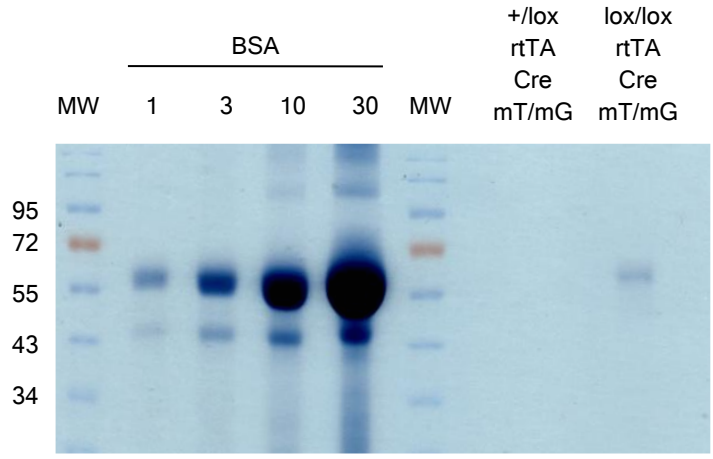

Figure 3.3: Inactivation of *Lmx1b* leads to albuminuria already after 1 week. 1, 3, 10, 30 µg of bovine serum albumin (BSA) and 0.2 µl of urine of both genotypes were separated on a 10% polyacrylamide gel and stained with amidoblack. Only homozygous *Lmx1b* mice developed proteinuria. MW stands for protein molecular weight marker in kDa.

ies of glomeruli isolated from *Lmx1b* knock-out mice have shown a significant increase of the mRNA levels of several genes in comparison to control mice (Burghardt et al., 2013). Due to their time-course of induction and their common physiological function three promising LMX1B target genes were chosen for further investigation. Two of them encode proteins associated with the actin cytoskeleton, they are Abra (Actin-binding Rho activating protein) and Arl4c (ADP-ribosylation factor-like 4C). The third candidate of the studies, which shows a characteristic time-course of its mRNA levels in the microarray, is Crct1 (Cysteine-rich C-terminal 1). Currently there is no biological information available regarding this gene, making it attractive as a research object. The

microarray data were confirmed by quantitative real-time PCR. Abra, Arl4c and Crct1 mRNA levels were increased in Cre-positive glomeruli compared with control Cre-negative glomeruli (Burghardt et al., 2013).

3.1.4 Stably transfected HeLa cell line synthesizing the human LMX1B in an inducible manner – HtTA-1/LMX1B cells

Part of the experiments presented in this thesis were performed on a stably transfected HeLa cell line synthesizing the human LMX1B protein in an inducible manner, called HtTA-1/LMX1B from here on. The cell line was obtained by the stable transfection of HtTA-1 cells with pUHD10-3/myc-LMX1B by Dr. Anne Rascle (Rascle et al., 2009). The expression of the human LMX1B cDNA is regulated by the tetracycline transactivator (tTA) consisting of the tet repressor (TetR) fused with the activating domain of virion protein 16 (VP16) of herpes simplex virus. There is no LMX1B expression in the cells growing in the medium containing doxycycline. On the other hand, in the doxycycline-free growth medium tTA binds to seven tet-operator domains (tetO7) and the expression of LMX1B in the cells is activated (Kohan, 2008). Figure 3.4 shows the schematic diagram of induction of the HtTA-1/LMX1B cell line and the Western blot analysis of protein lysates from HeLa cells which were grown in the presence or absence of doxycycline in the growth medium.

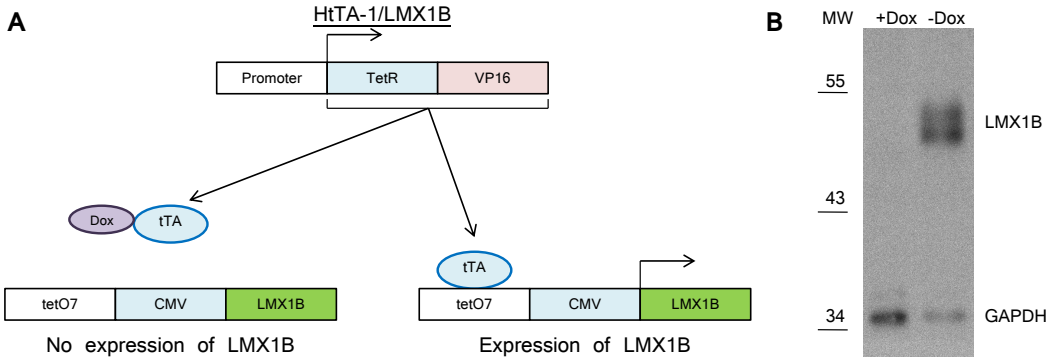

Figure 3.4: Induction of the HtTA-1/LMX1B cell line. (A) Scheme of the tet-off system [modified from (Kohan, 2008)]. The tetracycline-controlled transactivator (tTA) consists of the tet repressor fused with the activating domain of virion protein 26 (VP16) of herpes simplex virus. It is able to bind to seven copies of the tet operator thereby initiating transciption of a cDNA of interest. On the other side, doxycycline blocks the binding of tTA to the tet operator and transcription is stopped. (B) Protein lysates collected from HtTA-1/LMX1B cells grown for 4 days in the presence ("+ Dox") or in the absence ("- Dox") of doxycycline were separated on a 10% polyacrylamide gel. Subsequently, Western blot analysis was performed with antibodies directed against human LMX1B. GAPDH was used as a loading control. MW stands for protein molecular weight marker in kDa.

3.1.5 Promoter binding studies of the putative LMX1B target genes

The binding of LMX1B to its target genes is mediated by the central homeodomain which specifically recognizes the so-called FLAT (FAR-linked AT-rich) elements. These

elements were characterized for the first time in the promoter sequence of the rat insulin I gene (German et al., 1992). FLAT elements can be subdivided into two versions: FLAT-E (5'-TAATTA-3') and FLAT-F (5'-TTAATA-3')(Figure 3.5).

Functional studies using chromatin immunoprecipitation and luciferase reporter assay revealed that LMX1B regulates the expression of NF-κB target genes, such as IL-6 and IL-8 by binding to the FLAT-F elements within the proximal promoter of these genes in HeLa cells (Rascle et al., 2009).

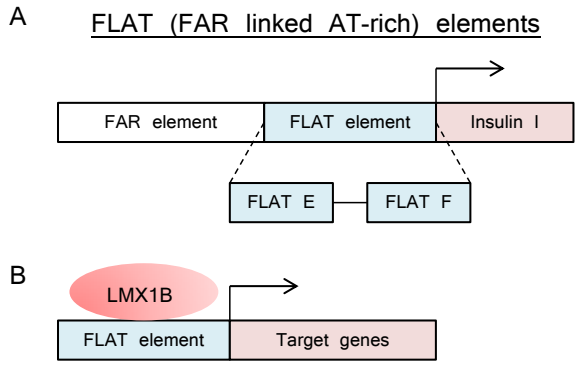

Figure 3.5: (A) Promoter structure of the rat insulin I gene with the Far and FLAT elements [modified from (German et al., 1992)]. FLAT elements can be subdivided into two versions: FLAT-E (5'-TAATTA-3') and FLAT-F (5'-TTAATA-3'). (B) Scheme of the transcriptional regulation of LMX1B target genes through binding of LMX1B to the FLAT elements in the promoter region of its target genes.

To demonstrate that the observed changes in the mRNA levels of Abra, Arl4c and Crct1 in the inducible podocyte-specific *Lmx1b* knock-out mice were caused by direct LMX1B binding to the FLAT elements within the promoter regions of these genes, bioinformatical studies were initiated. Human and murine promoter regions were screened for the presence of FLAT elements because it was planned to perform functional studies first in the HtTA-1/LMX1B cell line and then in the podocyte-specific *Lmx1b* knock-out mice. However, finally studies were performed only in HtTA-1/LMX1B cells, because chromatin immunoprecipitation assays were not sensitive enough to show Lmx1b promoter binding in primary podocytes (Burghardt et al., 2013). 6,000 bp upstream of the transcriptional start site were analyzed for the presence of FLAT elements by the UCSC genome browser and NCBI. The results of the bioinformatical studies are presented in Table 3.1.

Dr. Tillmann Burghardt analyzed FLAT elements within the promoter regions by applying chromatin immonoprecipitation (ChIP) and electrophoretic mobility shift (EMSA) assays in HtTA-1/LMX1B cells. He demonstrated that LMX1B binds to FLAT elements located at positions -2,731 and -2,303 within the human ABRA promoter and to a FLAT element located at position -5,417 of the human ARL4C promoter. These data were confirmed in a human podocyte cell line transiently transfected with an expression plasmid for the human LMX1B protein (Burghardt et al., 2013).

Abra				Arl4c				Crct1			
human		mouse		human		mouse		human		mouse	
F	E	F	E	F	E	F	E	F	E	F	E
-275	-372	-401	-2,431	-2,678	-2,568	-1,502	-3,309	-1,469		-3,529	
-682	-636	-619	-4,378	-2,688	-3,030	-2,515	-3,610	-1,507		-5,156	
-1,694	-1,874	-646	-4,471	-4,616	-5,241	-4,633	-5,207	-3,865			
-2,303	-2,411	-652		-5,074	-5,417	-4,982	-5,476	-5,136			
-2,731		-1,445		-5,576		-5,189					
-4,771		-1,885									
-5,164		-3,057									
		-3,113									
		-4,369									
		-5,371									

Table 3.1: Identification of FLAT elements within the human and murine Abra, Arl4c and Crct1 promoter fragments. F stands for FLAT-F and E for FLAT-E elements.

3.2 Functional analysis of the putative LMX1B target genes

3.2.1 Optimization of the luciferase assay for promoter studies

To determine the consequence of LMX1B binding to the promoter fragments of its putative target genes, these fragments were isolated from human genomic DNA and cloned into the pGL3-Basic luciferase reporter vector. The obtained constructs were studied using dual-luciferase reporter assays. Surprisingly, the data were impaired by unexpected effects of LMX1B on the pGL3-Basic vector alone (data not shown). Bioinformatical examination of the pGL3-Basic sequence revealed the presence of two FLAT-F elements within the vector backbone. To overcome the problem, promoter fragments were subcloned into the pGL4.10 *Firefly* luciferase reporter vector. pGL4 vector backbones were developed with a reduced number of transcription factor binding sites. FLAT elements within the vector backbone of the *Firefly* luciferase reporter vector pGL4.10 and the *Renilla* luciferase normalization vector pGL4.74 were removed as well. Nonetheless, the dual-luciferase reporter assay performance was impeded by unexpected effects of LMX1B on the *Renilla* vector used for normalization. LMX1B inhibits the expression of *Renilla* vector by approximately 70% (Figure 3.6, A). This leads to the increased relative *Firefly* luciferase activity of empty pGL4.10 vector in LMX1B-expressing HeLa cells (Figure 3.7, A). Therefore it was necessary to optimize the normalization method. The cells were transfected only with the *Firefly* luciferase reporter vector pGL4.10. *Firefly* luciferase activity was measured by using the Luciferase Assay Reagent and then samples were normalized to the relative mRNA level of the luciferase cDNA (*luc2*) by qPCR. The relative mRNA level of *Firefly* luciferase cDNA measured by qPCR was decreased by 25% in LMX1B-expressing HeLa cells (Figure 3.6, B). However, no significant differences were observed in the relative *Firefly* luciferase activity (Figure 3.7, B).

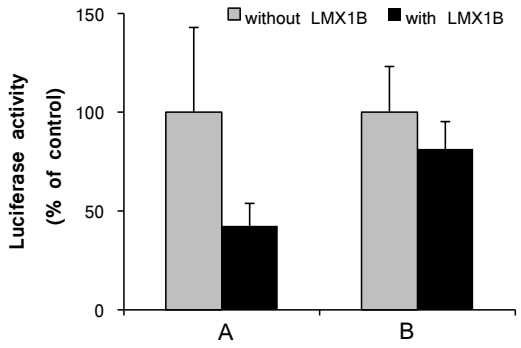

Figure 3.6: Optimization of the luciferase assay for promoter studies. Stably transfected HeLa cells inducibly producing LMX1B were transiently transfected with (A) the *Firefly* luciferase reporter vector pGL4.10 and the *Renilla* luciferase normalization vector pGL4.74, and (B) only the *Firefly* luciferase reporter vector pGL4.10. Histograms represent an average of (A) *Renilla* luciferase activity measured with the dual-luciferase assay and of (B) relative mRNA level of the *Firefly* luciferase cDNA (*luc2*) measured by qPCR. These data are the mean values relative to control (=100%) ± SDs.

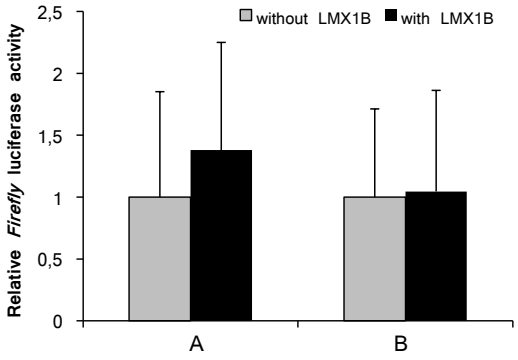

Figure 3.7: Relative *Firefly* luciferase activity of an empty pGL4.10 vector. Stably transfected HeLa cells inducibly producing LMX1B were transiently transfected with (A) the *Firefly* luciferase reporter vector pGL4.10 and the *Renilla* luciferase normalization vector pGL4.74, and with (B) the *Firefly* luciferase reporter vector pGL4.10 only. Histograms represent an average of relative *Firefly* luciferase activity of pGL4.10 normalized to (A) *Renilla* luciferase activity measured with the dual-luciferase reporter assay or to (B) relative mRNA levels of the *Firefly* luciferase cDNA (*luc2*) measured with qPCR. These data are the mean luciferase activity values relative to the basal promoter activity (=1) ± SDs.

3.2.2 Transcriptional regulation of the human *IL6*, *ABRA* and *ARL4C* genes by LMX1B

Luciferase reporter assays were performed in the HtTA-1/LMX1B cells transiently transfected with the constructs presented in Figure 3.8, A. To prove the correctness of the method the human *IL6* promoter fragment, which has shown 3-fold activation by LMX1B, was subcloned into the pGL4.10 *Firefly* luciferase reporter vector – hIL6.wt (Rascle et al., 2009). The human *IL6* promoter fragment contains one FLAT-F element located at position -140. In the present studies the human *IL6* promoter has shown 2-fold activation by LMX1B. The observed discrepancy between the present data and the previous stud-

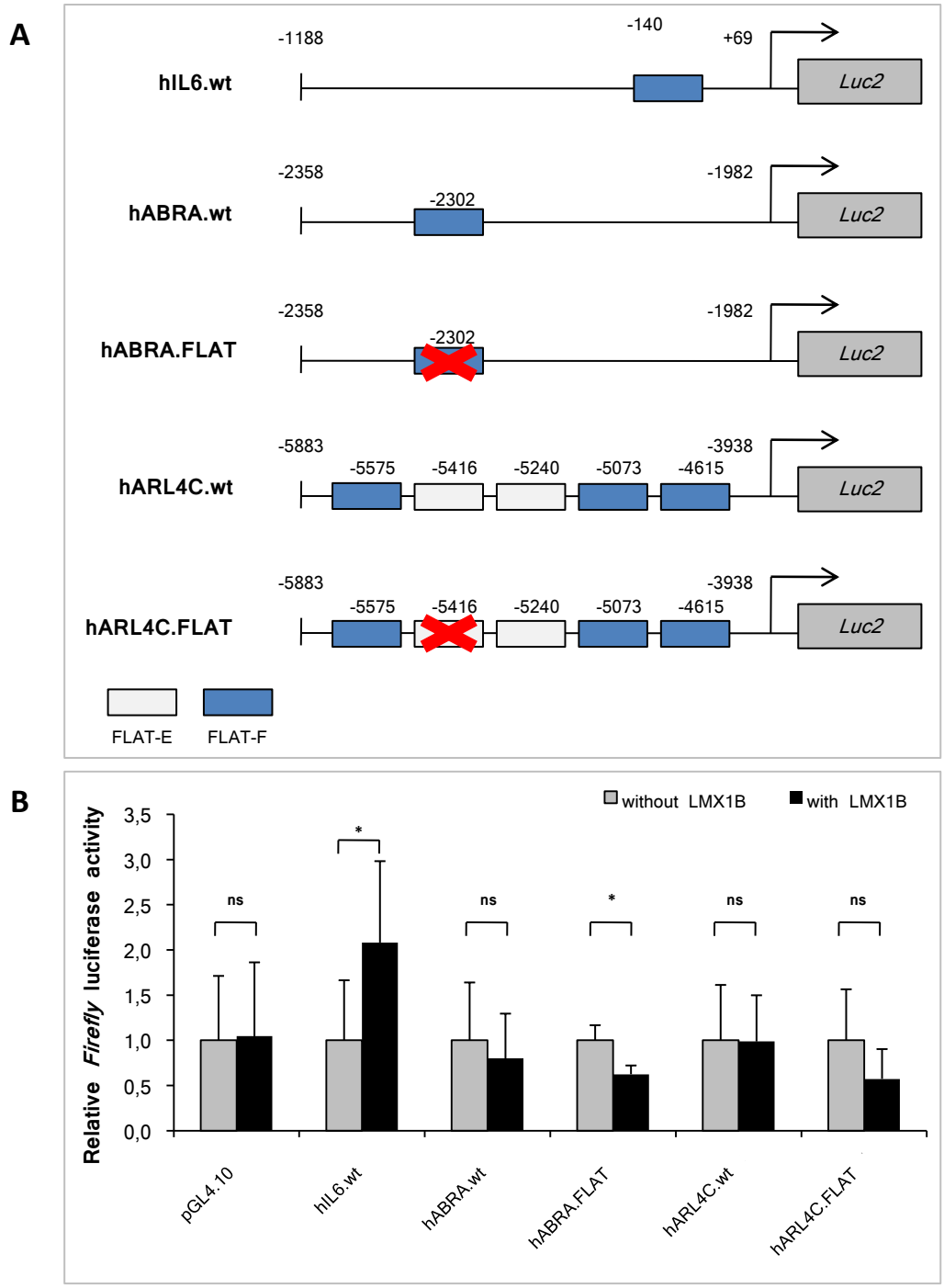

Figure 3.8: Effect of LMX1B on the human *IL6*, *ABRA* and *ARL4C* promoter fragments in stably transfected HeLa cells inducibly producing human LMX1B. (A) Schematic illustration of the *Firefly* reporter constructs with human *IL6*, *ABRA* and *ARL4C* promoter fragments containing FLAT-E (grey boxes) and FLAT-F (blue boxes) elements. Crossed boxes correspond to FLAT elements which have shown LMX1B binding (Burghardt et al., 2013) and which were mutated for these studies. hIL-6.wt, hABRA.wt, hARL4C.wt stands for constructs containing wild type promoter fragments, hABRA.FLAT and hARL4C.FLAT point mutations in the FLAT elements. (B) *Firefly* luciferase activity expressed relative to basal promoter activity (=1). Histograms represent an average of at least two independent experiments which were performed in triplicates (mean ± SD). Data were normalized to the relative expression of the luciferase cDNA (*luc2*) measured by qPCR. Here *ns* stands for data not significant, and * stands for $P<0.05$ (Student's t test).

ies could be explained by the use of the pGL4.10 backbone. Dr. Anne Rascle used the pGL3-Basic vector and performed dual-luciferase reporter assays, i.e. normalization was carried out with the *Renilla* vector.

The human *ABRA* (hABRA.wt) and *ARL4C* (hARL4C.wt) promoter fragments under investigation contain FLAT elements which in chromatin immunoprecipitation and gel shift assays showed interaction with LMX1B (Burghardt et al., 2013). This FLAT-F element within the human *ABRA* promoter and FLAT-E element within the human *ARL4C* promoter fragment are located at position -2,302 and -5,416, respectively. The relative *Firefly* luciferase activity under control of the human *ABRA* and *ARL4C* promoter fragments (hABRA.wt and hARL4C.wt) have shown a moderate, but not significant, downregulation by LMX1B in the HtTA-1/LMX1B cell line.

The effects of three point mutations in the FLAT-F element within the human *ABRA* promoter (5'-TATTAA-3' → 5'-TCTAGA-3') and of two point mutations in the FLAT-E element within the human *ARL4C* promoter (5'-TAATTA-3' → 5'-TGATGA-3') were analyzed by luciferase reporter assay (hABRA.FLAT and hARL4C.FLAT constructs in Figure 3.8, respectively). Promoter constructs bearing mutated FLAT elements have shown stronger inhibitory effects by LMX1B.

The data obtained lead to two hypotheses presented in Figure 3.9. In the first scenario LMX1B interacts with another transcription factor which downregulates the expression of a target gene. When LMX1B binds to FLAT elements, it is able to inhibit the activity of the other transcription factor (Figure 3.9, A). On the other hand, when the LMX1B binding elements are mutated, LMX1B can no longer bind to the promoter region and inhibit the other transcription factor, which as a result leads to a higher inactivation of the target genes (Figure 3.9, B). In the second scenario LMX1B blocks the access of another transription factor to the promoter (Figure 3.9, C). However, when the FLAT elements are mutated and LMX1B cannot bind, the other transcription factor is able to bind to the promoter and this negatively regulates the expression of the target genes (Figure 3.9, D).

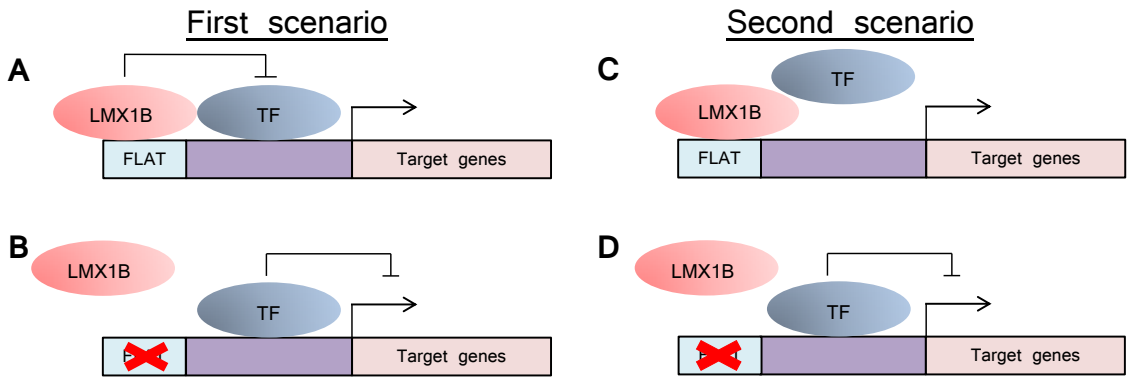

Figure 3.9: Hypotheses regarding the regulation of the human *ABRA* and *ARL4C* genes by LMX1B. (A) In the first scenario binding of LMX1B to the FLAT elements leads to the inhibition of another transcription factor (TF) which downregulates the expression of a target gene. (B) When the LMX1B binding elements are mutated, LMX1B can no longer inhibit the other transcription factor which in turn causes a downregulation of the target genes. (C) In the second scenario LMX1B blocks access of another transription factor to its target promoters. (D) When the FLAT elements are mutated, the other transcription factor is able to bind to the promoter and negatively regulate expression of the target genes.

3.3 Protein localization studies

The main goal of this part of the project was to identify the role of the putative LMX1B target genes in the development of nail-patella syndrome. A crucial piece of information concerns the subcellular localizations of the corresponding proteins and their interaction with the actin cytoskeleton in primary podocytes and in an immortalized human podocyte cell line. For this purpose cDNAs of Abra, Arl4c, and Crct1 were fused with a HA-epitope tag and miniSOG, thus giving us the opportunity to visualize the proteins by confocal and electron microscopy.

3.3.1 Subcellular localization of proteins encoded by putative LMX1B target genes in primary podocytes

The Kozak and HA-tag sequences were cloned upstream of the murine Abra, Arl4c and Crct1 cDNAs into the mammalian expression plasmid pcDNA3 (5'-Kozak-HA-cDNA-stop-3'). Primary podocytes were transiently transfected with the described expression vectors. Two days after transfection, podocytes were stained with a mouse anti-HA antibody and with an anti-mouse secondary antibody labeled with DyLight 405. Primary podocytes were co-stained with rhodamine-phalloidin in order to visualize F-actin.

Abra showed co-localization with actin filaments in primary podocytes (Figure 3.10, A-C), but neither Arl4c nor Crct1 co-localized with F-actin (Figure 3.10, D-J). Instead, immunofluorescence analysis of Arl4c and Crct1 showed staining in the cytoplasm of primary podocytes. Additionally, Arl4c demonstrated membrane-associated localization, predominantly at regions exhibiting membrane ruffling. The protein was localized at the distal ends of actin filaments (Figure 3.10, D-F). Crct1 showed association at membrane ruffles above cortical actin (Figure 3.10, H-J).

3.3.2 Abra, Arl4c, and Crct1 lead to the increased formation of F-actin

To determine the functional significance of LMX1B target genes on the actin cytoskeleton, primary podocytes isolated from quadruple transgenic *Lmx1b* heterozygous mice were transiently transfected with expression plasmids for Abra, Arl4c and Crct1. The cells were co-stained with rhodamine-phalloidin (described in Subsection 3.3.1). The phalloidin fluorescence which corresponds to the content of F-actin was quantified using ImageJ software. Primary podocytes transfected with expression plasmids for Abra, Arl4c, and Crct1 showed stronger phalloidin fluorescence in comparison to podocytes transfected with the empty pcDNA3 vector (control). Thus, phalloidin fluorescence in cells transfected with expression plasmids for Crct1, Abra, and Arl4c increased by 26%, 31%, and 41% compared to control, respectively (Figure 3.11). This experiment demonstrated that Abra, Arl4c, and Crct1 lead to the increased formation of filamentous actin (Burghardt et al., 2013).

3.3.3 Subcellular localization of wild-type and mutant Arl4c proteins in primary podocytes

ARL4C belongs to the family of GTP-binding proteins and cycles between an active GTP-bound and an inactive GDP-bound state. To study the significance of different forms of

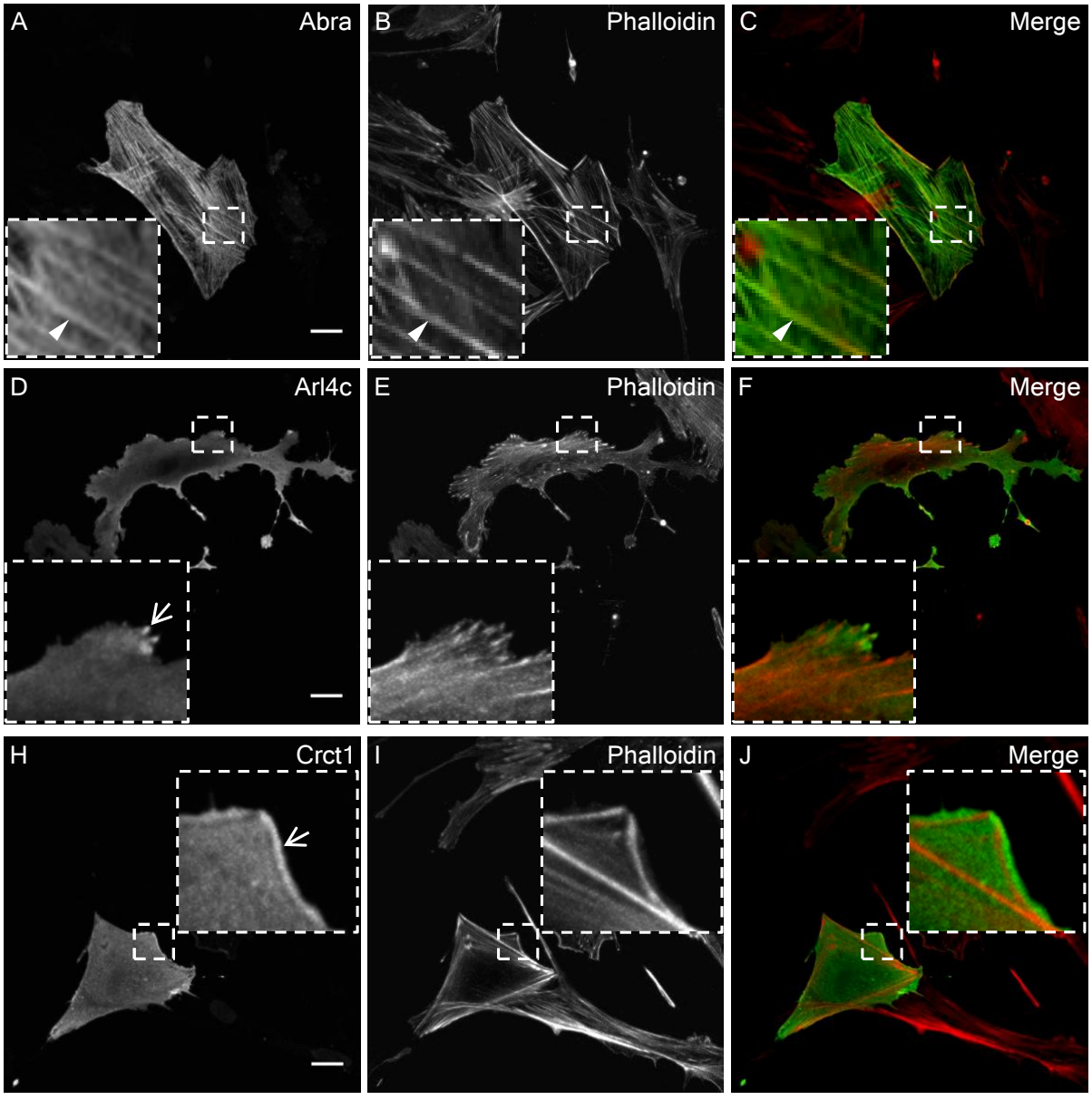

Figure 3.10: Subcellular localization of Abra, Arl4c and Crct1 in primary podocytes. Primary podocytes were transiently transfected with an expression vector encoding HA-tagged murine Abra, Arl4c and Crct1. Subsequently, cells were stained with a mouse anti-HA antibody and with an anti-mouse secondary antibody labeled with DyLight 405 (A, D, H). Primary podocytes were co-stained with rhodamine-phalloidin in order to visualize F-actin (B, E, I). Arrowheads illustrate Abra co-localization with F-actin. Arrows indicate localization of Arl4c and Crct1. Scale bars, 20 µm.

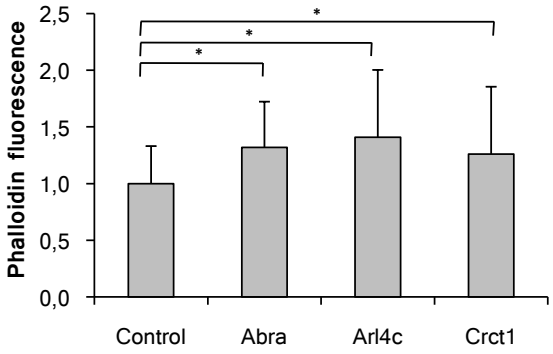

Figure 3.11: Quantification of F-actin in primary podocytes transiently transfected with expression plasmids for Abra, Arl4c, and Crct1. The studied proteins lead to the increased formation of F-actin. The control was transiently transfected with the empty vector and equals 1. Data shown are mean values ± SDs. * stands for $P<0.05$ (Student's t test).

Arl4c, primary podocytes isolated from quadruple transgenic *Lmx1b* heterozygous mice were transiently transfected with constructs expressing 1) the wild-type protein (Arl4c wt), 2) the inactive GDP-bound or dominant-negative form (Arl4c T27N) and 3) the active GTP-bound or constitutively active form (Arl4c Q71L). All Arl4c proteins were fused with the enhanced yellow fluorescent protein (EYFP) (Engel et al., 2004).

The wild-type Arl4c-EYFP (Arl4c wt) fusion protein showed cytoplasmic localization with no signal in the nucleus (Figure 3.12, A). This protein demonstrated also a punctate distribution within the cytoplasm and a membrane-associated localization, especially at lamellipodia and filopodia (Figure 3.12, A). The dominant-negative Arl4c mutant (Arl4c T27N) was distributed solely in the perinuclear region as small vesicular structures (Figure 3.12, D). The constitutively active Arl4c mutant (Arl4c Q71L) similarly to the wild-type protein (Arl4c wt) localized throughout the cytoplasm with additional distribution to lamellipodia (Figure 3.12, H). No colocalization was observed for wild-type and mutant Arl4c and F-actin (Figure 3.12, C, F, J).

3.3.4 Mutant Arl4c proteins lead to the greater formation of F-actin

The cellular distribution of wild-type and constituvely active forms of Arl4c might indicate that Arl4c interacts with the cytoskeleton (Engel et al., 2004). To determine the functional significance of wild-type and mutant forms of Arl4c on the actin cytoskeleton primary podocytes isolated from quadruple transgenic *Lmx1b* heterozygous mice were transiently transfected with plasmids expressing 1) the wild-type (Arl4c wt), 2) the inactive GDP-bound (Arl4c T27N) and 3) the active GTP-bound (Arl4c Q71L) Arl4c-EYFP fusion proteins and were co-stained with rhodamin-phalloidin to visualize F-actin. The phalloidin fluorescence was quantified using ImageJ software. Primary podocytes transfected with expression plasmids for wild-type and mutant Arl4c proteins showed stronger phalloidin fluorescence in comparison to the non-transfected podocytes (control). Phalloidin fluorescence in cells transfected with the expression plasmids for the wild-type form of Arl4c, the dominant-negative form of Arl4c (T27N), and constitutively active (Arl4c Q71L) Arl4c increased by 21%, 30% and 64% compared to control, respectively. This experiment confirmed the previously described effect of Arl4c on the

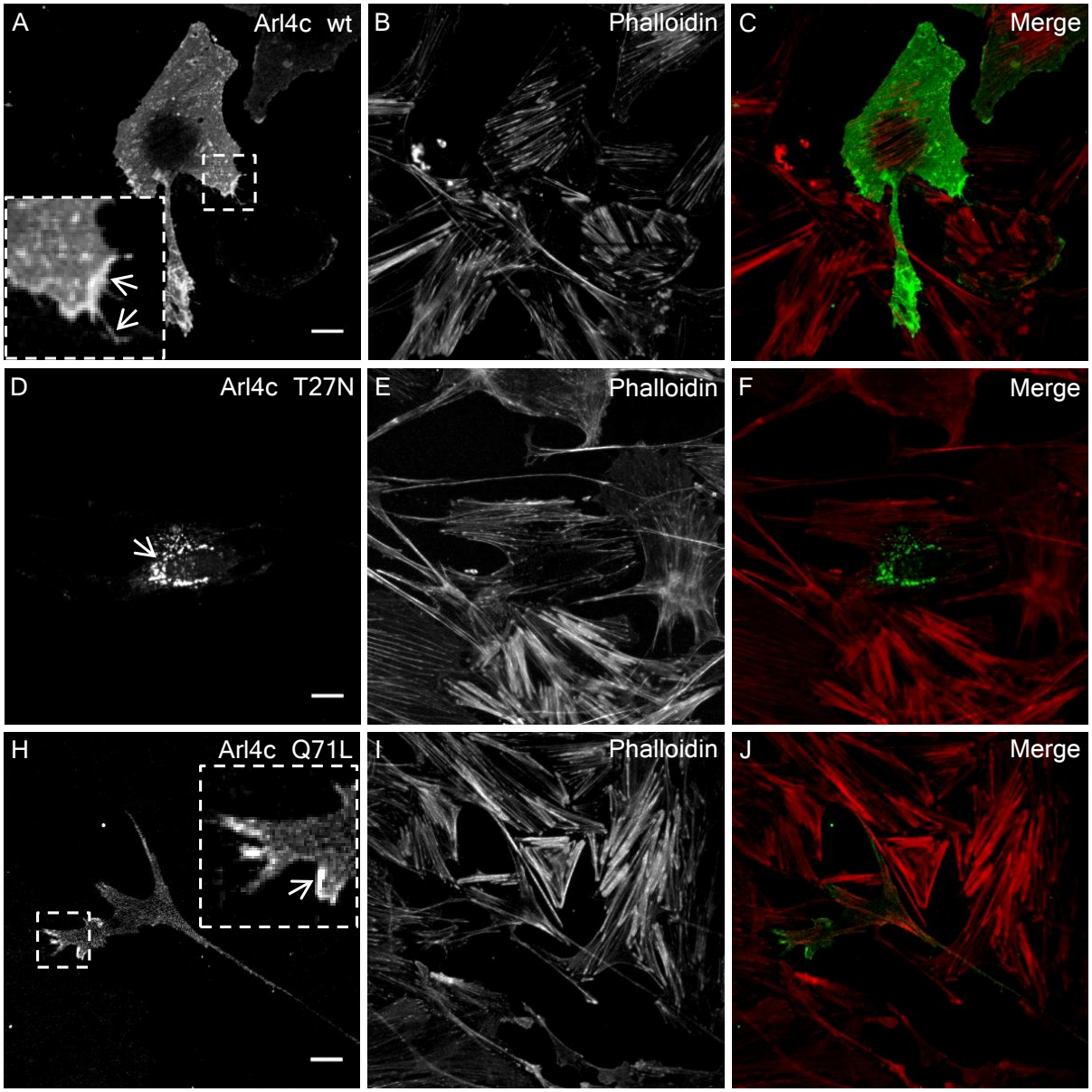

Figure 3.12: Subcellular localization of wild-type (Arl4c wt), dominant-negative (Arl4c T27N) and constitutively active (Arl4c Q71L) forms of Arl4c-EYFP fusion proteins in primary podocytes. Primary podocytes were transiently transfected with an expression vector encoding different forms of EYFP-tagged Arl4c (A, D, H) and subsequently co-stained with rhodamine-phalloidin (B, E, I). Arrows demonstrate protein localization. Scale bars, 20 µm.

actin cytoskeleton. Futhermore, dominant-negative (Arl4c T27N) and constitutively active (Arl4c Q71L) Arl4c mutant proteins lead to the greater stiffness of the actin cytoskeleton (Figure 3.13).

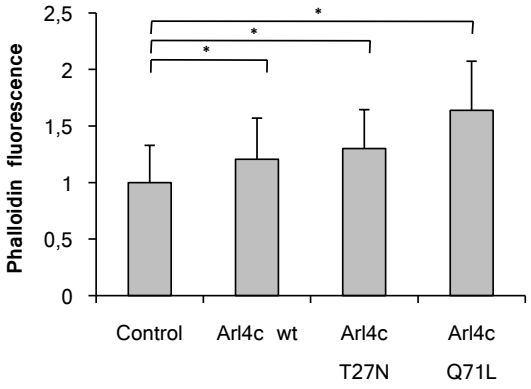

Figure 3.13: Quantification of F-actin in primary podocytes transiently transfected with expression plasmids for wild type (Arl4c wt), dominant-negative (Arl4c T27N) and constitutively active (Arl4c Q71L) forms of Arl4c. All 3 proteins lead to the increased formation of F-actin. The control represents non-transfected cells and equals 1. Data shown are mean values ± SDs. * stands for $P<0.05$.

3.3.5 Ultrastructural localization of Abra, Arl4c and Crct1 in a human podocyte cell line

To visualize the proteins under investigation by transmission electron microscopy the recently described miniSOG technique ("mini Singlet Oxygen Generator") was applied (Shu et al., 2011). Initially we encountered the difficulty that the green fluorescence emitted by the miniSOG protein was gone within a few seconds after excitation. A fellow PhD student, Benjamin Salecker, facilitated the search for transfected cells by subcloning the mCherry cDNA upstream of miniSOG (5'-mCherry-miniSOG-cDNA-3').

Conditionally immortalized human podocytes were transiently transfected with expression plasmids for Abra, Arl4c and Crct1 fused with mCherry-miniSOG. The subcellular distribution of the miniSOG-tagged proteins was equivalent to that of the HA-tagged proteins and is illustrated in Figure 3.14. In addition to the expected pattern, small punctate structures were detected within the cytoplasm of podocytes expressing Arl4c and Crct1. These proteins fused with a HA-tag, which is 36 times smaller than the mCherry-miniSOG tag, did not show such a pattern. The HA-tag consists of 9 amino acids which correspond to 1.1 kDa. On the contrary, the mCherry-miniSOG tag consists of 362 amino acids and has a mass of 39.8 kDa. Therefore, it is possible that the Arl4c and Crct1 fused with a larger tag are improperly folded.

Two days after transfection the podocytes were illuminated by an intense light from a mercury lamp for 10 min, using a standard fluorescein isothiocyanate filter. Photoconversion of fluorescent miniSOG protein generates singlet oxygen which catalyzes the polymerization of diaminobenzidine tetrachloride (DAB) into an osmiophilic polymer resolvable by electron microscopy (Shu et al., 2011). After photoconversion the podocytes were fixed and 70 nm thick sections were cut for further electron microscopic examination.

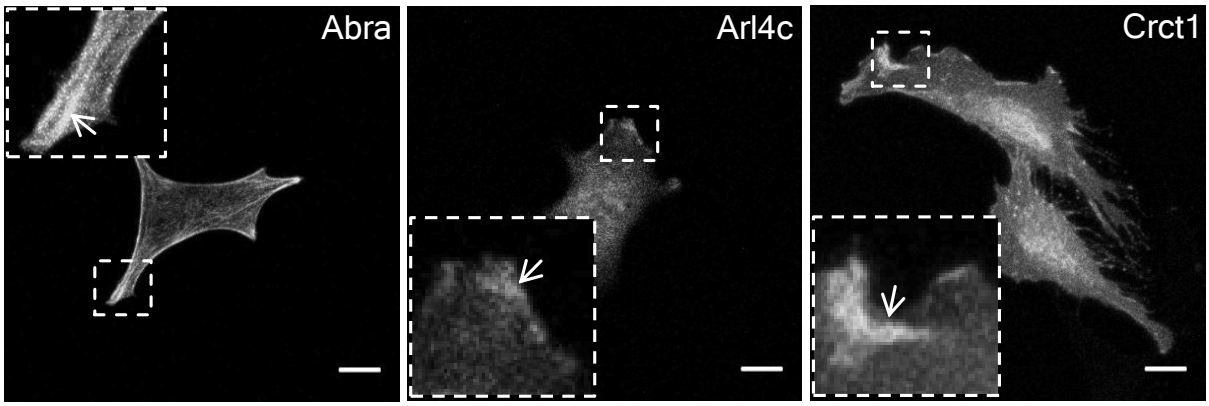

Figure 3.14: Subcellular localization of mCherry-miniSOG-tagged Abra, Arl4c and Crct1 in a human podocyte cell line. Arrowheads demonstrate protein localization. Scale bars, 10 μm.

Abra. A human podocyte cell line transfected with miniSOG-tagged Abra showed tremendous accumulation of an osmiophilic polymer at filamentous structures in the cytoplasm (Figure 3.15, A, C), thus confirming the previously described subcellular localization of HA-tagged Abra (Subsection 3.3.1). Actin filaments are known to be the smallest component of the cytoskeleton with a diameter of about 7 nm (Cooper, 2000). Electron microscopic images taken with a higher magnification illustrate filaments which might demonstrate Abra associated with actin (Figure 3.15, E). Interestingly, the examination of other ultrathin sections derived from the same podocyte revealed the membrane-associated distribution of Abra (Figure 3.15, B and D). No expression of Abra was detected in filopodia (Figure 3.15, F).

Arl4c. Expression of HA-tagged Arl4c in primary podocytes and subsequent staining with fluorescently labeled phalloidin showed no co-localization of Arl4c with filamentous actin (Subsection 3.3.1). However, electron microscopic studies of miniSOG-tagged Arl4c expressed in a human podocyte cell line revealed the polarized distribution of Arl4c at actin-like filamentous structures in the periphery of the cell (Figure 3.16, A-C). Detailed examination of other ultrathin section derived from another podocyte revealed a membrane-associated distribution of Arl4c at filopodia (Figure 3.16, D), supporting the previously described subcellular localization of HA-tagged Arl4c in primary podocytes (Subsection 3.3.1).

Crct1. Similarly to Abra and Arl4c, miniSOG-tagged Crct1 showed the membrane-associated localization at filopodia (Figure 3.17, A, B, D). A strong signal was observed at the site of contact with the neighboring cell (Figure 3.17, C). Additionally, filamentous structures were detected under the cell membrane of filopodia (Figure 3.17, B, D).

Non-transfected human podocytes. The transmission electron microscopy studies of non-transfected human podocytes did not reveal any specific localization of osmiophilic polymer. Images taken at a higher magnification illustrate fiber-like structures, however the signal intensities are weaker than those of the Abra-, Arl4c- and Crct1-expressing conditionally immortalized human podocytes (Figure 3.18, C, E). Detailed examination of the plasma membrane and filopodia of non-transfected cells did not show similar intensity of osmiophilic polymer in comparison to the transfected cells (Figure 3.18, D, F).

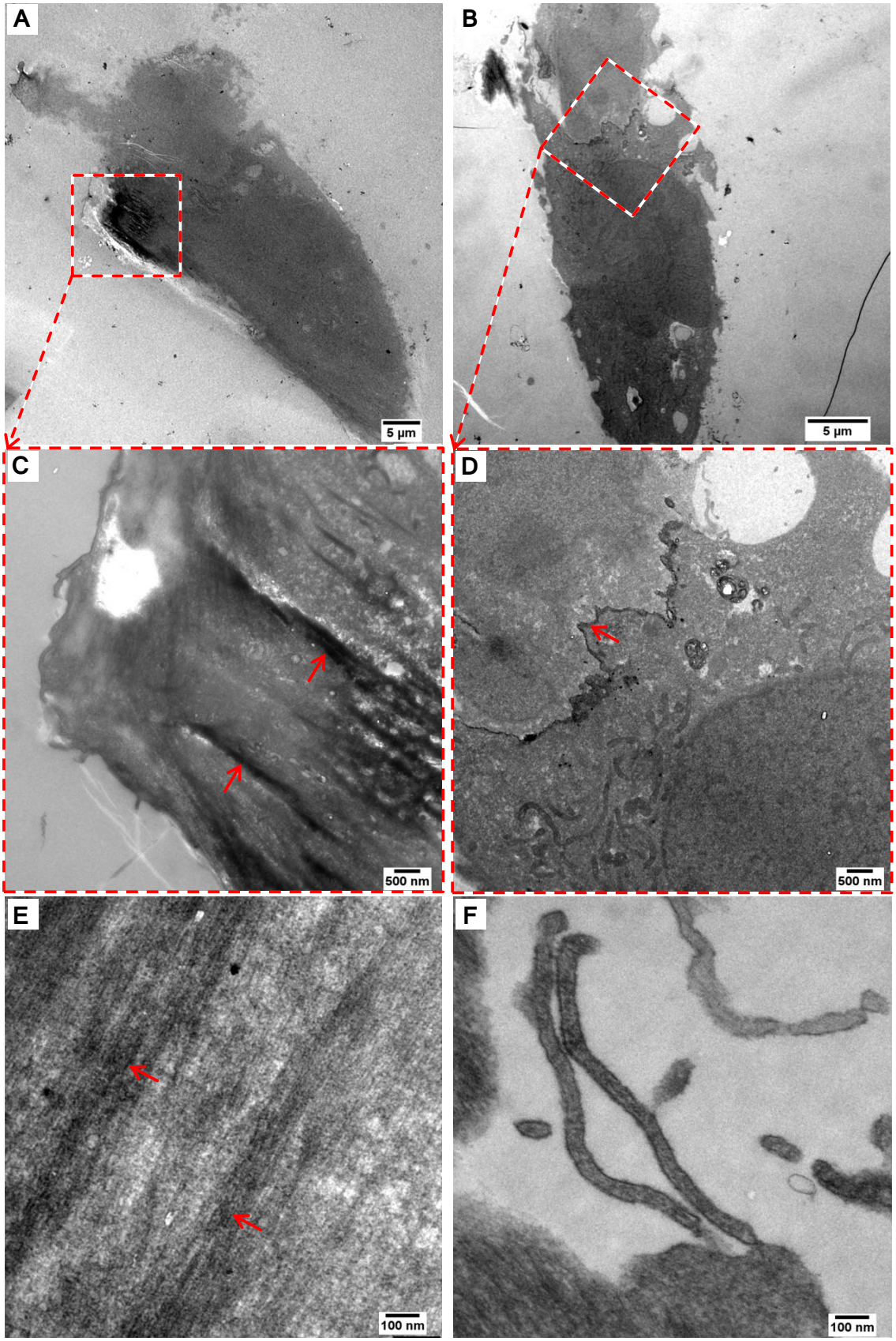

Figure 3.15: MiniSOG-tagged Abra in a human podocyte cell line showed (A, C, E) filamentous structures in the cytoplasm and (B, D) a membrane-associated localization. (C) and (D) are images taken with higher magnification of portions of (A) and (B), respectively. Red arrows illustrate the localization of the osmiophilic polymer. Images were taken by transmission electron microscopy.

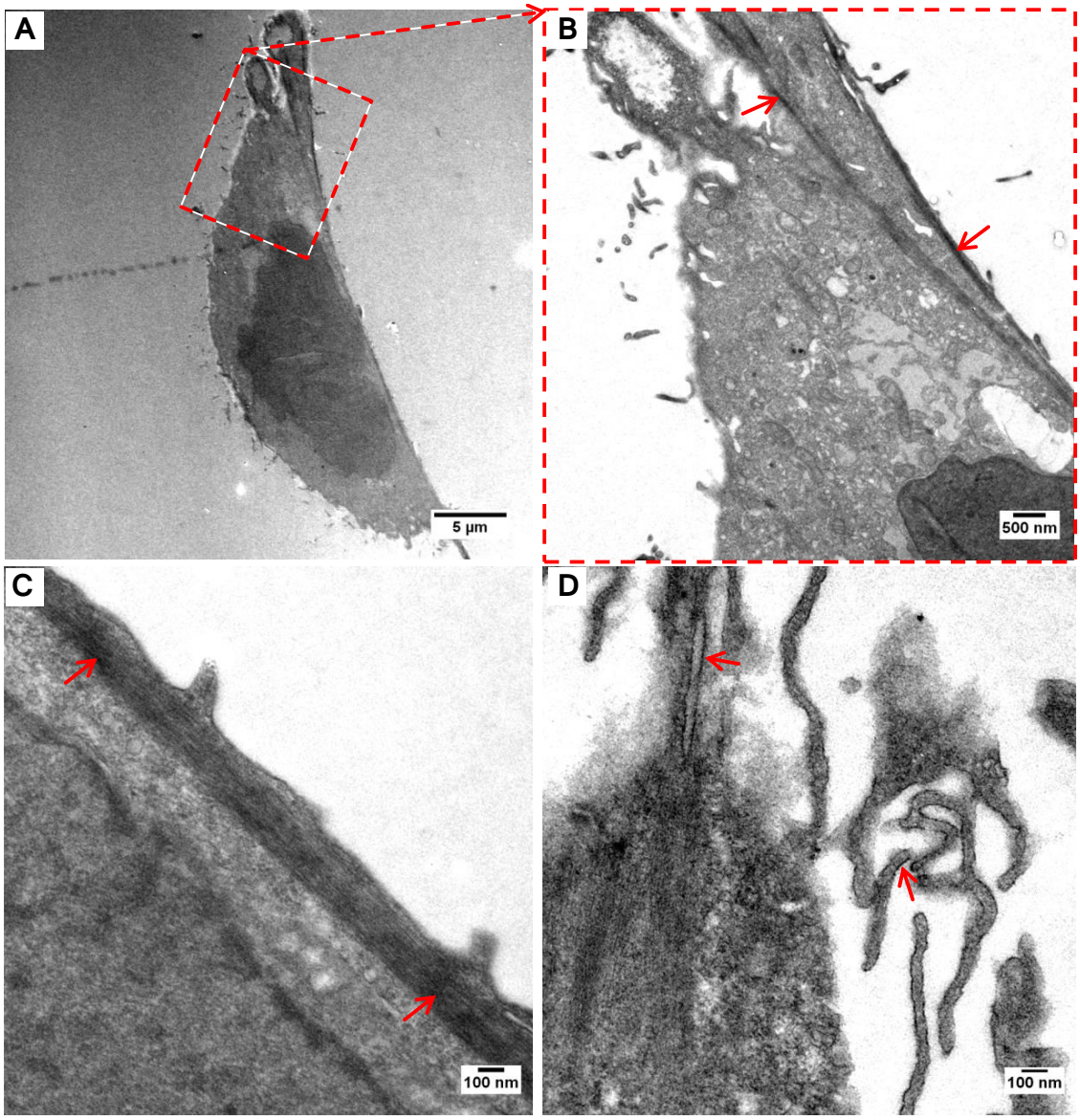

Figure 3.16: MiniSOG-tagged Arl4c in a human podocyte cell line shows (A-C) filamentous structures at the periphery of the cell and (D) a membrane-associated localization at filopodia. (B) is an image taken with higher magnification of portion of (A). Red arrows illustrate the localization of the osmiophilic polymer. Images were taken by transmission electron microscopy.

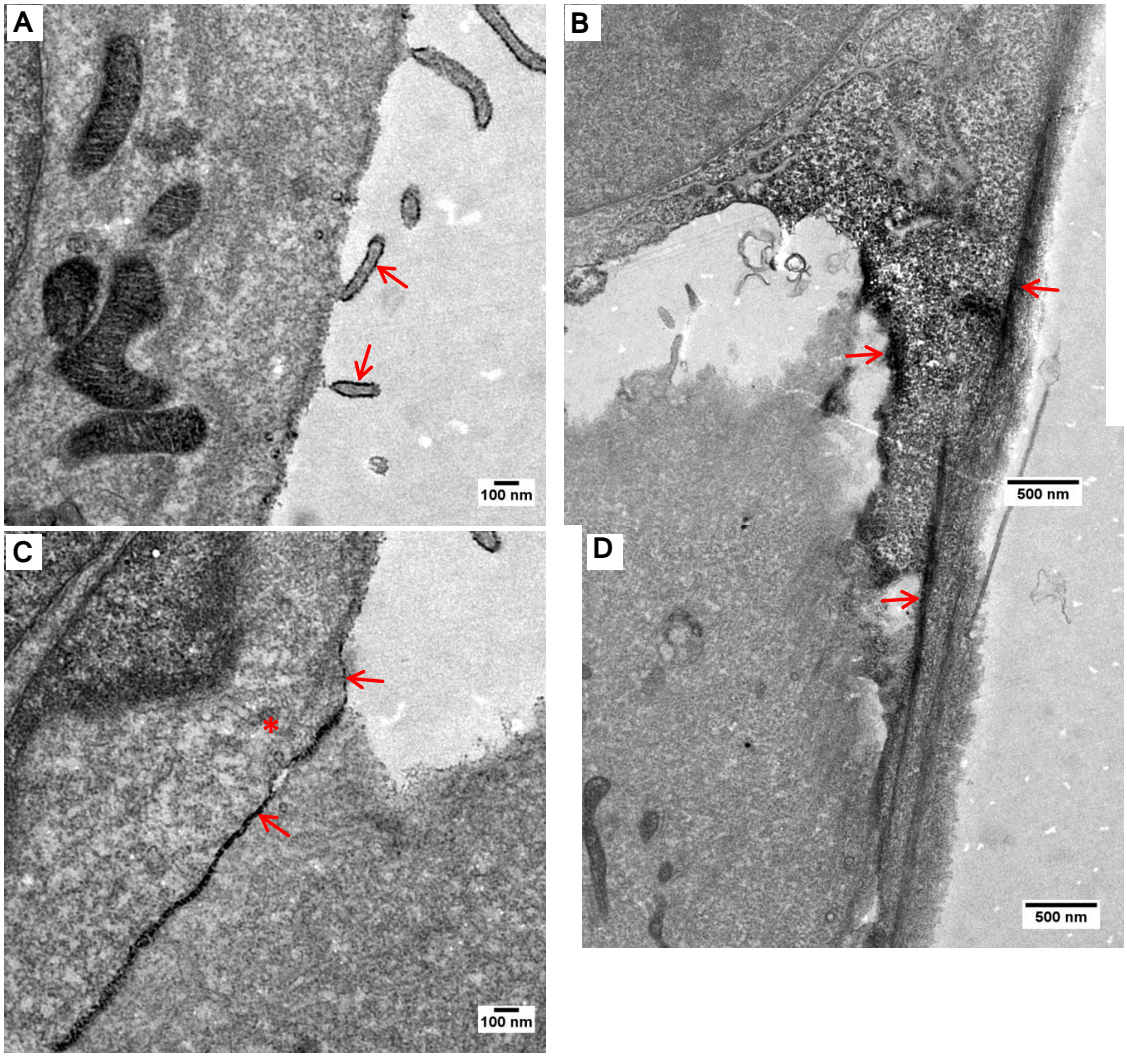

Figure 3.17: MiniSOG-tagged Crct1 in a human podocyte cell line shows a membrane-associated localization (A-D). Moreover, filamentous structures were detected under the cell membrane of filopodia (B, D). Red arrows illustrate the localization of the osmiophilic polymer. Red asterisk in panel (C) indicates the Crct1-expressing cell, whereas the neighboring cell was not transfected. Images were taken by transmission electron microscopy.

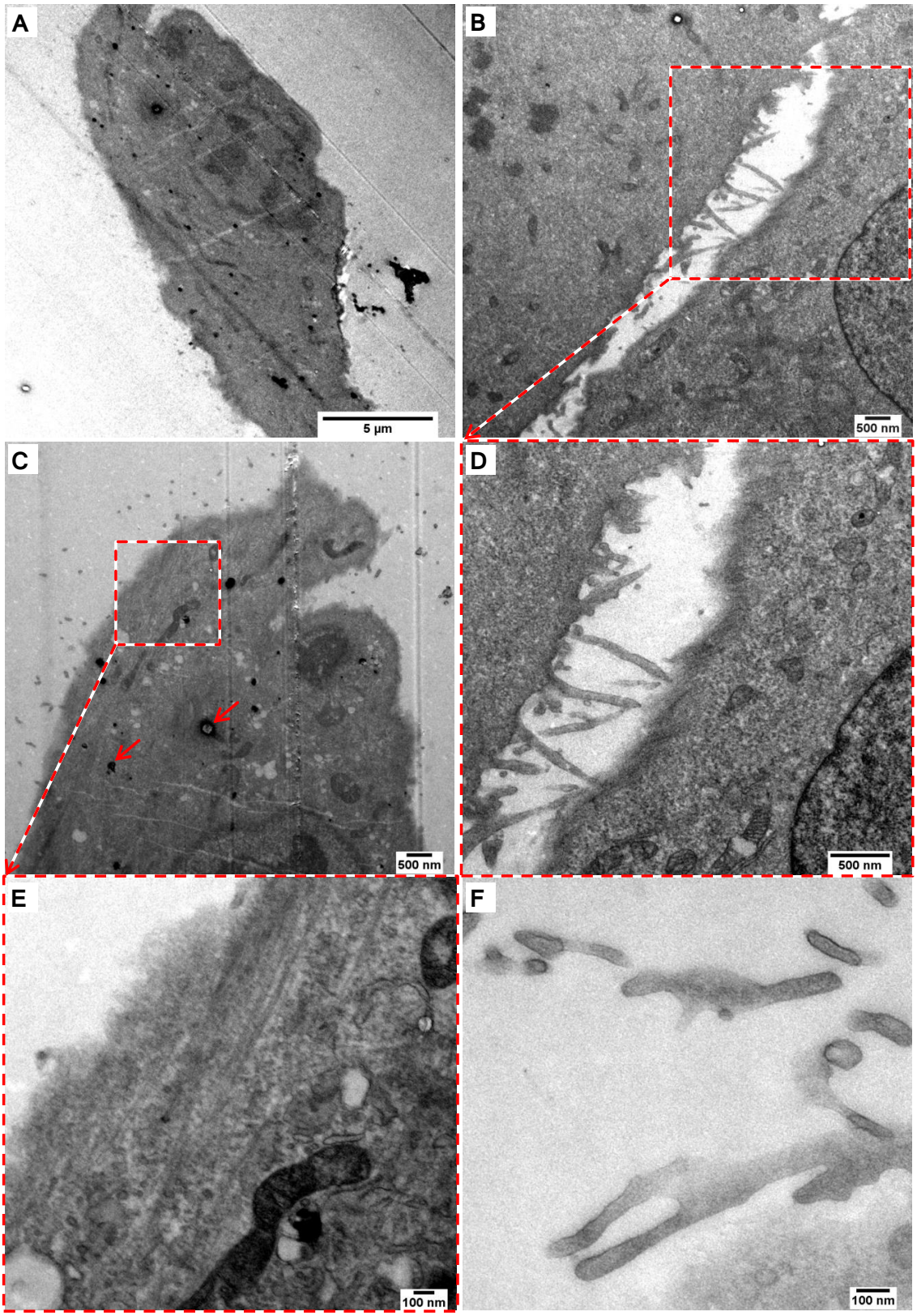

Figure 3.18: Transmission electron micrographs taken from non-transfected human podocytes. Detailed examination of the (A, C, E) cell membrane and cytoplasm, (B, D) cell-cell contact and (G) filopodia. Red arrows illustrate non-specific osmiophilic polymer precipitates.

3.4 Actin polymerization studies

In Subsection 3.3.2 it was demonstrated that primary podocytes transiently transfected with expression plasmids for Abra, Arl4c and Crct1 contain higher levels of filamentous actin. Moreover, primary podocytes isolated from *Lmx1b* knock-out mice have shown increased levels of filamentous actin as well (Burghardt et al., 2013). To further analyze the effects of LMX1B and its target genes on the actin cytoskeleton, filamentous (F) and globular (G) actin fractions were purified and F- to G-actin ratio was determined. Preliminary studies were performed in the HtTA-1/LMX1B cell line (Subsection 3.4.1). Further examinations of the F- to G-actin ratio in primary podocytes failed because it was not possible to isolate a sufficient number of cells. Additionally, studies in conditionally immortalized murine podocytes transiently transfected with expression plasmids for Abra, Arl4c, and Crct1 were performed (Subsection 3.4.2).

3.4.1 LMX1B has no effect on the F- and G-actin content in the HtTA-1/LMX1B cell line

HtTA-1/LMX1B cells were treated with 0.3 μM and 1 μM of latrunculin A, which inhibits the polymerization of actin by binding to G-actin. Subsequently cells were stained with Acti-stain 488 fluorescent phalloidin to visualize F-actin. The effect of latrunculin A on the actin cytoskeleton of HtTA-1/LMX1B cells was evident already 30 min after treatment (Figure 3.19, A).

The functionality of the assay was confirmed by immunoblotting F- and G-actin fractions purified from the latrunculin A-treated cells and subsequent quantification of the immunoblot signals. As expected, the F- to G-actin ratio in HtTA-1/LMX1B cells treated with latrunculin A was significantly reduced. 30 min after treatment with 0.3 μM and 1 μM latrunculin A the F- to G-actin ratio was reduced 2- and 5-fold in comparison to the ethanol-treated control cells, respectively (Figure 3.19, B-C).

The effect of LMX1B on the F- to G-actin ratio was analyzed in HtTA-1/LMX1B cells which were grown in the presence or absence of doxycycline for 4 days. The expression of LMX1B did not cause any significant changes on the actin cytoskeleton organization in the cells examined (Figure 3.20).

3.4.2 The expression of Abra, Arl4c, and Crct1 has no effect on the F- to G-actin ratio in a murine podocyte cell line

A murine podocyte cell line was treated with 0.2 μM and 1 μM of latrunculin A for 30 min and 2 h. After 30 min of treatment slight changes in the actin polymerization were visible. However, depolymerization of the actin cytoskeleton was more prominent after 2 h of treatment with the toxin (Figure 3.21, A). Therefore, to demonstrate functionality of the assay in conditionally immortalized murine podocytes, cells were treated with 0.2 μM and 1 μM of latrunculin A for 2 h. Treatment of conditionally immortalized murine podocytes with 0.2 μM and 1 μM latrunculin A for 2 h reduced the F- to G-actin ratio 1.6- and 3.8-fold in comparison to the ethanol-treated control cells, respectively (Figure 3.21, C).

In order to investigate the influence of putative LMX1B target genes on the actin cytoskeleton, conditionally immortalized murine podocytes were transiently transfected with expression plasmids for Abra, Arl4c and Crct1. Filamentous and globular actin fractions were purified and immunoblot signals were quantified. Murine podocytes expressing

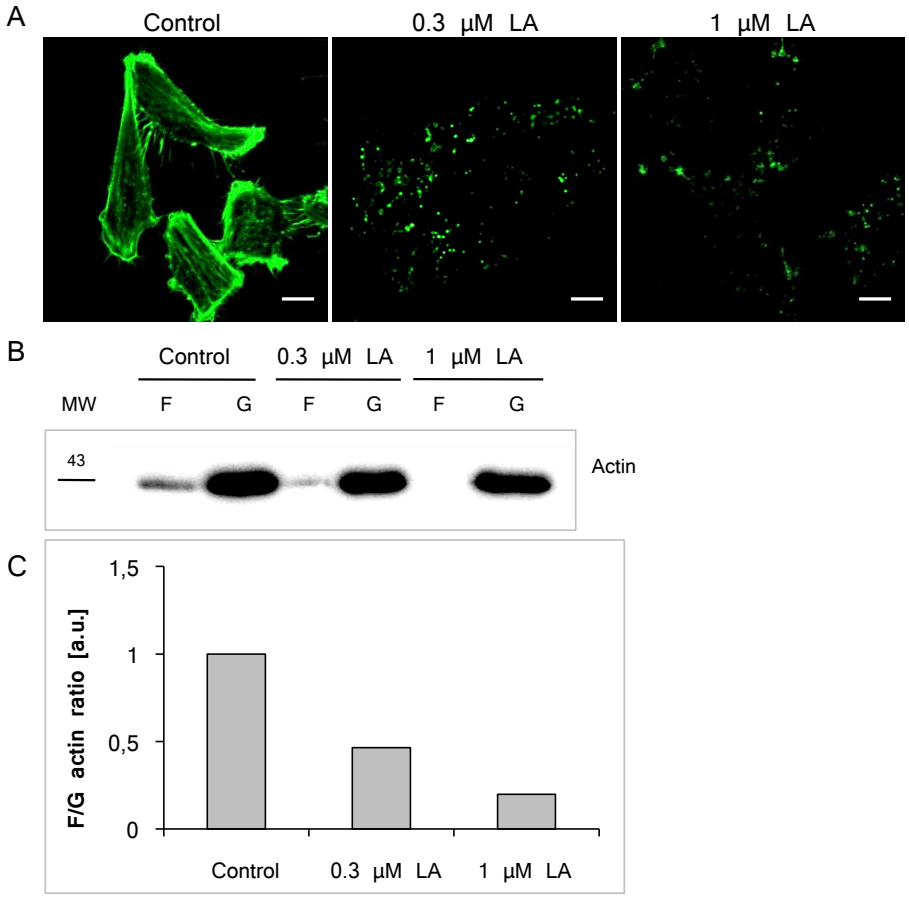

Figure 3.19: Influence of latrunculin A (LA) on the actin cytoskeleton in HtTA-1/LMX1B cells. The cells were treated with 0.3 µM and 1 µM latrunculin A for 30 min. (A) F-actin was visualized by staining with Acti-stain 488 fluorescent phalloidin. (B) The immunoblot illustrating filamentous (F) and globular (G) actin fractions purified from latrunculin A-treated HtTA-1/LMX1B cells. (C) Densitometric analysis of F- to G-actin ratio relative to control treated with ethanol (=1). Data were collected from one experiment. MW stands for protein molecular weight marker in kDa. Scale bars, 10 µm.

Abra showed a 19% increase in the F- to G-actin ratio, in contrast to podocytes expressing Arl4c and Crct1 which showed a reduction in the F- to G-actin ratio by 12 % and 25 %, respectively (Figure 3.22). However, the observed changes were not statistically significant.

3.5 Expression of recombinant Abra, Arl4c and Crct1 proteins in *Escherichia coli*

The complete coding sequences for murine Abra and Crct1, and the incomplete coding sequence for murine Arl4c (from 396 to 576 bp) were cloned into the bacterial expression vector pET21a. Expression of recombinant proteins was induced by isopropyl-1-thio-β-D-galactosidase (IPTG) in different strains of *Escherichia coli* – BL21(DE3), BL21(DE3)pLysS and Rosetta(DE3)pLysS at 25°C and 37°C for 1 h, 2 h, 4 h and overnight. Bacterial lysates were separated on a polyacrylamide gel. The optimized

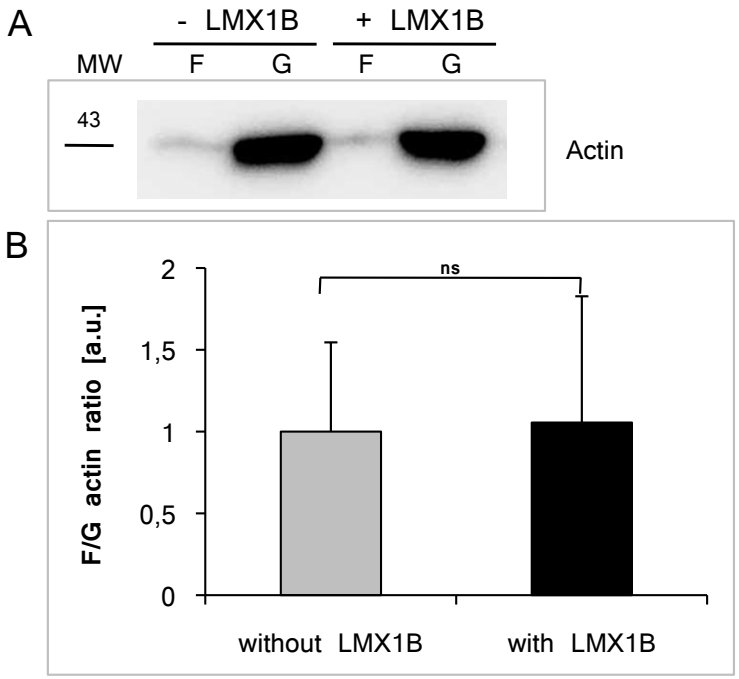

Figure 3.20: LMX1B has no effect on the F- to G-actin ratio in stably transfected HeLa cells inducibly producing LMX1B. HtTA-1/LMX1B cells were grown in the presence or absence of doxycycline for 4 days. (A) The immunoblot illustrating the filamentous (F) and globular (G) actin fractions collected from HeLa cells without ("-LMX1B") or with ("+LMX1B") LMX1B expression. (B) Densitometric analysis of F- and G-actin fractions collected from HeLa cells from four independent experiments. n=12 per group, where n refers to the number of analyzed F- and G-actin fractions. All data are presented as mean ± SDs. Here *ns* stands for data not significant, and MW stands for protein molecular weight marker in kDa.

parameters for the highest protein expression induced by IPTG are summarized in Table 3.2.

Protein	Bacterial strain	Time of induction	Temperature
Abra	Rosetta(DE3)pLysS	o/n	37°C
Arl4c	Rosetta(DE3)pLysS	2 h	37°C
Crct1	BL21(DE3)pLysS	o/n	37°C

Table 3.2: Optimized parameters for the highest expression of recombinant Abra, Arl4c and Crct1 induced by IPTG

Recombinant proteins were purified from the bacteria on Ni^{2+}-charged His-Bind resin. Purified proteins were separated on polyacrylamide gels and analyzed with an anti-His-Tag monoclonal antibody (Figure 3.23). The predicted molecular weights including the N-terminal T7-Tag and the C-terminal His-Tag of Abra, Arl4c and Crct1 are 43.2 kDa, 8.5 kDa and 13.1 kDa, respectively.

After the purification of proteins Prof. Dr. Rainer Deutzmann identified Abra and Arl4c peptide sequences by mass spectrometry. Crct1 peptide sequences were not identified because of the high cysteine contents within the sequence. Only one peptide, comprising the T7-tag, was found in the Crct1 protein by mass spectrometry.

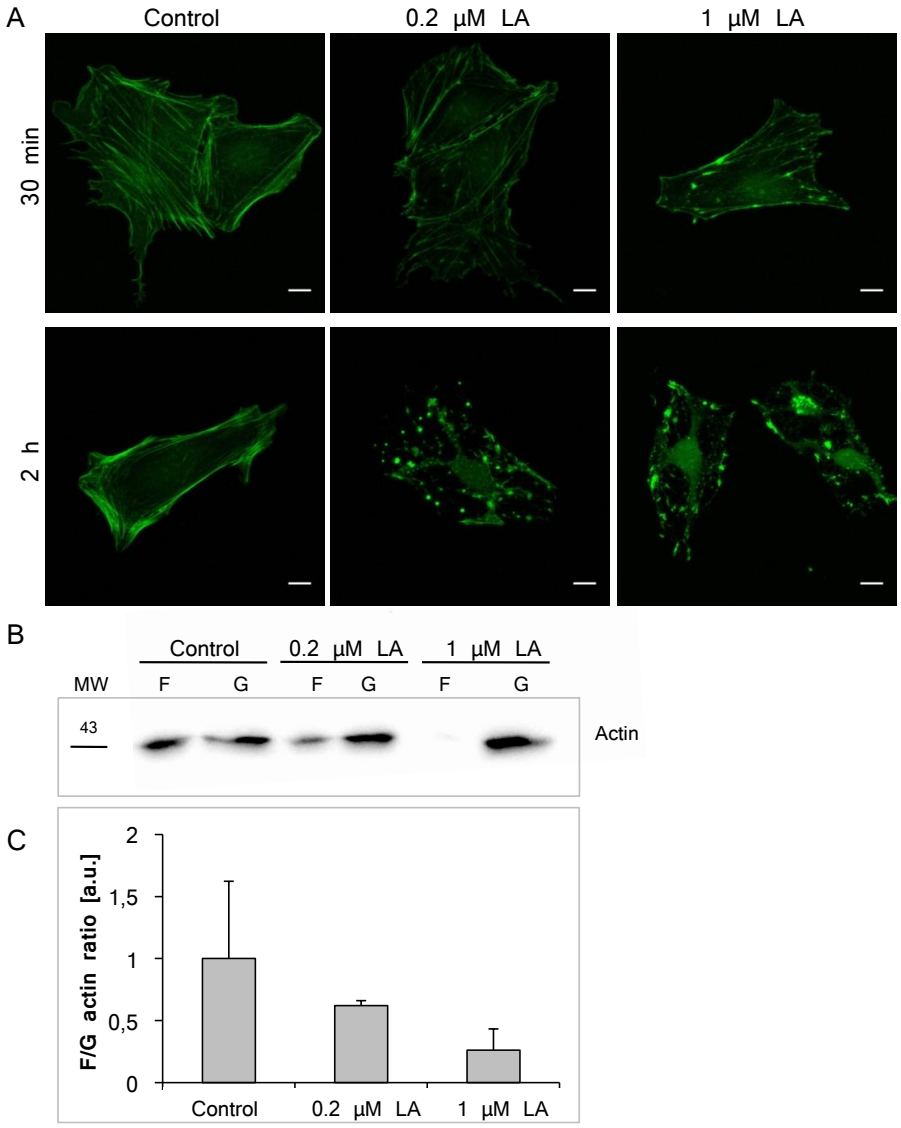

Figure 3.21: Latrunculin A-treated murine podocytes showed significant F-actin depolymerization. (A) Murine podocytes were treated with 0.2 µM and 1 µM latrunculin A for 30 min and 2 h and then stained with Acti-stain 488 fluorescent phalloidin to visualize F-actin. Control cells were treated with ethanol. (B) The representative immunoblot illustrating the filamentous (F) and globular (G) actin fractions collected from the murine podocyte cell line treated with 0.2 µM and 1 µM for 2 h. (C) Densitometric analysis of F- and G-actin fractions purified from latrunculin A-treated murine podocytes relative to control (=1). Data were collected from three independent experiments. n=3 per group, where n refers to the number of F-actin and G-actin fractions analyzed. All data are presented as mean ± SDs. MW stands for protein molecular weight marker in kDa. Scale bars, 10 µm.

3.6 Generation, affinity purification, and characterization of rabbit antibodies directed against Abra, Arl4c, and Crct1

To generate polyclonal antibodies rabbits were immunized with the purified recombinant Abra, Arl4c and Crct1 proteins described in Section 3.5 (two rabbits each, six rabbits

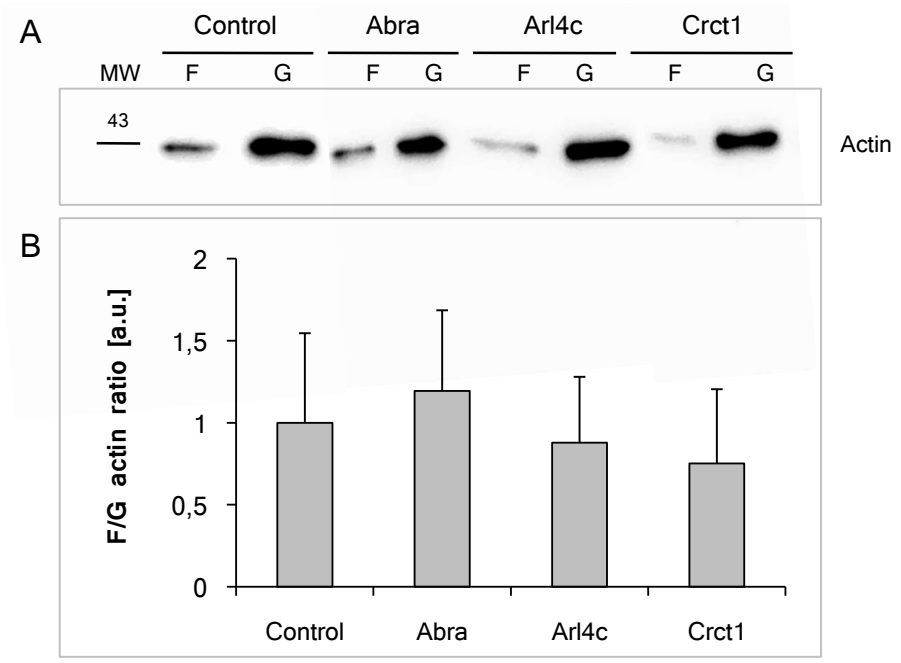

Figure 3.22: The expression of Abra, Arl4c and Crct1 has no effect on the F- to G-actin ratio in a murine podocyte cell line. (A) Representative immunoblot illustrating the effects of Abra, Arl4c and Crct1 on filamentous (F) and globular (G) actin fractions, which were collected from the murine podocyte cell line transiently transfected with expression plasmids for Abra, Arl4c, and Crct1. Control cells were transfected with empty pcDNA3. (B) Densitometric analysis from three independent experiments. n=8-9 per group, where n refers to the number of analysed F-actin and G-actin fractions. All data are presented as mean ± SDs.

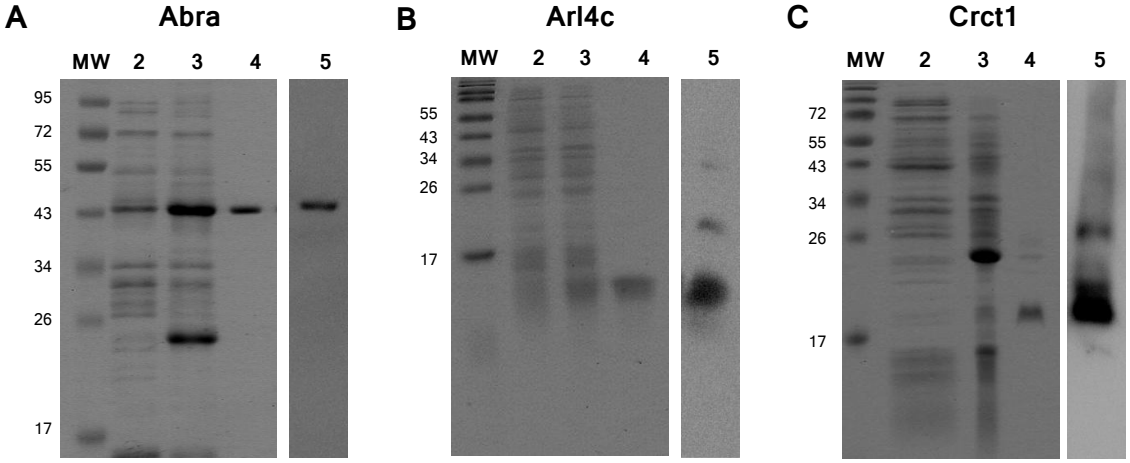

Figure 3.23: Expression and purification of recombinant murine (A) Abra, (B) Arl4c and (C) Crct1 proteins expressed in *Escherichia coli*. (MW) protein molecular weight marker in kDa, (lane 2) bacterial lysate before induction by 1 mM IPTG, (Lane 3) crude bacterial lysate after induction, (Lane 4) recombinant proteins purified from bacterial lysate by column chromatography using Ni^{2+}-charged His-Bind resin, and (Lane 5) Western blot analysis of the recombinant proteins with an anti-His-Tag monoclonal antibody.

in total). The obtained antisera were tested in COS-7 cells transiently transfected with expression plasmids for Abra, Arl4c and Crct1. Abra and Arl4c were detected with the antisera, but not Crct1 (Figure 3.24). The expected molecular weights including the N-terminal HA-Tag of Abra, Arl4c and Crct1 are 42.4 kDa, 22.2 kDa and 12.3 kDa, respectively.

To eliminate multiple nonspecific bands detected by Western blot using anti-Abra and anti-Arl4c antibodies it was decided to affinity-purify the rabbit antisera. Affinity purification eliminated nonspecific bands by Western blot (Figure 3.25). Moreover, the background signal detected by immunofluorescence staining was significantly reduced. Figures of cells stained with the crude antisera are not presented. For further studies of Crct1 a commercial goat anti-Crct1 antibody was used.

Prior to the examination of kidney sections with anti-Abra, anti-Arl4c and anti-Crct1 antibodies immunofluorescence stainings of a murine podocyte cell line transiently transfected with expression plasmids for HA-tagged Abra, Arl4c and Crct1 were performed. Transfected podocytes were double-stained with an anti-HA antibody and with anti-Abra, anti-Arl4c and anti-Crct1 antibodies. The proper subcellular distribution of the proteins and co-localization of signals from the immunostainings are shown in Figure 3.26.

3.7 Expression of endogenous Abra, Arl4c and Crct1 after the podocyte-specific inactivation of Lmx1b

Three-month-old female inducible podocyte-specific *Lmx1b* knock-out ($Lmx1b^{lox/lox}$, rtTA, Cre) and control ($Lmx1b^{lox/lox}$, rtTA) mice were administered 2 mg/ml doxycycline for 7 days. Animals were perfusion-fixed and their kidneys were embedded in paraffin and in Tissue-Tek O.C.T. Paraffin-embedded (Figure 3.27) and frozen (Figure 3.28) kidney sections were stained with our own anti-Abra and anti-Arl4c antibodies as well as with the commercial anti-Crct1 antibodies.

The anti-Abra antibodies recognized an epitope in some cells of the glomerulus in paraffin-embedded kidney sections. However, no differences in the expression level of Abra between induced triple-transgenic and control animals were observed (Figure 3.27). No distinct signal for endogenous Abra in frozen kidney sections stained with the anti-Abra antibody was observed (Figure 3.28). Immunofluorescence stainings of paraffin-embedded and frozen kidney sections with the anti-Arl4c antibodies were not successful (Figures 3.27 and 3.28). The endogenous Crct1 protein was significantly induced in the glomeruli of the induced podocyte-specific *Lmx1b* knock-out mice (Figures 3.27 and 3.28).

3.8 Paxillin expression is affected in conditionally immortalized murine podocytes expressing Abra and Crct1, but not Arl4c

Burghardt *et al.* demonstrated that primary podocytes isolated from inducible podocyte-specific *Lmx1b* knock-out mice better adhere to a laminin-coated surface than podocytes from control mice (Burghardt et al., 2013). However, the focal contact area of primary podocytes with or without an inactivated *Lmx1b* gene examined by immunofluorescence staining with an anti-paxillin antibody showed no difference (Burghardt et al., 2013).

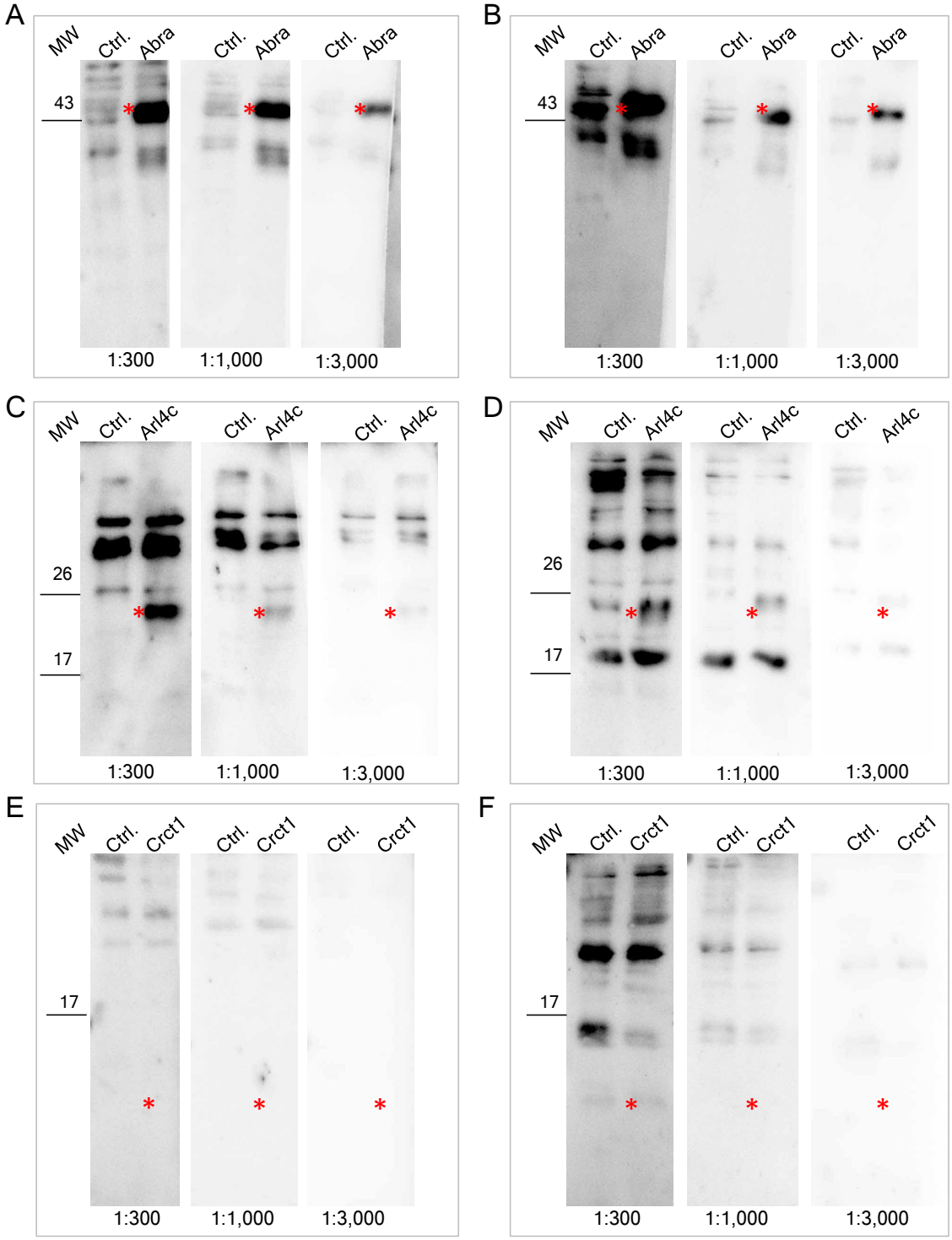

Figure 3.24: Titration of the rabbit antisera. 12 µg of total protein lysates extracted from COS-7 cells transiently transfected with the empty pcDNA3 vector (Ctrl.) or with pcDNA3 plasmids encoding Abra, Arl4c and Crct1 were separated on 15 % polyacrylamide gels. Separated proteins were transferred to a PVDF membrane. The membranes were first incubated with rabbit antisera diluted 1:300, 1:1,000 and 1:3,000 and then with HRP-conjugated anti-rabbit antibodies. Tested antisera obtained from rabbit 1 (A, C, E) or rabbit 2 (B, D, F). MW stands for protein molecular weight marker in kDa. Red asterisks correspond to the expected size of the proteins of interest.

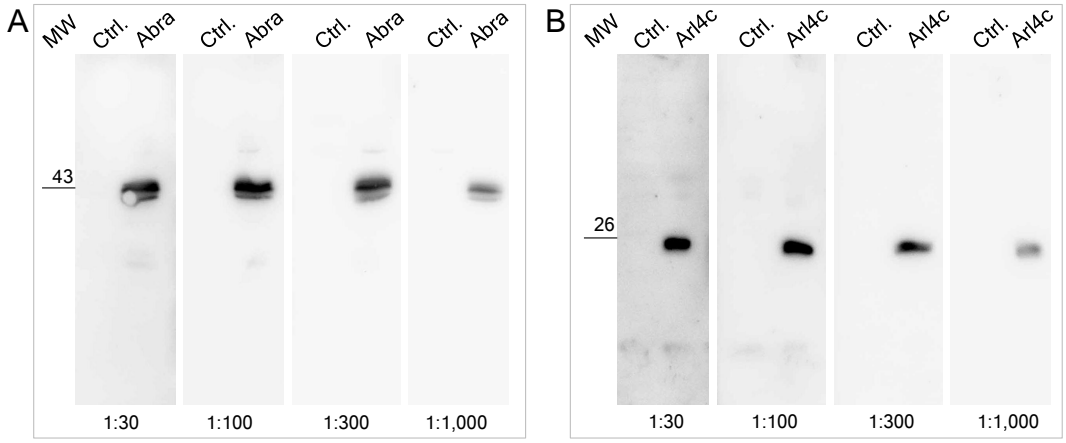

Figure 3.25: Titration of affinity-purified (A) anti-Abra and (B) anti-Arl4c antibodies. 20 µg of total protein lysates extracted from COS-7 cells transiently transfected with empty pcDNA3 vector (Ctrl.) or with pcDNA3 plasmids encoding Abra and Arl4c were separated on 12 % polyacrylamide gels. Separated proteins were transferred to a PVDF membranes. The membranes were first incubated with purified anti-Abra and anti-Arl4c rabbit antibodies diluted 1:30, 1:100, 1:300 and 1:1,000 and then with HRP-conjugated anti-rabbit antibodies. MW stands for protein molecular weight marker in kDa.

To investigate the influence of the putative LMX1B target genes on paxillin expression, conditionally immortalized murine podocytes were transiently transfected with expression plasmids for Abra, Arl4c, and Crct1. Protein samples from cells were separated on a 10% polyacrylamide gel and then transferred to a PVDF membrane. The membrane was then incubated with anti-paxillin and anti-GAPDH antibodies. Surprisingly, paxillin expression was increased in transfected podocytes regarding to the control. Thus, Abra and Crct1 induced the expression of paxillin 1.7-fold and Arl4c induced the expression of paxillin 1.3-fold (Figure 3.29).

3.9 Turnover of proteins involved in the formation of the actin cytoskeleton and focal adhesions

In several experiments Burghardt *et al.* demonstrated that LMX1B affects the organization of the actin cytoskeleton. For example, fibronectin-coated nanobeads attached to primary podocytes from *Lmx1b* knock-out mice moved significantly less than the beads attached to podocytes from control mice. Additionally, *Lmx1b*-deficient primary podocytes showed stronger phalloidin staining. Furthermore, primary podocytes isolated from inducible podocyte-specific *Lmx1b* knock-out mice adhered better to a laminin-coated surface than podocytes from control mice (Burghardt et al., 2013).

In view of these facts, the turnover of proteins involved in the regulation of the actin cytoskeleton and focal adhesions could provide essential pieces of information. For this purpose several proteins were investigated by Fluorescence Recovery After Photobleaching (FRAP). Initially FRAP studies were performed in stably transfected HeLa cells inducibly producing LMX1B (Subsection 3.9.1). After the identification of proteins which showed significant changes in their turnover studies were continued in primary podocytes isolated from quadruple transgenic mice (Subsection 3.9.2).

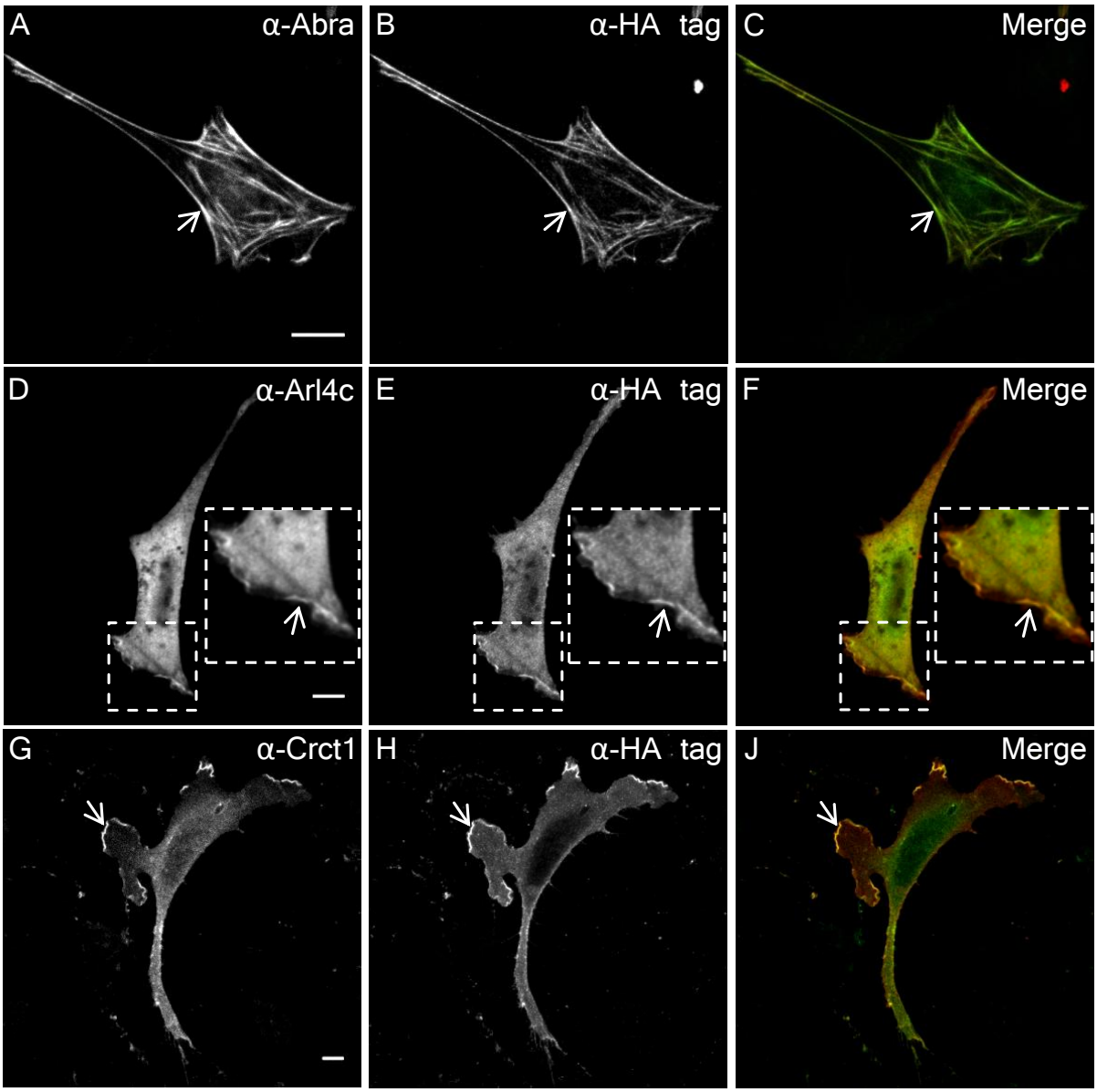

Figure 3.26: Immunofluorescence stainings of a murine podocyte cell line transiently transfected with expression plasmids for (A-C) Abra, (D-F) Arl4c and (G-I) Crct1 fused with a HA-tag. Cells were stained with (A) anti-Abra, (D) anti-Arl4c, (G) anti-Crct1 and (B, E, H) anti-HA-tag antibodies. Arrows show co-localization of the signal from the different antibodies. Scale bars, 10 µm.

3.9.1 FRAP studies in the HtTA-1/LMX1B cell line

Currently approximately 150 proteins involved in the formation of the actin cytoskeleton and focal adhesions are known (Zaidel-Bar et al., 2007). To study the effects of LMX1B on the actin cytoskeleton, the mobilities of several proteins such as α-actinin-1, α-actinin-4, actin, focal adhesion kinase (FAK), non-muscle myosin 9 heavy chain (MYH9), paxillin, talin, utrophin, vasodilator-stimulated phosphoprotein (VASP), vinculin and zyxin were studied using FRAP. Experiments were performed in the HtTA-1/LMX1B cell line grown in the presence or absence of doxycycline for 4 days. HtTA-1/LMX1B cells were

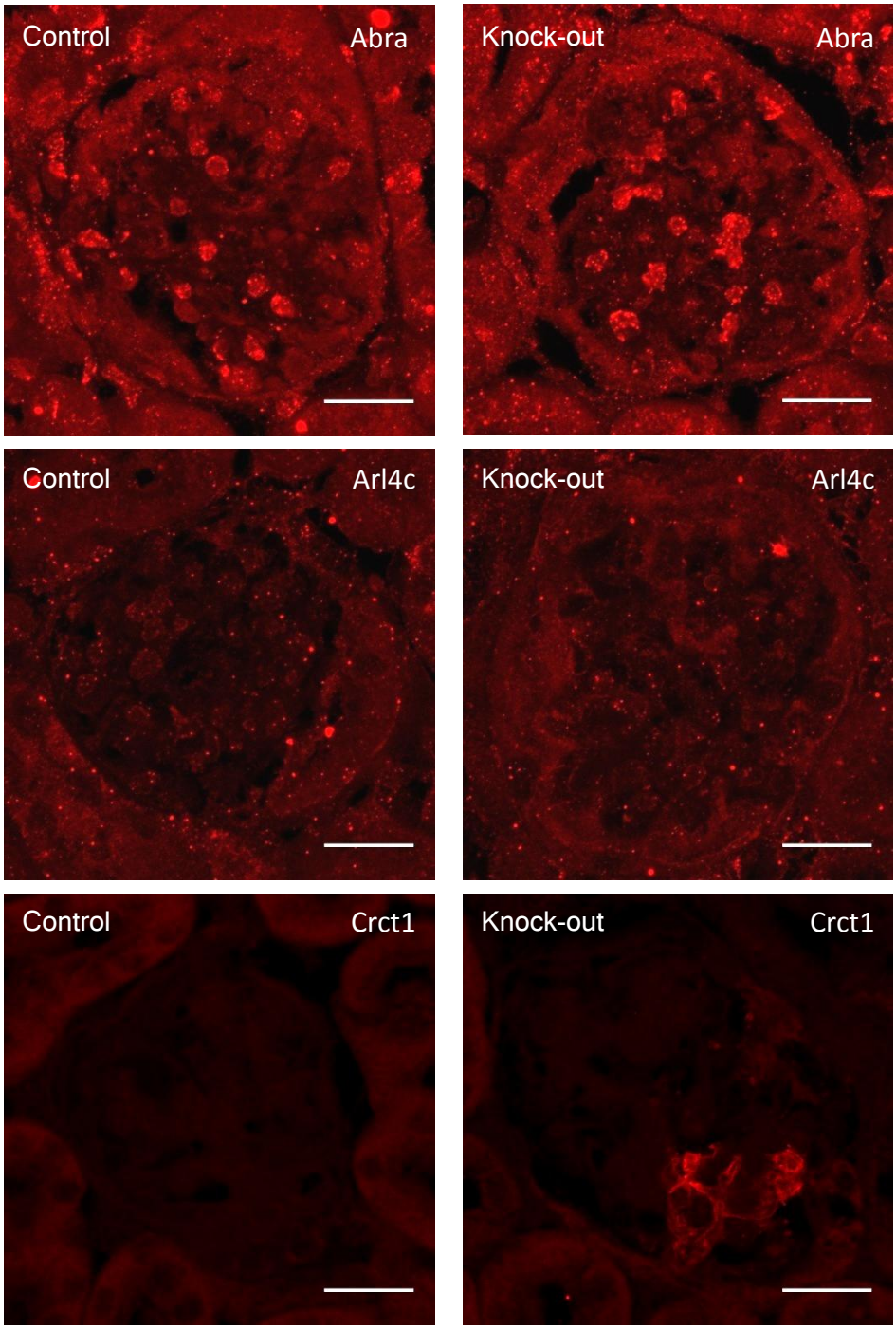

Figure 3.27: Staining for endogenous Abra, Arl4c and Crct1 in paraffin-embedded kidney sections. Kidneys were isolated from inducible podocyte-specific *Lmx1b* knock-out and control (Lmx1b$^{lox/lox}$, rtTA) mice administered 2 mg/ml doxycycline for 7 days. Sections were stained with anti-Abra, anti-Arl4c and anti-Crct1 antibodies. Scale bars, 20 µm.

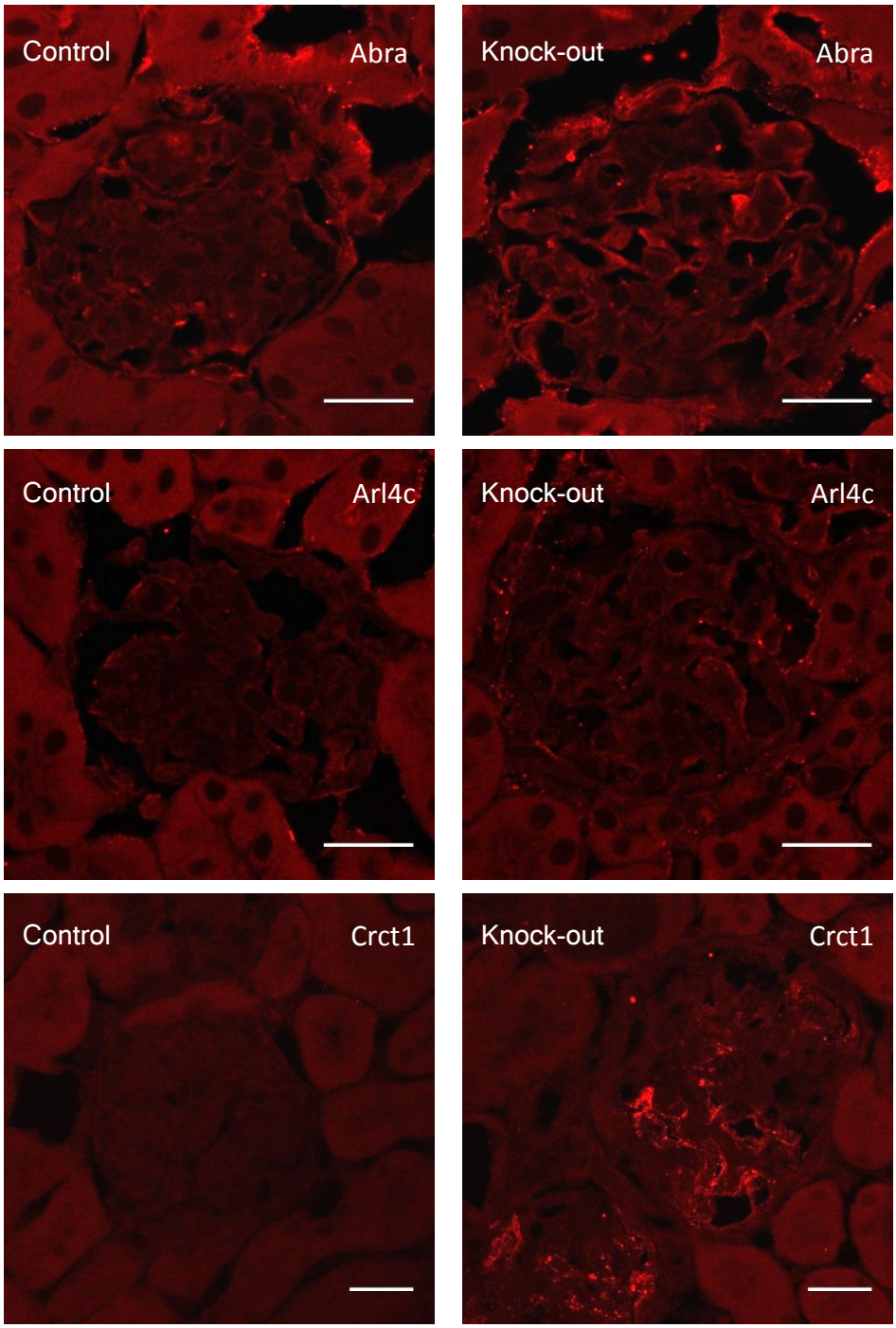

Figure 3.28: Staining for endogenous Abra, Arl4c, and Crct1 in frozen kidney sections. Kidney were isolated from inducible podocyte-specific *Lmx1b* knock-out and control ($Lmx1b^{lox/lox}$, rtTA) mice administered 2 mg/ml doxycycline for 7 days. Scale bars, 20 µm.

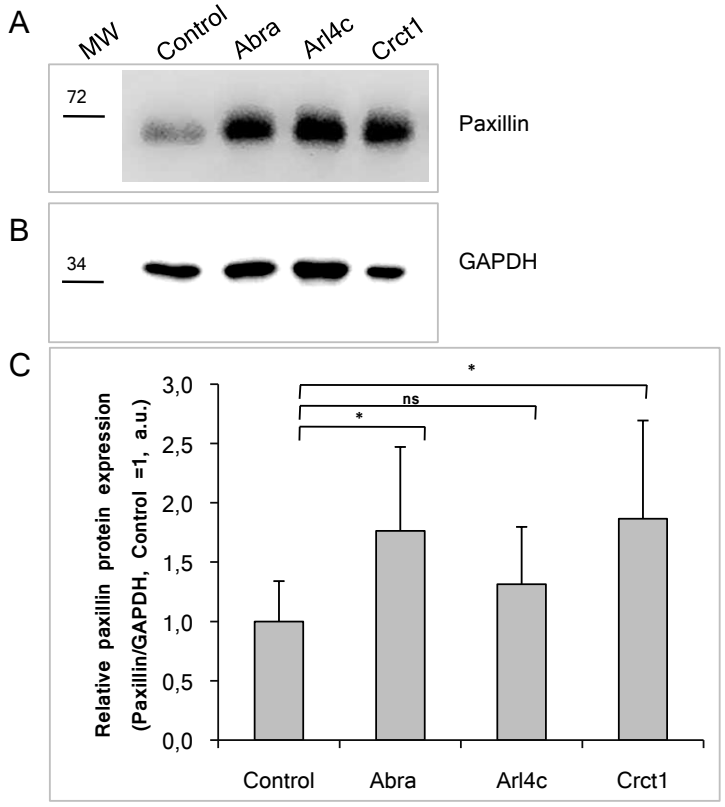

Figure 3.29: Paxillin expression is significantly affected in conditionally immortalized murine podocytes expressing Abra and Crct1, but not Arl4c. 10 μg of total protein lysates extracted from conditionally immortalized murine podocytes transiently transfected with an empty pcDNA3 vector (Control) or with pcDNA3 plasmids encoding Abra, Arl4c and Crct1 were separated on a 10% polyacrylamide gel. Separated proteins were transferred to a PVDF membrane. The membranes were incubated with mouse anti-paxillin and rabbit anti-GAPDH antibodies and then with HRP-conjugated anti-mouse and anti-rabbit antibodies, respectively. Representative immunoblots stained with (A) anti-paxillin and (B) anti-GAPDH antibodies. GAPDH was used as a loading control. (C) Histograms represent an average from at least three independent experiments made in triplicates (mean ± SDs). MW, *ns* and * stands for protein molecular weight marker in kDa, data not significant and $P<0.05$ (Student's t test), respectively.

transiently transfected with the expression plasmids for the cytoskeletal proteins. On the next day, the region of interest in the transfected cells was bleached and recovery of fluorescence was tracked over time. A single exponential equation was fitted to every measurement and three kinetic parameters – the recovery half-time $t_{1/2}$, the mobile fraction (MF) and the rate constant for the exchange of molecules between the bleached region and the surrounding area (K) were analyzed (Table 3.3).

The results obtained from HtTA-1/LMX1B cells transiently transfected with expression plasmids for α-actinin-1, α-actinin-1 and actin showed a similar tendency. In the presence of LMX1B the turnover of these proteins was faster. LMX1B significantly accelerated the recovery half-times of α-actinin-1, α-actinin-4, and actin by 35%, 19% and 48%, respectively. The rate constant for the exchange of molecules between the bleached region and the surrounding area increased 1.6-, 1.2-, and 1.5-fold for α-actinin-1, α-actinin-4 and actin, respectively. No significant changes were observed in the mobile fractions of all

tested cytoskeletal proteins. LMX1B showed no effect on the mobility of focal adhesion kinase, non-muscle myosin 9 heavy chain, paxillin, talin, utrophin, vasodilator-stimulated phosphoprotein, vinculin and zyxin in the HtTA-1/LMX1B cell line. The relative recovery half-times of proteins involved in the regulation of the actin cytoskeleton in HtTA-1/LMX1B and the recovery curves of normalized fluorescence intensities are presented in Figure 3.30 and Figure 3.31, respectively.

	$t_{1/2}$ [s]		MF [%]		K [1/s]	
LMX1B	+	−	+	−	+	−
α-actinin-1	3.5	5.4	72.3	78.6	0.27	0.17
α-actinin-4	6.3	7.7	72.3	69.0	0.13	0.11
Actin	1.4	2.7	85.9	84.3	0.62	0.42
FAK	0.7	0.7	80.7	77.6	1.59	1.69
MYH9	11.3	13.5	66.5	65.0	0.09	0.07
Paxillin	2.2	2.0	69.3	72.2	0.47	0.49
Talin	0.8	0.9	68.8	71.9	1.50	1.31
Utrophin	2.5	2.2	76.4	79.1	0.31	0.35
VASP	1.1	0.9	79.6	80.5	1.12	1.26
Vinculin	3.2	4.0	62.7	71.8	0.32	0.29
Zyxin	1.6	1.8	83.8	82.9	0.66	0.55

Table 3.3: Kinetic parameters of focal adhesion proteins and proteins associated with the actin cytoskeleton obtained from FRAP measurements in the HtTA-1/LMX1B cell line. "+", data obtained from Hela cells with LMX1B expression, "-", data obtained from Hela cells without LMX1B expression, $t_{1/2}$ denotes the recovery half-time, MF, the mobile fraction shown as percentage of total fraction (sum of mobile and immobile fractions $\bar{1}00\%$), and K, the rate constant for the exchange of molecules between the bleached region and the surrounding area. FAK, MYH9 and VASP stands for focal adhesion kinase, non muscle myosin heavy chain 9, and vasodilator-stimulated phosphoprotein, respectively.

3.9.2 FRAP studies in primary podocytes isolated from quadruple transgenic mice

Due to the effect of LMX1B on the mobility of α-actinin-1, α-actinin-4 and actin in HtTA-1/LMX1B cells, these proteins were subsequently analyzed in primary podocytes. Glomeruli isolated from quadruple transgenic *Lmx1b* heterozygous mice (Control) and *Lmx1b* homozygous mice (KO) administered 2 mg/ml of doxycycline for 7 days were cultured for 5 days to allow the outgrowth of podocytes. Then podocytes were transiently transfected with expression plasmids for α-actinin-1, α-actinin-4 and actin. 2 days after transfection, the region of interest in the transfected cells was bleached and recovery of fluorescence was tracked over time. A single exponential equation was fitted to every measurement and three kinetic parameters – the recovery half-time $t_{1/2}$, the mobile fraction (MF) and the rate constant for the exchange of molecules between the bleached region and the surrounding area (K) – were analyzed (Table 3.4).

Similarly to the results obtained from stably transfected HeLa cells inducibly producing LMX1B, mobilities of the proteins of interest were faster in the presence of LMX1B. The recovery half-times of α-actinin-1 and actin in podocytes from *Lmx1b* heterozygous mice (Control) were accelerated by 30% and 28%, respectively. However, the recovery

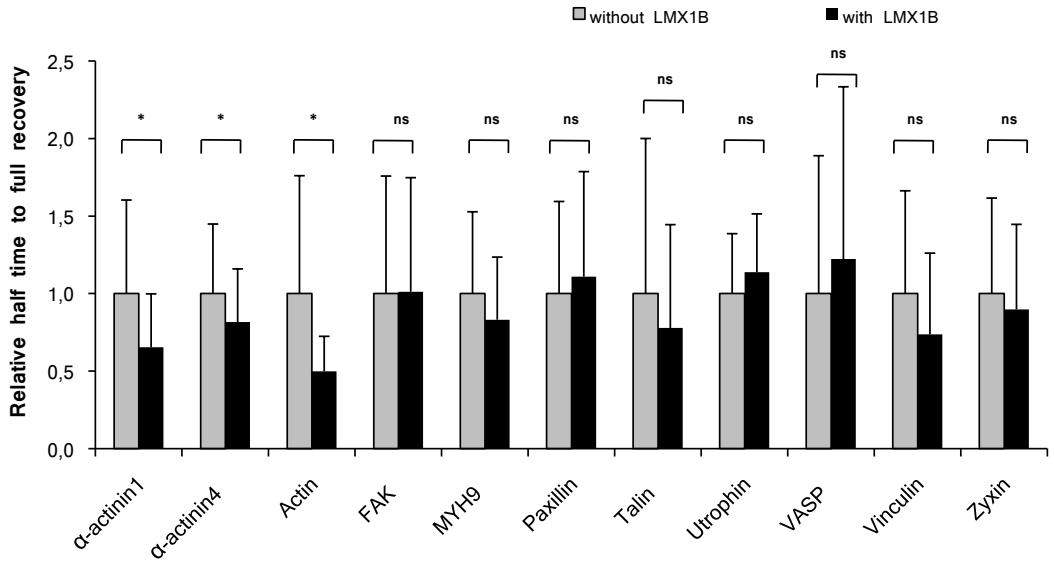

Figure 3.30: Relative recovery half-times of proteins involved in the regulation of the actin cytoskeleton in HtTA-1/LMX1B cells. The half-time to full recovery measured in cells without LMX1B expression equals 1. Histograms represent an average of at least three independent experiments (mean ± SDs). Here *ns* stands for data not significant, and * stands for $P<0.01$ (Student's t test).

half-time of α-actinin-4 was increased only by 12%. As expected, the rate constant for the exchange of molecules between the bleached region and the surrounding area increased 1.2-, 1.3-, 1.5-fold for α-actinin-1, α-actinin-4 and actin, respectively. Surprisingly, the mobile fraction of α-actinin-1 in *Lmx1b*-deficient podocytes decreased 13.7% relative to control podocytes. Mobile fractions of α-actinin-4 and actin showed no significant changes. The relative recovery half-times of proteins involved in the regulation of the actin cytoskeleton in primary podocytes and the recovery curves of normalized fluorescence intensities are presented in Figure 3.32 and Figure 3.33, respectively.

	$t_{1/2}$ [s]		MF [%]		K [1/s]	
	Control	**KO**	**Control**	**KO**	**Control**	**KO**
α-actinin-1	8.4	12.0	59.2	42.5	0.11	0.09
α-actinin-4	7.8	8.9	54.2	56.7	0.12	0.09
Actin	6.2	8.6	74.0	73.3	0.15	0.10

Table 3.4: Kinetic parameters of α-actinin-1, α-actinin-4 and actin obtained from FRAP measurements in primary podocytes isolated from quadruple transgenic *Lmx1b* heterozygous mice (Control) and *Lmx1b* homozygous mice (KO). $t_{1/2}$ denotes the recovery half-time, MF, the mobile fraction shown as percentage of total fraction (sum of mobile and immobile fractions $\bar{1}00\%$), and K, the rate constant for the exchange of molecules between the bleached region and the surrounding area.

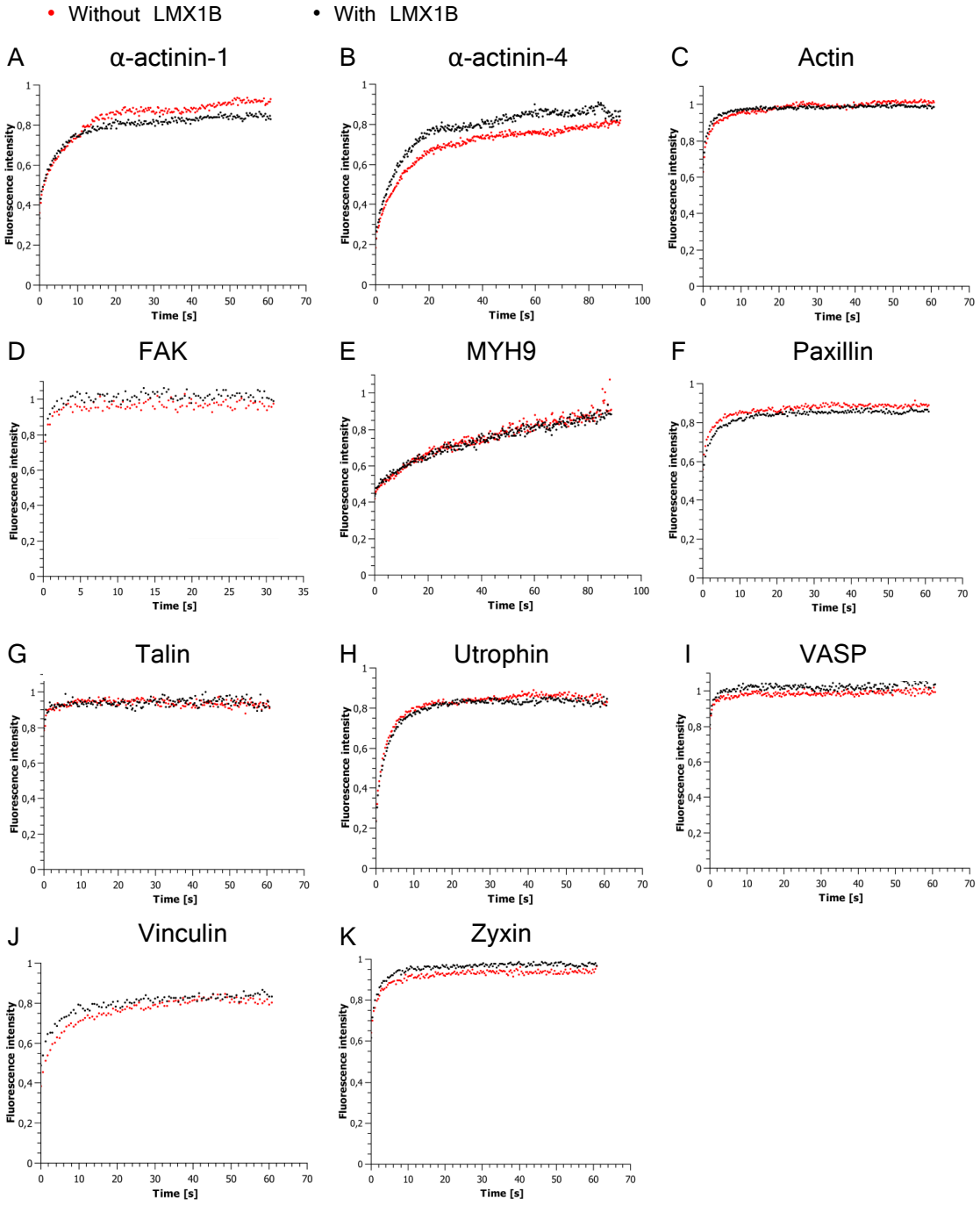

Figure 3.31: Turnover of proteins involved in the regulation of the actin cytoskeleton and focal adhesions in HtTA-1/LMX1B cells. Recovery curves of normalized fluorescence intensities of (A) EGFP-tagged α-actinin-1, (B) EGFP-tagged α-actinin-4, (C) EGFP-tagged actin, (D) mEmerald-tagged focal adhesion kinase (FAK), (E) mEmerald-tagged non-muscle myosin 9 heavy chain (MYH9), (F) mCherry-tagged paxillin, (G) mEmerald-tagged talin, (H) GFP-tagged utrophin, (I) mEmerald-tagged vasodilator-stimulated phosphoprotein (VASP), (J) venus-tagged vinculin and (K) mCherry-tagged zyxin in the HtTA-1/LMX1B cell line with (black) and without (red) LMX1B expression. Every curve was normalized by setting the pre-bleach intensity to 1. Approximately 60 recovery curves were analyzed. Data were collected from at least three independent experiments.

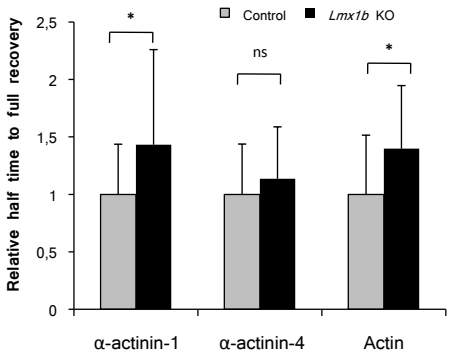

Figure 3.32: The relative recovery half-times of proteins involved in the regulation of the actin cytoskeleton in primary podocytes isolated from quadruple transgenic $Lmx1b^{lox/lox}$ (*Lmx1b* KO) and $Lmx1b^{+/lox}$ (Control) mice. The half-time to full recovery measured in primary podocytes obtained from $Lmx1b^{+/lox}$ (Control) mice equals 1. Histograms represent an average of at least three independent experiments (mean ± SDs). Here *ns* stands for data not significant, and * stands for $P<0.01$ (Student's t test).

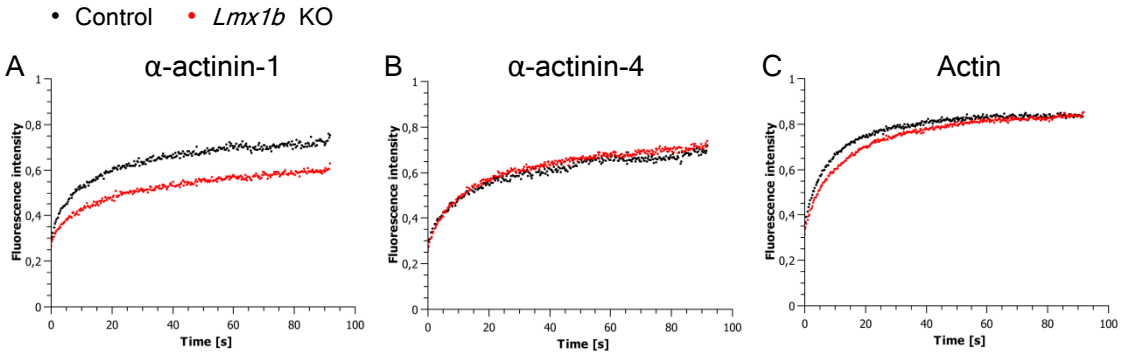

Figure 3.33: Turnover of proteins involved in the regulation of the actin cytoskeleton in primary podocytes isolated from quadruple transgenic mice. Recovery curves of normalized fluorescence intensities of (A) mCherry-tagged α-actinin-1, (B) α-actinin-4, and (C) actin in primary podocytes isolated from quadruple transgenic $Lmx1b^{lox/lox}$ (*Lmx1b* KO – red) and $Lmx1b^{+/lox}$ (Control – black) mice. Every curve was normalized by setting the pre-bleach intensity to 1. Approximately 30 recovery curves were analyzed. Data were collected from at least three independent experiments.

Chapter 4

Discussion

Approximately 40% of NPS patients suffer from renal symptoms which result from a thickened glomerular basement membrane and foot process effacement (Sweeney et al., 2003; Witzgall, 2008; Lemley, 2009). More than 140 mutations in the *LMX1B* gene have been identified in patients with NPS. Roughly 18% of these mutations are concentrated in the homeodomain which mediates the binding of LMX1B to its target genes (Bongers et al., 2002). As reported previously, LMX1B regulates the transcription of several genes, including the *Col4a3*, the *Col4a4*, the *Cd2ap*, and the *Nphs2* genes which code for the α3 and α4 chains of collagen IV in the GBM, for the CD2-associated protein, and for podocin, respectively (Morello et al., 2001; Miner et al., 2002). However, the expression of podocin and of the α3 and α4 chains of collagen IV is not altered in the constitutive podocyte-specific *Lmx1b* knock-out mice (Suleiman et al., 2007) and in kidney biopsies from NPS patients (Heidet et al., 2003). In order to understand the molecular mechanisms which lead to the development of NPS, it is necessary to answer the following question: which genes are regulated by LMX1B? In search for the downstream targets of LMX1B, microarray studies of glomeruli isolated from inducible podocyte-specific *Lmx1b* knock-out mice were performed. This analysis revealed that the expression of several genes was altered in *Lmx1b* knock-out mice, compared with findings for control mice, following the administration of doxycycline (Burghardt et al., 2013). For further investigation three promising LMX1B target genes, which have shown an upregulation after *Lmx1b* inactivation, were chosen: *Abra*, *Arl4c* and *Crct1*.

4.1 Effect of LMX1B on its putative target genes

Previous reports demonstrated that LMX1B is able to regulate transcription of its target genes by binding to the adenine and thymine-rich sites in the promoter region, the FLAT elements (German et al., 1992; Morello et al., 2001; Miner et al., 2002; Rohr et al., 2002; Rascle et al., 2009). Bioinformatic studies of 6-kbp promoter fragments of the putative LMX1B target genes led to the identification of several FLAT elements (Table 3.1). Additionally, the recruitment of LMX1B to FLAT elements within the *ABRA* and *ARL4C* promoter regions was demonstrated by ChIP and EMSA assays (Burghardt et al., 2013). To understand how LMX1B regulates the transcription of these genes, luciferase assays of reporter constructs bearing FLAT elements, which have shown binding of LMX1B, were performed. In HtTA-1/LMX1B cells ABRA and ARL4C expression were modestly reduced by LMX1B (Subsection 3.2.2). The previously described microarray data demonstrated that in the mouse kidney LMX1B negatively regulates expression of the

same genes (Burghardt et al., 2013), but the effects in the mouse were stronger. The discrepancies between the data obtained from the two approaches could be explained for example by: (a) the difference of LMX1B cofactors in the mouse kidney and in HtTA-1/LMX1B cell line, (b) the investigated promoter fragments contained only a short region possibly without other regulatory regions of DNA necessary for their correct transcription, and (c) the absence of histones in the reporter constructs. Surprisingly, mutations in the FLAT sequence within the investigated promoter fragments caused stronger inhibitory effects by LMX1B. Collectively, the obtained data lead to two hypotheses. In the first scenario LMX1B collaborates with the other transcription factor which downregulates the expression of a target gene. When LMX1B binds to the FLAT elements within its target genes, it inhibits the activity of a transcriptional repressor. Mutations in the FLAT element impede the binding of LMX1B to its target genes so that LMX1B is no longer able to inhibit the transcriptional repressor. Thereby, a higher inactivation of LMX1B downstream targets is caused. In another scenario, the binding of LMX1B to the FLAT element blocks the access to the promoter by the other transcription factor. However, when the FLAT element is mutated and LMX1B is not able to bind it, the other transcription factor binds to the promoter and negatively regulates expression of the target genes (Figure 3.9).

4.2 Subcellular and ultrastructural localization of Abra, Arl4c and Crct1

The subcellular localization of proteins provides key insights into their function, interaction and cellular signaling pathways (Stadler et al., 2013). Among the various possibilities to visualize the proteins under investigation, the immunofluorescence technique was chosen. Therefore the coding sequences of mouse Abra, Arl4c and Crct1 were fused to the human influenza hemagglutinin (HA) epitope tag (Pati, 1992) and expressed in primary podocytes. In this study, Abra was associated with actin stress fibers (Subsection 3.3.1) as previously demonstrated (Arai et al., 2002), suggesting that Abra provides structural support for cells. However, neither Arl4c nor Crct were associated with actin filaments. Instead they were distributed diffusely in the cytoplasm of primary podocytes (Subsection 3.3.1). Additionally, Arl4c demonstrated a membrane-associated localization, predominantly at regions exhibiting membrane ruffling. The protein accumulated at the ends of actin filaments, similarly to focal adhesion proteins. Arl4c is known to interact with the focal adhesion protein paxillin via ARNO, also known as cytohesin-2 (Torii et al., 2010). Therefore, this implies that Arl4c plays a role in cell attachment and spreading. Because Arl4c belongs to the family of small GTPases (Jacobs et al., 1999), its subcellular distribution depends on binding to GTP or GDP. Additional studies on Arl4c fused with EYFP demonstrated that the wild-type form and the constitutively active GTP-bound mutant of Arl4c were associated with the plasma membrane in filopodia and lamellipodia, while the inactive GDP-bound Arl4c mutant was detected in the perinuclear region of the cell as small vesicular structures (Subsection 3.3.3). The data obtained are in agreement with previous findings showing distinct subcellular distributions for Arl4c (Engel et al., 2004). Engel *et al.* proposed a possible involvement of Arl4c in actin filament assembly and/or reorganization (Engel et al., 2004). The overexpression studies of Crct1 demonstrated for the first time its membrane-associated localization at lamellipodia above cortical actin (Subsection 3.3.1), where it may initiate actin polymerization.

The ultrastructural localization of proteins in cells and tissues became possible due to the invention of the immunogold labeling technique by Faulk and Taylor in 1971 (Faulk and Taylor, 1971). However, this technique has several limitations. For example, it is necessary to generate high-affinity and highly selective antibodies. Strong fixation, which is necessary for optimal preservation of ultrastructure and visibility of cellular organelles, can hamper the diffusion of antibodies and gold particles (Hermann et al., 1996; Zhu et al., 2011). Substitution of gold particles by eosin resulted in improved penetration of eosin-conjugated antibodies, but cell permeabilization was still necessary (Deerinck et al., 1994). The discovery of genetically encoded tags such as ReAsH (Gaietta et al., 2002) or miniSOG (Shu et al., 2011) significantly improved the ultrastructural visualization of proteins in cells. Therefore, to visualize Abra, Arl4c and Crct1 by transmission electron microscopy, it was decided to use the miniSOG tag. Unexpectedly, localization of transfected cells with a fluorescence microscope encountered one difficulty: green fluorescence emitted by the miniSOG protein was gone within a few seconds after excitation. This problem was solved by a fellow PhD student, Benjamin Salecker, who subcloned the mCherry cDNA upstream of miniSOG (5'-mCherry-miniSOG-cDNA of interest-3').

miniSOG-fused Abra, Arl4c, and Crct1 were successfully localized by transmission electron microscopy in a human podocyte cell line. The data indicate that the proteins can be detected at several intracellular sites. Abra was localized at actin-like filamentous structures in the cytoplasm, thus confirming the previously described data obtained from confocal microscopy. Additionally, the membrane-associated distribution of Abra was detected at lamellipodia, possibly at the leading edge of the cell. Arl4c was localized at actin-like filamentous structures, but possibly at the trailing edge of the cell. These findings suggest a role for Abra and Arl4c in cell migration. However, to gain a better understanding of the role played by these proteins in cell migration, additional studies, such as the spatio-temporal regulation of Abra and Arl4c activity in motile cells, need to be performed. Arl4c and Crct1 have shown a membrane-associated distribution at filopodia. Moreover, Crct1 was localized to actin-like filamentous structures at cell protrusions and at sites of contact to the neighboring cell (Subsection 3.3.5). These data indicate that in podocytes Crct1 links membrane proteins of foot processes to the slit diaphragm.

The results of the subcellular and ultrastructural localization of Abra, Arl4c and Crct1 by confocal and electron microscopy suggest their functional involvement with the actin cytoskeleton. The present study confirmed the specific association of Abra with F-actin (Figure 3.10, C), where it may stimulate formation and/or stabilization of microfilaments (Arai et al., 2002). Additionally, Abra, Arl4c and Crct1 have shown a localization near the plasma membrane where they may also play a role in actin polymerization (Wang, 1985). In summary, these findings suggest that LMX1B controls two different sets of proteins through their transcriptional regulation: one set initiates actin formation at plasma membrane, and the other stabilizes F-actin once it is formed (Figure 4.1).

4.3 Regulation of the actin cytoskeleton by LMX1B and its target genes

A number of glomerular diseases originating from podocyte dysfunction involve the actin cytoskeleton. Upon podocyte injury the coordinated parallel bundles of actin filaments change into an interwoven network and the expression of actin increases (Shirato et al.,

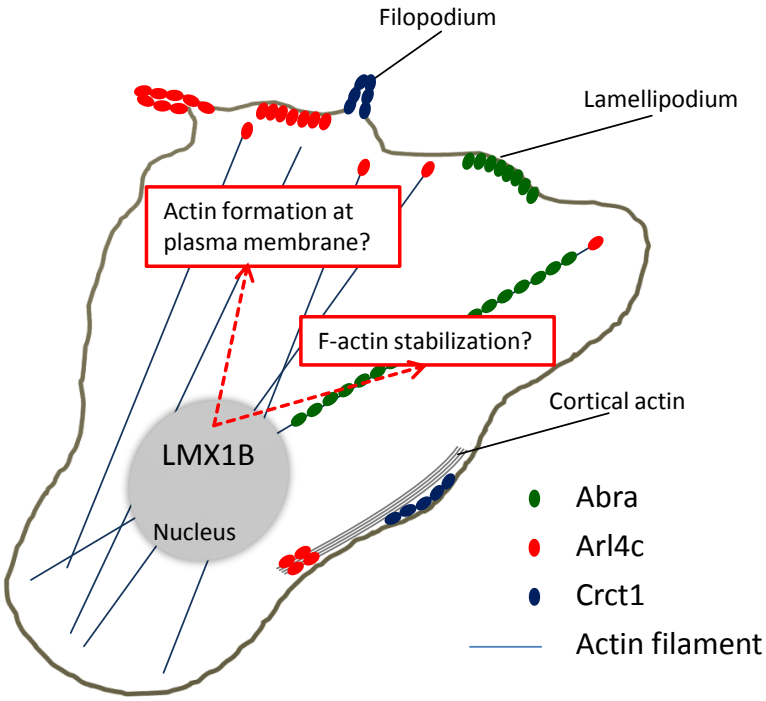

Figure 4.1: Scheme of subcellular and ultrastructural localization of Abra, Arl4c and Crct1. Abra (green ellipses) is associated with actin stress fibers and with membrane at lamellipodia. Arl4c (red ellipses) is are associated with membrane at lamellipodia and filopodia. It is localized at the ends of F-actin filaments. Additionally, Arl4c is possibly associated with a cortical actin. Crct1 (blue ellipses) is associated with membrane at lamellipodia above the cortical actin and at filopodia. Moreover, it is distributed at actin-like filamentous structures at cell protrusions and at sites of contact to the neighboring cell. In summary, LMX1B controls two different set of proteins through their transcriptional regulation: one set initiates actin polymerization at plasma membrane, and the other, stabilizes F-actin.

1996; Kerjaschki, 2001). Foot process effacement in the podocyte-specific *Lmx1b* knockout mice is obvious. However, primary podocytes isolated 1 week after the inactivation of *Lmx1b* demonstrated a decreased motility and an increased formation of F-actin. These data suggest a possible role of LMX1B in the dysregulation of the actin cytoskeleton by increasing its stiffness (Burghardt et al., 2013). To determine whether the putative LMX1B targets regulate the actin cytoskeleton, primary podocytes were transiently transfected with expression plasmids for Abra, Arl4c and Crct1 and stained with phalloidin. Transfected podocytes showed a stronger fluorescence (Subsection 3.3.2), indicating that the proteins under investigation lead to the increased formation of F-actin (Burghardt et al., 2013). These findings are consistent with published studies demonstrating the role of Abra in the stimulation of F-actin formation (Arai et al., 2002) and the importance of Arl4c in the rearrangement of actomyosin (Matsumoto et al., 2014).

Overexpression of constitutively active Arl4c, Arl4c Q71L, significantly stimulated the formation of F-actin. Surprisingly, overexpression of dominant-negative Arl4c, Arl4c T27N, also stimulated the formation of F-actin, though to a smaller extent (Subsection 3.3.4). The data obtained can be explained by the fact that Arl4c T27N, which is predicted to be in the GDP-bound form, possibly loses its nucleotide (Macia et al., 2004). Biochemical

studies of another small GTP-binding protein, Arf6, by Macia *et al.* revealed that the Arf6 T27N mutant cannot be used to mimic the GDP-bound form. This mutant cannot bind GDP and was unstable (Macia et al., 2004). Macia *et al.* suggested that other small G-proteins could suffer from a similar problem. Therefore, to investigate the cellular functions of Arl4c can be used alternative dominant-negative mutant which carries the T44N mutation.

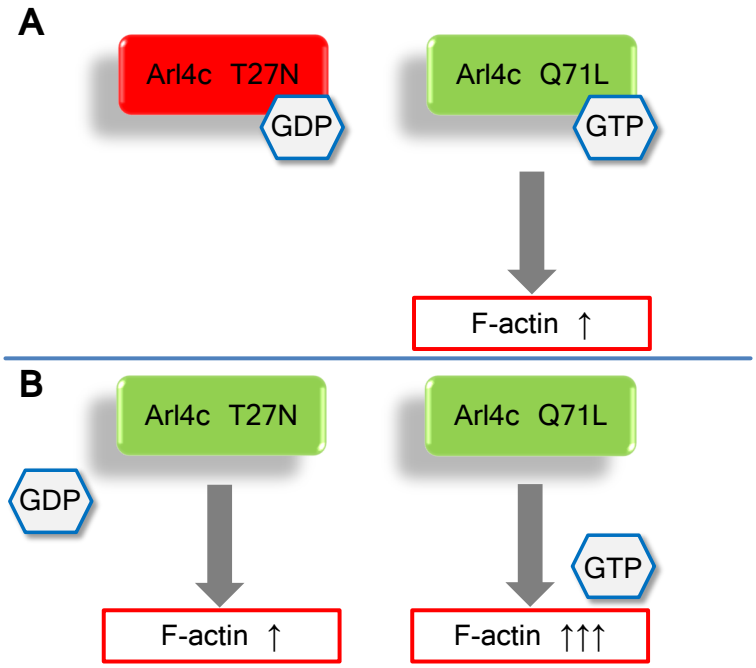

Figure 4.2: Regulation of F-actin formation by Arl4c mutant proteins. Two mutants of Arl4c, Arl4c T27N and Arl4c Q71L, mimic the GDP- and GTP-bound forms, respectively. (A) According to expectations only the activation of Arl4c (Arl4c Q71L) leads to the increased formation of F-actin. (B) In the present study both the dominant-negative and the constitutively active mutant forms of Arl4c displayed increased F-actin formation, suggesting that Arl4c T27N, which is predicted to be in the GDP-bound form, loses its nucleotide. The dominant-negative mutant, Arl4c T27N, stimulated the formation of F-actin to a smaller extent (↑) in comparison to constitutively active Arl4c Q71L (↑↑↑).

The actin cytoskeleton is crucial in mediating cell shape changes as well as in maintaining stable cell shape. It is able to behave either fluid-like to accommodate structural rearrangements, or solid-like to preserve cell shape (Norstrom and Gardel, 2011). The transition between fluid- and solid-like behavior is associated with changes in the concentration of cross-linker protein(s) and of F-actin, and modulations of F-actin length (Stricker et al., 2010). Therefore, to determine the possible reason for the formation of a stiffer actin cytoskeleton after the inactivation of *Lmx1b* or after the expression of Abra, Arl4c and Crct1, the F- to G-actin ratio was examined. The expression of LMX1B and its targets did not cause any significant changes in the polymerization of F-actin in HtTA-1/LMX1B cells and in a murine podocyte cell line, respectively (Subsections 3.4.1 and 3.4.2). The estimation of the F- to G-actin ratio in primary podocytes failed because it was not possible to isolate a sufficient number of cells. Alternatively, to measure G-actin fluorescently labelled deoxyribonuclease I (DNaseI) can be used for further experiments (Cramer et al., 2002; Flavahan et al., 2005). Assuming that LMX1B and its targets have no influence on

the F- to G-actin ratio in primary podocytes as well, the observed increase in F-actin level may result from the decrease in cell size. In fact, podocytes which expressed LMX1B target genes were significantly smaller than the control podocytes (data not shown). However, it remains unknown whether the cells were shrunken or the total cell volume was decreased. A reduction in intracellular space was likely associated with an increased density of microfilaments. As a result it could lead to increased phalloidin intensity. Altogether these data suggest that LMX1B causes changes in podocyte morphology which lead to the F-actin reorganization and generation of stiffer actin cytoskeleton with no alterations in net F- to G-actin ratio. The proposed scheme for the formation of a stiffer actin cytoskeleton by LMX1B and its target genes is shown in Figure 4.3.

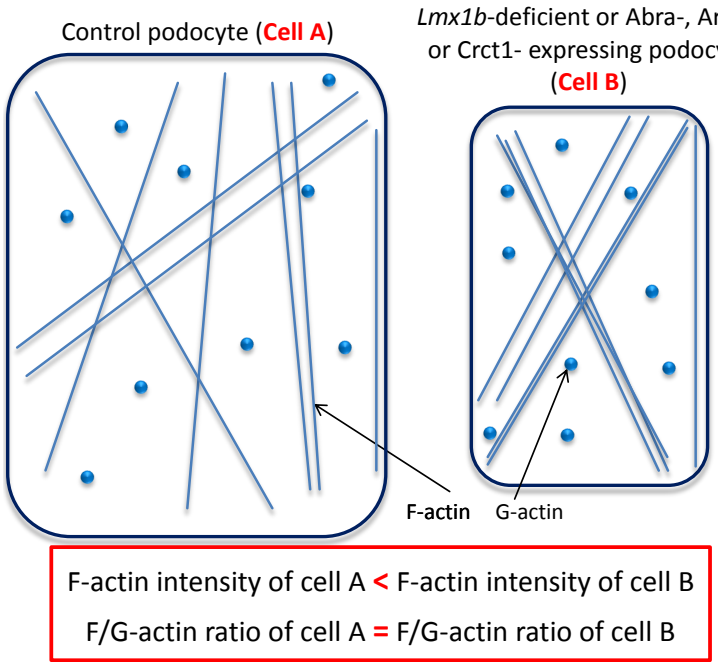

Figure 4.3: Scheme for the generation of a stiffer actin cytoskeleton by LMX1B and its target genes. LMX1B causes changes in podocyte morphology which lead to the F-actin reorganization with no alterations in net F- to G-actin ratio. Possibly LMX1B and its target genes increase the stiffness of actin filaments by cross-linking them to thick, tightly packed bundles.

Previously it was demonstrated that the stiffness of actin filaments is enhanced by actin-associated proteins such as α-actinin and filamin (Esue et al., 2009). Therefore to comprehend better the mechanisms of regulation of the actin cytoskeleton by LMX1B and its target genes, the expression of these proteins in *Lmx1b*-deficient podocytes can be examined in detail in the future.

4.4 Glomerular distribution of Abra, Arl4c and Crct1 after the podocyte-specific inactivation of *Lmx1b*

For studying the glomerular distribution of Abra, Arl4c and Crct1 after the podocyte-specific inactivation of *Lmx1b*, immunofluorescence analysis of kidney sections were performed. Because commercial specific antibodies were unavailable, these antibodies were

generated.

To produce recombinant Abra, Arl4c and Crct1, the complete coding sequences for murine Abra and Crct1 and the incomplete for murine Arl4c (132 to 192 amino acids) were cloned into the expression vector pET-21a. The recombinant proteins were solubilized from inclusion bodies and then purified on Ni^{2+}-charged His-Bind resin. As was demonstrated by Western blot analysis, the recombinant proteins were detected with an anti-His-Tag antibody. However, only Abra was detected at the predicted molecular weight of approximately 43 kDa. Arl4c and Crct1, which are predicted to be 8.5 kDa and 13.1 kDa proteins, respectively, migrated slightly higher on polyacrylamide gels. Additional upper bands for Arl4c and Crct1 of approximately 17 kDa and 26 kDa, respectively, which correspond to twice the molecular weight predicted, were detected as well. The upper bands could be explained by either 1) an incomplete reduction of the samples or 2) the possible dimerization of the proteins. Peptide sequences of Abra and Arl4c, including the upper band of Arl4c, were identified by mass spectrometry. Crct1 peptide sequences were not identified by mass spectrometry probably because of the high cysteine contents within the sequence. Only one peptide, comprising the T7-tag, was found for the Crct1 protein (Section 3.5). The identification of the His-tag and the T7-tag suggests that the purifed recombinant protein is Crct1. In the final step two rabbits were immunized with each protein preparation.

The specificity of the antisera was validated by Western blot (Bordeaux et al., 2010). The anti-Abra and anti-Arl4c antibodies were able to recognize the respective antigens in transiently transfected COS-7 cells (Section 3.6). However, the anti-Crct1 antibody was not able to recognize Crct1 and for further studies a commercial goat anti-Crct1 antibody was used. Because in Western blots multiple nonspecific bands were observed, it was decided to affinity-purify the rabbit antisera before further applications. After this step the specificity of antibodies was validated again by Western blot. Additionally the proper distribution of Abra, Arl4c, and Crct1 was demonstrated by double immunofluorescence stainings of a murine podocyte cell line transiently transfected with expression plasmids for HA-tagged Abra, Arl4c and Crct1 with an anti-HA and anti-Abra, anti-Arl4c and anti-Crct1 antibodies (Section 3.6).

The analysis of paraffin-embedded kidney sections revealed that Abra was located in some cells of the glomerulus. However, no differences in the expression level of Abra after the podocyte-specific inactivation of *Lmx1b* were observed. No distinct signal for Abra in frozen kidney sections stained with the anti-Abra antibody was observed (Section 3.7). The difference in the results obtained with tissues embedded according to two different protocols could be explained by using heat-mediated epitope retrieval of paraffin-embedded kidney sections. This step breaks protein cross-linkages formed during perfusion with paraformaldehyde, thus "unmasking" the epitope of interest (Leong and Leong, 2007).

Immunofluorescence stainings of paraffin-embedded and frozen kidney sections with the anti-Arl4c antibodies were not successful (Section 3.7). If Arl4c is present in the kidneys, then possible reason for not being detected could be post-translational modifications of Arl4c, the inability of the anti-Arl4c antibodies to penetrate into the tissue, or low expression levels of Arl4c. The use of other antibodies that recognize other Arl4c epitopes may solve the problem.

Examination of paraffin-embedded and frozen kidney sections stained with the anti-Crct1 antibodies revealed that the expression of Crct1 was markedly increased in the glomeruli of the inducible podocyte-specific *Lmx1b* knock-out mice compared with control

kidney sections (Section 3.7). To further clarify the exact glomerular localization of Crct1, double-immunofluorescence stainings must be performed with the anti-Crct1 antibody and podocyte markers like nephrin, podocin, CD2-associated protein, podocalyxin (Koop et al., 2003), WT-1, vimentin, synaptopodin, or α-actinin-4 (Testagrossa et al., 2013), endothelial cells markers like CD31 or CD34 (Takano et al., 2007), and with mesangial cells marker like α-smooth muscle actin (α-SMA) (Takano et al., 2007) .

4.5 Influence of the putative LMX1B target genes on cell-matrix contacts

Structural and functional anomalies in the glomerular filtration barrier including podocyte foot process effacement lead to proteinuria (Bains et al., 1997; Zhang and Huang, 2012). During proteinuria podocytes detach from the basement membrane (Whiteside et al., 1989; Whiteside et al., 1993; Mundel and Shankland, 2002). The exact molecular mechanisms behind this are not completely understood. Koukouritaki *et al.* demonstrated an enhanced expression of paxillin in experimental nephrotic syndrome, suggesting its possible role in regulating the adhesion of podocytes to the GBM (Koukouritaki et al., 1998). Burghardt *et al.* observed that more podocytes grew out of freshly isolated glomeruli after the inactivation of *Lmx1b*. In a replating assay, primary podocytes isolated from inducible podocyte-specific *Lmx1b* knock-out mice better adhered to a laminin-coated surface than podocytes from control mice (Burghardt et al., 2013). However, the focal contact area of primary podocytes with or without an inactivated *Lmx1b* gene examined by immunofluorescence staining with an anti-paxillin antibody showed no difference (Burghardt et al., 2013). To get a better insight on the role of the putative LMX1B target genes on cell-matrix contacts, protein lysates of conditionally immortalized murine podocytes transiently transfected with expression plasmids for Abra, Arl4c and Crct1 were analyzed by Western blot for paxillin expression. Surprisingly, paxillin expression was significantly affected in podocytes expressing Abra and Crct1, but not Arl4c (Section 3.8).

It was demonstrated previously that the activation of RhoA modulates actin polymerization which is initiated by the recruitment of paxillin-vinculin complexes and FAK to cell adhesomes (Zhang et al., 2012). Moreover, it is known that Abra activates RhoA (Arai et al., 2002) while Arl4c inhibits this small GTPase protein (Matsumoto et al., 2014). Therefore the differences in the effect of Abra and Arl4c on paxillin expression could be explained by their opposite effect on RhoA. It would be interesting to confirm this hypothesis and to examine additionally whether Crct1 and LMX1B could be implicated in the regulation of RhoA.

Taken together, these observations suggest a possible role of Abra and Crct1 in the initiation of actin polymerization and/or enhanced podocyte adhesion via paxillin. From the experiments shown here we cannot conclude whether RhoA is involved in this pathway. Therefore, additional studies must be performed such as assessment of RhoA activation, Western blot with antibodies directed against other cell adhesion proteins, as well as replating and migration assays of murine podocytes transiently transfected with expression plasmids for Abra, Arl4c and Crct1 to corroborate such a hypothesis.

4.6 Role of LMX1B in the regulation of cell-matrix adhesion dynamics

Podocyte foot processes are highly dynamic structures and their motility must be finely regulated in order to maintain the correct function of the glomerular filtration barrier (Peti-Peterdi and Sipos, 2010; Welsh and Saleem, 2011; Noris and Remuzzi, 2012). Changes in their dynamics, such as hyper- or hypomotility, can lead to foot process effacement (Wang et al., 2012; Kistler et al., 2012). Focal adhesion proteins such as $\alpha_3\beta_1$-integrin, actin, talin, vinculin and α-actinin enable podocytes to attach to the glomerular basement membrane and play an essential role in the regulation of actin cytoskeleton dynamics and cell motility (Lauffenburger and Horwitz, 1996; Smoyer et al., 1997).

Burghardt *et al.* demonstrated that LMX1B affects actin cytoskeleton organization and dynamics. For example, *Lmx1b*-deficient primary podocytes showed stronger phalloidin staining. Additionally, fibronectin-coated nanobeads attached to primary podocytes from *Lmx1b* knock-out mice moved significantly less than beads attached to podocytes from control mice. Furthermore, *Lmx1b*-deficient primary podocytes adhered better to a laminin-coated surface than podocytes from control mice (Burghardt et al., 2013). In view of these facts, the further analysis of the role of LMX1B in the dynamics of the podocyte actin cytoskeleton is essential in deciphering the molecular mechanisms that lead to proteinuria and foot process effacement in nail-patella syndrome. For this purpose the turnover of several proteins involved in the regulation of the actin cytoskeleton and focal adhesions was investigated by Fluorescence Recovery After Photobleaching (FRAP).

The data revealed that LMX1B was required to accelerate the dynamics of α-actinin-1, α-actinin-4 and actin, but not that of focal adhesion kinase, non-muscle myosin heavy chain IIA, paxillin, talin, utrophin, vasodilator-stimulated phosphoprotein, vinculin or zyxin in HtTA-1/LMX1B cells (Subsection 3.9.1). There were only very small immobile fractions of the proteins, suggesting that these focal adhesion proteins are highly dynamic. The mobile and immobile fractions as well as the rate constant for the exchange of molecules between the bleached region and the surrounding area were not significantly affected by LMX1B (Subsection 3.9.1). In accordance with previous studies (Lavelin et al., 2013), we demonstrated that all proteins of interest were recovered in less than one or only a few seconds. Thus, Lavelin *et al.* demonstrated that FAK, paxillin, talin, VASP, vinculin and zyxin in HeLa cells showed a comparable half-time of recovery of about 0.5-2 s (Lavelin et al., 2013). In contrast, utrophin in oocytes and α-actinin-1 in fibroblasts demonstrated slower recovery half-times of approximately 39.3 s, and 5 min, respectively (Burkel et al., 2007; Edlund et al., 2001). In endothelial cells actin is exchanged in focal adhesions with a half-time of more than 1 min (Le Dévédec et al., 2012), while at the leading edge of HeLa cells with approximately 5 s (Lorente et al., 2014). The differences in dynamics of all proteins of interest can be explained by the origin of HtTA-1/LMX1B cell line derived from a cervical cancer. Lorente *et al.* suggested that a high level of actin dynamics is a common characteristic of some cancer cells and is essential for its invasion and metastasis (Lorente et al., 2014). In fact, the investigations of the turnover of α-actinin-1, α-actinin-4 and actin in primary podocytes isolated from quadruple transgenic mice demonstrated decreased protein dynamics, however within a similar range, from 6 to 8 s (vs. from 1 to 6 s). The inactivation of *Lmx1b* lead to the decreased mobility of these proteins. However, the changes in the turnover of α-actinin-4 were not statistically significant. Surprisingly, the mobile fraction of α-actinin-

1 in *Lmx1b*-deficient podocytes decreased 13.7% relative to control podocytes. Mobile fractions of α-actinin-4 and actin showed no significant changes (Subsection 3.9.2).

These studies demonstrated for the first time that the protein turnover of α-actinin-1 and actin was notably affected by the inactivation of *Lmx1b*. The dynamics of these proteins was significantly decreased. However, LMX1B did not induce changes in the dynamics of α-actinin-4, which is known to cause focal segmental glomerulosclerosis (Kaplan et al., 2000). Taken together, these results support the idea that LMX1B is involved in the regulation of actin cytoskeleton (Burghardt et al., 2013). By decreasing the mobility of α-actinin-1 and actin, LMX1B may strengthen the linkage between podocytes and the extracellular matrix. Additionally, it stabilizes F-actin at the cell edge. The next questions to be addressed are: does LMX1B regulate the dynamics of α-actinin-1 and actin via its target genes, and is it essential for focal adhesion assembly and disassembly as well?

4.7 Summary

The main purpose of this work was to clarify the molecular pathway(s) regulated by LMX1B. Therefore the putative LMX1B target genes, which are upregulated after the inactivation of *Lmx1b*, were characterized. Bioinformatic studies of 6-kbp long promoter fragments of the putative LMX1B target genes led to the identification of LMX1B binding elements (FLAT elements) within the *ABRA* and *ARL4C* promoter regions which were then analyzed using luciferase reporter assays. Their importance was verified by site-directed mutagenesis studies.

Essential information was obtained from the subcellular localization of the corresponding proteins and their interaction with the actin cytoskeleton in primary podocytes and in an immortalized human podocyte cell line. For this purpose Abra, Arl4c and Crct1 were fused with a HA-epitope tag and miniSOG. This allowed us to visualize the proteins by confocal and electron microscopy. Additionally the regulation of the actin cytoskeleton by LMX1B and its target genes was investigated.

To localize Abra, Arl4c and Crct1 in the kidney, it was necessary to produce rabbit antibodies directed against these proteins. Therefore, recombinant Abra, Arl4c and Crct1 proteins were generated in *Escherichia coli* and polyclonal antibodies were produced.

To determine the role of LMX1B for the maintenance of the podocyte actin cytoskeleton, several proteins involved in the formation of the actin cytoskeleton including actin, α-actinin-1, α-actinin-4, focal adhesion kinase, non-muscle myosin heavy chain IIA, paxillin, talin, utrophin, vasodilator stimulated phosphoprotein, vinculin and zyxin were chosen for fluorescence recovery after photobleaching (FRAP) studies.

Figure 4.4 demonstrates a scheme detailing the effects of *Lmx1b* inactivation and summarizes the data obtained in this work. The inactivation of *Lmx1b* in adult mice resulted in proteinuria and foot process effacement one week later (Burghardt et al., 2013). This was associated with the increase in the mRNA levels of Abra, Arl4c and Crct1. The inactivation of *Lmx1b* and overexpression of Abra, Arl4c and Crct1 caused an increased stiffness of the actin cytoskeleton. Moreover, *Lmx1b* inactivation affected the dynamics of α-actinin-1 and actin.

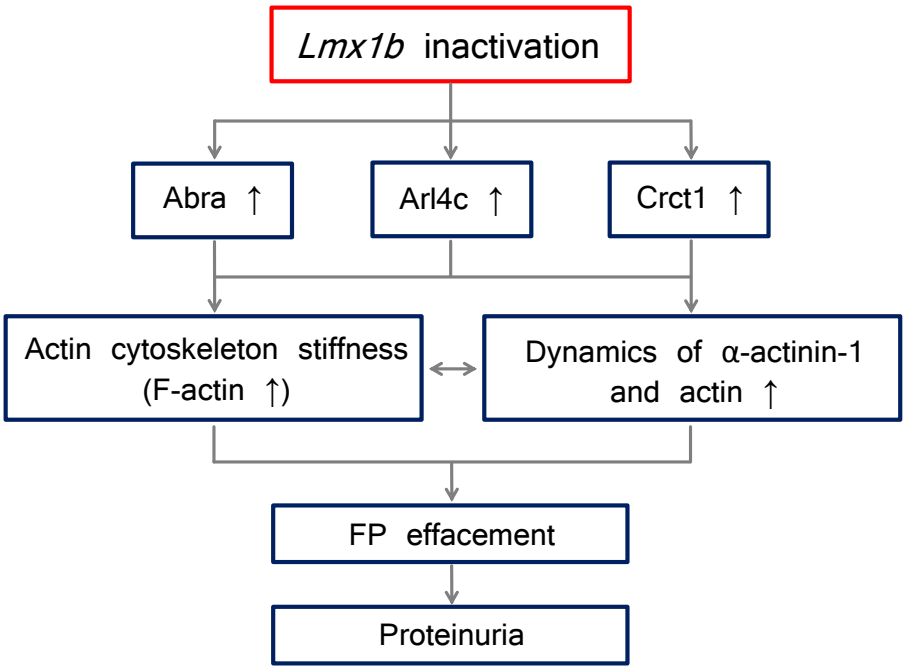

Figure 4.4: Scheme detailing the effects of *Lmx1b* inactivation. One week of inactivation of *Lmx1b* in adult mice resulted in proteinuria with foot process effacement (Burghardt et al., 2013). This was associated with the increase in the mRNA levels of Abra, Arl4c and Crct1. The inactivation of *Lmx1b* and overexpression of Abra, Arl4c and Crct1 caused stiffness of actin cytoskeleton by increasing F-actin. Moreover, *Lmx1b* inactivation affected the dynamics of α-actinin-1 and actin.

4.8 Perspectives

The transfection effeciency of HtTA-1/LMX1B cells and conditionally immortalized murine podocytes was approximately 20 %. Additionally, HtTA-1/LMX1B cells probably are missing some cofactors which are present in podocytes. To facilitate further investigations, the generation of a murine podocyte cell line which expresses LMX1B targets is necessary. During this PhD project attempts to generate these cell line were performed. However, the transduction of a murine podocyte cell line with lentiviruses was not successful. The pLVPT-rtTR-KRAB-2SM2 lentiviral vector containing the cDNA of interest has a significant disadvantage since it has no mammalian selection marker. The additional selection of transduced cells is necessary to avoid the amplification of non-transduced cells.

The physiological significance of the identified LMX1B target genes can be studied by RNA interference. Therefore, the lentiviral vectors coding for several anti-Arl4c shRNAs were generated. Unfortunately, these vectors were not tested during this PhD thesis.

Current techniques which are used to visualize the actin-associated proteins generated some artifacts during fixation, permeablization, and immunofluorescence staining (Arcangeletti et al., 1997). Fluorescence recovery after photobleaching, which was applied in this work, allows to observe the dynamics of these proteins in living cells. To provide both spatial and temporal information on protein dynamics in focal adhesions the simultaneous fluorescence loss in photobleaching (FLIP)-FRAP can be used (Mattern et al., 2004; Le Dévédec et al., 2012). A key question for future investigations concerns the assem-

bly and disassembly of focal adhesions. To this end, time-lapse microscopy can be used. Primary podocytes can be treated with the Rho-kinase inhibitor Y-27632 and reorganization of focal adhesions can be monitored. On the other hand, removal of the Rho-kinase inhibitor will allow to observe the *de novo* formation of focal adhesions (Lavelin et al., 2013).

Bibliography

Alberts, B., Johnson, A., Lewis, J., Raff, M., Roberts, K., and Walter, P. (2008). The cytoskeleton. *Molecular biology of the cell. Fifth Edition*, Chapter 16:965–1052.

Albiges, L., Molinie, V., and Escudier, B. (2012). Non-clear cell renal cell carcinoma: does the mammalian target of rapamycin represent a rational therapeutic target? *Oncologist*, 17(8):1051–1062.

Arai, A., Spencer, J. A., and Olson, E. N. (2002). Stars, a striated muscle activator of rho signaling and serum response factor-dependent transcription. *J Biol Chem*, 277(27):24453–24459.

Arcangeletti, C., Sütterlin, R., Aebi, U., De Conto, F., Missorini, S., Chezzi, C., and Scherrer, K. (1997). Visualization of prosomes (mcp-proteasomes), intermediate filament and actin networks by "instantaneous fixation" preserving the cytoskeleton. *J Struct Biol*, 119(1):35–58.

Arrondel, C., Vodovar, N., Knebelmann, B., Grünfeld, J. P., Gubler, M. C., Antignac, C., and Heidet, L. (2002). Expression of the nonmuscle myosin heavy chain iia in the human kidney and screening for myh9 mutations in epstein and fechtner syndromes. *J Am Soc Nephrol*, 13(1):65–74.

Bains, R., Furness, P. N., and Critchley, D. R. (1997). A quantitative immunofluorescence study of glomerular cell adhesion proteins in proteinuric states. *J Pathol*, 183(3):272–280.

Barrientos, T., Frank, D., Kuwahara, K., Bezprozvannaya, S., Pipes, G. C., Bassel-Duby, R., Richardson, J. A., Katus, H. A., Olson, E. N., and Frey, N. (2007). Two novel members of the ablim protein family, ablim-2 and -3, associate with stars and directly bind f-actin. *J Biol Chem*, 282(11):8393–8403.

Ben-Bassat, M., Cohen, L., and Rosenfeld, J. (1971). The glomerular basement membrane in the nail-patella syndrome. *Arch Pathol*, 92(5):350–355.

Birnboim, H. C. and Doly, J. (1979). A rapid alkaline extraction procedure for screening recombinant plasmid dna. *Nucleic Acids Res*, 7(6):1513–1523.

Blattner, S. M., Hodgin, J. B., Nishio, M., Wylie, S. A., Saha, J., Soofi, A. A., Vining, C., Randolph, A., Herbach, N., Wanke, R., Atkins, K. B., Gyung Kang, H., Henger, A., Brakebusch, C., Holzman, L. B., and Kretzler, M. (2013). Divergent functions of the rho gtpases rac1 and cdc42 in podocyte injury. *Kidney Int*, 84(5):920–930.

Boerries, M., Grahammer, F., Eiselein, S., Buck, M., Meyer, C., Goedel, M., Bechtel, W., Zschiedrich, S., Pfeifer, D., Laloë, D., Arrondel, C., Gonçalves, S., Krüger, M., Harvey, S. J., Busch, H., Dengjel, J., and Huber, T. B. (2013). Molecular fingerprinting of the podocyte reveals novel gene and protein regulatory networks. *Kidney Int*, 83(6):1052–1064.

Bongers, E. M., Gubler, M. C., and Knoers, N. V. (2002). Nail-patella syndrome. overview on clinical and molecular findings. *Pediatr Nephrol*, 17(9):703–712.

Bordeaux, J., Welsh, A., Agarwal, S., Killiam, E., Baquero, M., Hanna, J., Anagnostou, V., and Rimm, D. (2010). Antibody validation. *Biotechniques*, 48(3):197–209.

Bradford, M. M. (1976). A rapid and sensitive method for the quantitation of microgram quantities of protein utilizing the principle of protein-dye binding. *Anal Biochem*, 72:248–254.

Brindle, N. P., Holt, M. R., Davies, J. E., Price, C. J., and Critchley, D. R. (1996). The focal-adhesion vasodilator-stimulated phosphoprotein (vasp) binds to the proline-rich domain in vinculin. *Biochem J*, 318 (Pt 3):753–757.

Burghardt, T., Kastner, J., Suleiman, H., Rivera-Milla, E., Stepanova, N., Lottaz, C., Kubitza, M., Böger, C. A., Schmidt, S., Gorski, M., de Vries, U., Schmidt, H., Hertting, I., Kopp, J., Rascle, A., Moser, M., Heid, I. M., Warth, R., Spang, R., Wegener, J., Mierke, C. T., Englert, C., and Witzgall, R. (2013). Lmx1b is essential for the maintenance of differentiated podocytes in adult kidneys. *J Am Soc Nephrol*, 24(11):1830–1848.

Burkel, B. M., von Dassow, G., and Bement, W. M. (2007). Versatile fluorescent probes for actin filaments based on the actin-binding domain of utrophin. *Cell Motil Cytoskeleton*, 64(11):822–832.

Burridge, K. and Connell, L. (1983a). A new protein of adhesion plaques and ruffling membranes. *J Cell Biol*, 97(2):359–367.

Burridge, K. and Connell, L. (1983b). Talin: a cytoskeletal component concentrated in adhesion plaques and other sites of actin-membrane interaction. *Cell Motil*, 3(5-6):405–417.

Chen, H. C., Appeddu, P. A., Parsons, J. T., Hildebrand, J. D., Schaller, M. D., and Guan, J. L. (1995). Interaction of focal adhesion kinase with cytoskeletal protein talin. *J Biol Chem*, 270(28):16995–16999.

Cooper, G. M. (2000). Structure and organization of actin filaments. *The Cell: A Molecular Approach*, 2nd edition:Chapter 11.

Cramer, L. P., Briggs, L. J., and Dawe, H. R. (2002). Use of fluorescently labelled deoxyribonuclease i to spatially measure g-actin levels in migrating and non-migrating cells. *Cell Motil Cytoskeleton*, 51(1):27–38.

Crawford, A. W. and Beckerle, M. C. (1991). Purification and characterization of zyxin, an 82,000-dalton component of adherens junctions. *J Biol Chem*, 266(9):5847–5853.

Crawford, A. W., Michelsen, J. W., and Beckerle, M. C. (1992). An interaction between zyxin and alpha-actinin. *J Cell Biol*, 116(6):1381–1393.

Critchley, D. R. and Gingras, A. R. (2008). Talin at a glance. *J Cell Sci*, 121(Pt 9):1345–1347.

Critchley, D. R., Holt, M. R., Barry, S. T., Priddle, H., Hemmings, L., and Norman, J. (1999). Integrin-mediated cell adhesion: the cytoskeletal connection. *Biochem Soc Symp*, 65:79–99.

Österreicher, W. (1930). Gemeinsame vererbung von anonychie bzw. onychatrophie, patellardefekt und luxatio radii. dominantes auftreten in 5 generationen. *Ztschr. Konstitutionslehre*, 15:465–476.

Deerinck, T. J., Martone, M. E., Lev-Ram, V., Green, D. P., Tsien, R. Y., Spector, D. L., Huang, S., and Ellisman, M. H. (1994). Fluorescence photooxidation with eosin: a method for high resolution immunolocalization and in situ hybridization detection for light and electron microscopy. *J Cell Biol*, 126(4):901–910.

Del Pozo, E. and Lapp, H. (1970). Ultrastructure of the kidney in the nephropathy of the nail–patella syndrome. *Am J Clin Pathol*, 54(6):845–851.

Drenckhahn, D. and Franke, R. P. (1988). Ultrastructural organization of contractile and cytoskeletal proteins in glomerular podocytes of chicken, rat, and man. *Lab Invest*, 59(5):673–682.

Dreyer, S. D., Zhou, G., Baldini, A., Winterpacht, A., Zabel, B., Cole, W., Johnson, R. L., and Lee, B. (1998). Mutations in lmx1b cause abnormal skeletal patterning and renal dysplasia in nail patella syndrome. *Nat Genet*, 19(1):47–50.

Dunston, J. A., Hamlington, J. D., Zaveri, J., Sweeney, E., Sibbring, J., Tran, C., Malbroux, M., O'Neill, J. P., Mountford, R., and McIntosh, I. (2004). The human lmx1b gene: transcription unit, promoter, and pathogenic mutations. *Genomics*, 84(3):565–576.

Ebashi, S. and Ebashi, F. (1965). Alpha-actinin, a new structural protein from striated muscle. *J Biochem*, 58(1):7–12.

Edlund, M., Lotano, M. A., and Otey, C. A. (2001). Dynamics of alpha-actinin in focal adhesions and stress fibers visualized with alpha-actinin-green fluorescent protein. *Cell Motil Cytoskeleton*, 48(3):190–200.

Engel, T., Lueken, A., Bode, G., Hobohm, U., Lorkowski, S., Schlueter, B., Rust, S., Cullen, P., Pech, M., Assmann, G., and Seedorf, U. (2004). Adp-ribosylation factor (arf)-like 7 (arl7) is induced by cholesterol loading and participates in apolipoprotein al-dependent cholesterol export. *FEBS Lett*, 566(1-3):241–246.

Esue, O., Tseng, Y., and Wirtz, D. (2009). Alpha-actinin and filamin cooperatively enhance the stiffness of actin filament networks. *PLoS One*, 4(2):e4411.

Farquhar, M. G., Vernier, R. L., and Good, R. A. (1957). An electron microscope study of the glomerulus in nephrosis, glomerulonephritis, and lupus erythematosus. *J Exp Med*, 106(5):649–660.

Faulk, W. P. and Taylor, G. M. (1971). An immunocolloid method for the electron microscope. *Immunochemistry*, 8(11):1081–1083.

Flavahan, N. A., Bailey, S. R., Flavahan, W. A., Mitra, S., and Flavahan, S. (2005). Imaging remodeling of the actin cytoskeleton in vascular smooth muscle cells after mechanosensitive arteriolar constriction. *Am J Physiol Heart Circ Physiol*, 288(2):H660–H669.

Fogl, C., Puckey, L., Hinssen, U., Zaleska, M., El-Mezgueldi, M., Croasdale, R., Bowman, A., Matsukawa, A., Samani, N. J., Savva, R., and Pfuhl, M. (2012). A structural and functional dissection of the cardiac stress response factor ms1. *Proteins*, 80(2):398–409.

Foley, K. S. and Young, P. W. (2014). The non-muscle functions of actinins: an update. *Biochem J*, 459(1):1–13.

Fong, E. E. (1946). Iliac horns (symmetrical bilateral central posterior iliac processes). *Radiology*, 47(5):517.

Gaietta, G., Deerinck, T. J., Adams, S. R., Bouwer, J., Tour, O., Laird, D. W., Sosinsky, G. E., Tsien, R. Y., and Ellisman, M. H. (2002). Multicolor and electron microscopic imaging of connexin trafficking. *Science*, 296(5567):503–507.

Galeano, B., Klootwijk, R., Manoli, I., Sun, M., Ciccone, C., Darvish, D., Starost, M. F., Zerfas, P. M., Hoffmann, V. J., Hoogstraten-Miller, S., Krasnewich, D. M., Gahl, W. A., and Huizing, M. (2007). Mutation in the key enzyme of sialic acid biosynthesis causes severe glomerular proteinuria and is rescued by n-acetylmannosamine. *J Clin Invest*, 117(6):1585–1594.

Geiger, B., Tokuyasu, K. T., Dutton, A. H., and Singer, S. J. (1980). Vinculin, an intracellular protein localized at specialized sites where microfilament bundles terminate at cell membranes. *Proc Natl Acad Sci U S A*, 77(7):4127–4131.

German, M. S., Wang, J., Chadwick, R. B., and Rutter, W. J. (1992). Synergistic activation of the insulin gene by a lim-homeo domain protein and a basic helix-loop-helix protein: building a functional insulin minienhancer complex. *Genes Dev*, 6(11):2165–2176.

Gossen, M. and Bujard, H. (1992). Tight control of gene expression in mammalian cells by tetracycline-responsive promoters. *Proc Natl Acad Sci USA*, 89(12):5547–5551.

Grange, J., Moody, J. D., Ascione, M. P., and Hansen, M. D. (2013). Zyxin-vasp interactions alter actin regulatory activity in zyxin-vasp complexes. *Cell Mol Biol Lett*, 18(1):1–10.

Grishman, E. and Churg, J. (1975). Focal glomerular sclerosis in nephrotic patients: an electron microscopic study of glomerular podocytes. *Kidney Int*, 7(2):111–122.

Guéguen, P., Rouault, K., Chen, J. M., Raguénès, O., Fichou, Y., Hardy, E., Gobin, E., Pan-Petesch, B., Kerbiriou, M., Trouvé, P., Marcorelles, P., Abgrall, J. F., Le Maréchal, C., and Férec, C. (2013). A missense mutation in the alpha-actinin 1 gene (actn1) is the cause of autosomal dominant macrothrombocytopenia in a large french family. *PLoS One*, 8(9):e74728.

Hagel, M., George, E. L., Kim, A., Tamimi, R., Opitz, S. L., Turner, C. E., Imamoto, A., and Thomas, S. M. (2002). The adaptor protein paxillin is essential for normal development in the mouse and is a critical transducer of fibronectin signaling. *Mol Cell Biol*, 22(3):901–915.

Halbrügge, M. and Walter, U. (1989). Purification of a vasodilator-regulated phosphoprotein from human platelets. *Eur J Biochem*, 185(1):41–50.

Hall, A. (1998). Rho gtpases and the actin cytoskeleton. *Science*, 279(5350):509–514.

Harris, J. J., McCarthy, H. J., Ni, L., Wherlock, M., Kang, H., Wetzels, J. F., Welsh, G. I., and Saleem, M. A. (2013). Active proteases in nephrotic plasma lead to a podocin-dependent phosphorylation of vasp in podocytes via protease activated receptor-1. *J Pathol*, 229(5):660–671.

Heidet, L., Bongers, E. M., Sich, M., Zhang, S. Y., Loirat, C., Meyrier, A., Broyer, M., Landthaler, G., Faller, B., Sado, Y., Knoers, N. V., and Gubler, M. C. (2003). In vivo expression of putative lmx1b targets in nail-patella syndrome kidneys. *Am J Pathol*, 163(1):145–155.

Hemmings, L., Barry, S. T., and Critchley, D. R. (1995). Cell-matrix adhesion: structure and regulation. *Biochem Soc Trans*, 23(3):619–626.

Hermann, R., Walther, P., and Müller, M. (1996). Immunogold labeling in scanning electron microscopy. *Histochem Cell Biol*, 106(1):31–9.

Hildebrand, J. D., Schaller, M. D., and Parsons, J. T. (1995). Paxillin, a tyrosine phosphorylated focal adhesion-associated protein binds to the carboxyl terminal domain of focal adhesion kinase. *Mol Biol Cell*, 6(6):637–647.

Hoffman, L. M., Nix, D. A., Benson, B., Boot-Hanford, R., Gustafsson, E., Jamora, C., Menzies, A. S., Goh, K. L., Jensen, C. C., Gertler, F. B., Fuchs, E., Fässler, R., and Beckerle, M. C. (2003). Targeted disruption of the murine zyxin gene. *Mol Cell Biol*, 23(1):70–79.

Hofmann, I., Thompson, A., Sanderson, C. M., and Munro, S. (2007). The arl4 family of small g proteins can recruit the cytohesin arf6 exchange factors to the plasma membrane. *Curr Biol*, 17(8):711–716.

Honda, K., Yamada, T., Endo, R., Ino, Y., Gotoh, M., Tsuda, H., Yamada, Y., Chiba, H., and Hirohashi, S. (1998). Actinin-4, a novel actin-bundling protein associated with cell motility and cancer invasion. *J Cell Biol*, 140(6):1383–1393.

Horwitz, A., Duggan, K., Buck, C., Beckerle, M. C., and Burridge, K. (1986). Interaction of plasma membrane fibronectin receptor with talin–a transmembrane linkage. *Nature*, 320(6062):531–533.

Ilić, D., Furuta, Y., Kanazawa, S., Takeda, N., Sobue, K., Nakatsuji, N., Nomura, S., Fujimoto, J., Okada, M., and Yamamoto, T. (1995). Reduced cell motility and enhanced focal adhesion contact formation in cells from fak-deficient mice. *Nature*, 377(6549):539–544.

Jacobs, S., Schilf, C., Fliegert, F., Koling, S., Weber, Y., Schürmann, A., and Joost, H. G. (1999). Adp-ribosylation factor (arf)-like 4, 6, and 7 represent a subgroup of the arf family characterization by rapid nucleotide exchange and a nuclear localization signal. *FEBS Lett*, 456(3):384–388.

John, S. W., Weitzner, G., Rozen, R., and Scriver, C. R. (1991). A rapid procedure for extracting genomic dna from leukocytes. *Nucleic Acids Res*, 19(2):408.

Johnstone, D. B., Zhang, J., George, B., Léon, C., Gachet, C., Wong, H., Parekh, R., and Holzman, L. B. (2011). Podocyte-specific deletion of myh9 encoding non-muscle myosin heavy chain 2a predisposes mice to glomerulopathy. *Mol Cell Biol*, 31(10):2162–2170.

Jones, N., Blasutig, I. M., Eremina, V., Ruston, J. M., Bladt, F., Li, H., Huang, H., Larose, L., Li, S. S., Takano, T., Quaggin, S. E., and Pawson, T. (2006). Nck adaptor proteins link nephrin to the actin cytoskeleton of kidney podocytes. *Nature*, 440(7085):818–823.

Kaplan, J. M., Kim, S. H., North, K. N., Rennke, H., Correia, L. A., Tong, H. Q., Mathis, B. J., Rodríguez-Pérez, J. C., Allen, P. G., Beggs, A. H., and Pollak, M. R. (2000). Mutations in actn4, encoding alpha-actinin-4, cause familial focal segmental glomerulosclerosis. *Nat Genet*, 24(3):251–256.

Kerjaschki, D. (2001). Caught flat-footed: podocyte damage and the molecular bases of focal glomerulosclerosis. *J Clin Invest*, 108(11):1583–1587.

Kieser, W. (1939). Die sog. flughaut beim menschen. ihre beziehung zum status dysraphicus und ihre erblichkeit. *Ztschr Mensch Vererb Konstitutionsl*, 23:594–619.

Kistler, A. D., Altintas, M. M., and Reiser, J. (2012). Podocyte gtpases regulate kidney filter dynamics. *Kidney Int*, 81(11):1053–1055.

Kohan, D. E. (2008). Progress in gene targeting: using mutant mice to study renal function and disease. *Kidney Int*, 74(4):427–437.

Koop, K., Eikmans, M., Baelde, H. J., Kawachi, H., De Heer, E., Paul, L. C., and Bruijn, J. A. (2003). Expression of podocyte-associated molecules in acquired human kidney diseases. *J Am Soc Nephrol*, 14(8):2063–2071.

Kos, C. H., Le, T. C., Sinha, S., Henderson, J. M., Kim, S. H., Sugimoto, H., Kalluri, R., Gerszten, R. E., and Pollak, M. R. (2003). Mice deficient in alpha-actinin-4 have severe glomerular disease. *J Clin Invest*, 111(11):1683–1690.

Koukouritaki, S. B., Tamizuddin, A., and Lianos, E. A. (1998). Enhanced expression of the cytoskeletal-associated protein, paxillin, in experimental nephrotic syndrome. *J Investig Med*, 46(6):284–289.

Kreidberg, J. A., Donovan, M. J., Goldstein, S. L., Rennke, H., Shepherd, K., Jones, R. C., and Jaenisch, R. (1996). Alpha 3 beta 1 integrin has a crucial role in kidney and lung organogenesis. *Development*, 122(11):3537–3547.

Kretzler, M., Teixeira, V. P., Unschuld, P. G., Cohen, C. D., Wanke, R., Edenhofer, I., Mundel, P., Schlöndorff, D., and Holthöfer, H. (2001). Integrin-linked kinase as a candidate downstream effector in proteinuria. *FASEB J*, 15(10):1843–1845.

Kuwahara, K., Barrientos, T., Pipes, G. C., Li, S., and Olson, E. N. (2005). Muscle-specific signaling mechanism that links actin dynamics to serum response factor. *Mol Cell Biol*, 25(8):3173–3181.

Lauffenburger, D. A. and Horwitz, A. F. (1996). Cell migration: a physically integrated molecular process. *Cell*, 84(3):359–369.

Lavelin, I., Wolfenson, H., Patla, I., Henis, Y. I., Medalia, O., Volberg, T., Livne, A., Kam, Z., and Geiger, B. (2013). Differential effect of actomyosin relaxation on the dynamic properties of focal adhesion proteins. *PLoS One*, ;8(9):e73549.

Le Dévédec, S. E., Geverts, B., de Bont, H., Yan, K., Verbeek, F. J., Houtsmuller, A. B., and van de Water, B. (2012). The residence time of focal adhesion kinase (fak) and paxillin at focal adhesions in renal epithelial cells is determined by adhesion size, strength and life cycle status. *J Cell Sci*, 125(Pt 19):4498–4506.

Lemley, K. V. (2009). Kidney disease in nail-patella syndrome. *Pediatr Nephrol*, 24(12):2345–2354.

Leong, T. Y. and Leong, A. S. (2007). How does antigen retrieval work? *Adv Anat Pathol*, 14(2):129–131.

Lorente, G., Syriani, E., and Morales, M. (2014). Actin filaments at the leading edge of cancer cells are characterized by a high mobile fraction and turnover regulation by profilin i. *PLoS One*, 9(1):e85817.

Ma, H., Togawa, A., Soda, K., Zhang, J., Lee, S., Ma, M., Yu, Z., Ardito, T., Czyzyk, J., Diggs, L., Joly, D., Hatakeyama, S., Kawahara, E., Holzman, L., Guan, J. L., and Ishibe, S. (2010). Inhibition of podocyte fak protects against proteinuria and foot process effacement. *J Am Soc Nephrol*, 21(7):1145–1156.

Macia, E., Luton, F., Partisani, M., Cherfils, J., Chardin, P., and Franco, M. (2004). The gdp-bound form of arf6 is located at the plasma membrane. *J Cell Sci*, 117(Pt 11):2389–2398.

Mahadeva, H., Brooks, G., Lodwick, D., Chong, N. W., and Samani, N. J. (2002). ms1, a novel stress-responsive, muscle-specific gene that is up-regulated in the early stages of pressure overload-induced left ventricular hypertrophy. *FEBS Lett*, 521(1-3):100–104.

Matsumoto, S., Fujii, S., Sato, A., Ibuka, S., Kagawa, Y., Ishii, M., and Kikuchi, A. (2014). A combination of wnt and growth factor signaling induces arl4c expression to form epithelial tubular structures. *EMBO J*, 33(7):702–718.

Matsuura, S., Kondo, S., Suga, K., Kinoshita, Y., Urushihara, M., and Kagami, S. (2011). Expression of focal adhesion proteins in the developing rat kidney. *J Histochem Cytochem*, 59(9):864–874.

Mattern, K. A., Swiggers, S. J., Nigg, A. L., Löwenberg, B., Houtsmuller, A. B., and Zijlmans, J. M. (2004). Dynamics of protein binding to telomeres in living cells: implications for telomere structure and function. *Mol Cell Biol*, 24(12):5587–5594.

McIntosh, I., Dreyer, S. D., Clough, M. V., Dunston, J. A., Eyaid, W., Roig, C. M., Montgomery, T., Ala-Mello, S., Kaitila, I., Winterpacht, A., Zabel, B., Frydman, M., Cole, W. G., Francomano, C. A., and Lee, B. (1998). Mutation analysis of lmx1b gene in nail-patella syndrome patients. *Am J Hum Genet*, 63(6):1651–1658.

Müller, T., Rumpel, E., Hradetzky, S., Bollig, F., Wegner, H., Blumenthal, A., Greinacher, A., Endlich, K., and Endlich, N. (2011). Non-muscle myosin iia is required for the development of the zebrafish glomerulus. *Kidney Int*, 80(10):1055–1063.

Miao, J., Fan, Q., Cui, Q., Zhang, H., Chen, L., Wang, S., Guan, N., Guan, Y., and Ding, J. (2009). Newly identified cytoskeletal components are associated with dynamic changes of podocyte foot processes. *Nephrol Dial Transplant*, 24(11):3297–3305.

Miner, J. H., Morello, R., Andrews, K. L., Li, C., Antignac, C., Shaw, A. S., and Lee, B. (2002). Transcriptional induction of slit diaphragm genes by lmx1b is required in podocyte differentiation. *J Clin Invest*, 109(8):1065–1072.

Miyanaga, A., Honda, K., Tsuta, K., Masuda, M., Yamaguchi, U., Fujii, G., Miyamoto, A., Shinagawa, S., Miura, N., Tsuda, H., Sakuma, T., Asamura, H., Gemma, A., and Yamada, T. (2013). Diagnostic and prognostic significance of the alternatively spliced actn4 variant in high-grade neuroendocrine pulmonary tumours. *Ann Oncol*, 24(1):84–90.

Morello, R., Zhou, G., Dreyer, S. D., Harvey, S. J., Ninomiya, Y., Thorner, P. S., Miner, J. H., Cole, W., Winterpacht, A., Zabel, B., Oberg, K. C., and Lee, B. (2001). Regulation of glomerular basement membrane collagen expression by lmx1b contributes to renal disease in nail patella syndrome. *Nat Genet*, 27(2):205–208.

Mundel, P. and Kriz, W. (1995). Structure and function of podocytes: an update. *Anat Embryol (Berl)*, 192(5):385–397.

Mundel, P. and Shankland, S. J. (2002). Podocyte biology and response to injury. *J Am Soc Nephrol*, 13(12):3005–3015.

Murphy, W. M., Moretta, F. L., and Jukkola, A. F. (1979). Epithelial foot-process effacement in patients with proteinuria. *Am J Clin Pathol*, 72(4):529–532.

Muzumdar, M. D., Tasic, B., Miyamichi, K., Li, L., and Luo, L. (2007). A global double-fluorescent cre reporter mouse. *Genesis*, 45(9):593–605.

Noakes, P. G., Miner, J. H., Gautam, M., Cunningham, J. M., Sanes, J. R., and Merlie, J. P. (1995). The renal glomerulus of mice lacking s-laminin/laminin beta 2: nephrosis despite molecular compensation by laminin beta 1. *Nat Genet*, 10(4):400–406.

Noris, M. and Remuzzi, G. (2012). Non-muscle myosins and the podocyte. *Clin Kidney J*, 5:94101.

Norstrom, M. and Gardel, M. L. (2011). Shear thickening of f-actin networks crosslinked with non-muscle myosin iib. *Soft Matter*, 2011(7):3228–3233.

Orlando, R. A., Takeda, T., Zak, B., Schmieder, S., Benoit, V. M., McQuistan, T., Furthmayr, H., and Farquhar, M. G. (2001). The glomerular epithelial cell anti-adhesin podocalyxin associates with the actin cytoskeleton through interactions with ezrin. *J Am Soc Nephrol*, 12(8):1589–1598.

Pati, U. K. (1992). Novel vectors for expression of cdna encoding epitope-tagged proteins in mammalian cells. *Gene*, 114(2):285–288.

Peti-Peterdi, J. and Sipos, A. (2010). A high-powered view of the filtration barrier. *J Am Soc Nephrol*, 21(11):1835–1841.

Pollak, M. R. (2002). Inherited podocytopathies: Fsgs and nephrotic syndrome from a genetic viewpoint. *J Am Soc Nephrol*, 13(12):3016–3023.

Pozzi, A. and Zent, R. (2012). Hold tight or you'll fall off: Cd151 helps podocytes stick in high-pressure situations. *J Clin Invest*, 122(1):13–16.

Price, G. J., Jones, P., Davison, M. D., Patel, B., Bendori, R., Geiger, B., and Critchley, D. R. (1989). Primary sequence and domain structure of chicken vinculin. *Biochem J*, 259(2):453–461.

Quaggin, S. E. (2002). Transcriptional regulation of podocyte specification and differentiation. *Microsc Res Tech*, 57(4):208–211.

Raats, C. J., Bakker, M. A., van den Born, J., and Berden, J. H. (1997). Hydroxyl radicals depolymerize glomerular heparan sulfate in vitro and in experimental nephrotic syndrome. *J Biol Chem*, 272(42):26734–26741.

Raats, C. J., van den Born, J., Bakker, M. A., Oppers-Walgreen, B., Pisa, B. J., Dijkman, H. B., Assmann, K. J., and Berden, J. H. (2000). Expression of agrin, dystroglycan, and utrophin in normal renal tissue and in experimental glomerulopathies. *Am J Pathol*, 156(5):1749–1765.

Rascle, A., Neumann, T., Raschta, A. S., Neumann, A., Heining, E., Kastner, J., and Witzgall, R. (2009). The lim-homeodomain transcription factor lmx1b regulates expression of nf-kappa b target genes. *Exp Cell Res*, 315(1):76–96.

Rascle, A., Suleiman, H., Neumann, T., and Witzgall, R. (2007). Role of transcription factors in podocytes. *Nephron Exp Nephrol*, 106(2):e60–e66.

Regele, H. M., Fillipovic, E., Langer, B., Poczewki, H., Kraxberger, I., Bittner, R. E., and Kerjaschki, D. (2000). Glomerular expression of dystroglycans is reduced in minimal change nephrosis but not in focal segmental glomerulosclerosis. *J Am Soc Nephrol*, 11(3):403–412.

Reinhard, M., Giehl, K., Abel, K., Haffner, C., Jarchau, T., Hoppe, V., Jockusch, B. M., and Walter, U. (1995). The proline-rich focal adhesion and microfilament protein vasp is a ligand for profilins. *EMBO J*, 14(8):1583–1589.

Renwick, J. H. and Lawler, S. D. (1955). Genetical linkage between the abo and nail-patella loci. *Ann Hum Genet*, 19(4):312–331.

Roeckerath, W. (1951). Hereditary osteo-onychodysplasia. *Fortschr Geb Rontgenstr*, 75(6):700–712.

Rohr, C., Prestel, J., Heidet, L., Hosser, H., Kriz, W., Johnson, R. L., Antignac, C., and Witzgall, R. (2002). The lim-homeodomain transcription factor lmx1b plays a crucial role in podocytes. *J Clin Invest*, 109(8):1073–1082.

Saleem, M. A., O'Hare, M. J., Reiser, J., Coward, R. J., Inward, C. D., Farren, T., Xing, C. Y., Ni, L., Mathieson, P. W., and Mundel, P. (2002). A conditionally immortalized human podocyte cell line demonstrating nephrin and podocin expression. *J Am Soc Nephrol*, 13(3):630–638.

Schaller, M. D., Borgman, C. A., Cobb, B. S., Vines, R. R., Reynolds, A. B., and Parsons, J. T. (1992). pp125fak a structurally distinctive protein-tyrosine kinase associated with focal adhesions. *Proc Natl Acad Sci U S A*, 89(11):5192–5196.

Schaller, M. D., Otey, C. A., Hildebrand, J. D., and Parsons, J. T. (1995). Focal adhesion kinase and paxillin bind to peptides mimicking beta integrin cytoplasmic domains. *J Cell Biol*, 130(5):1181–1187.

Schleutermann, D. A., Bias, W. B., Murdoch, J. L., and McKusick, V. A. (1969). Linkage of the loci for the nail-patella syndrome and adenylate kinase. *Am J Hum Genet*, 21(6):606–630.

Seri, M., Pecci, A., Di Bari, F., Cusano, R., Savino, M., Panza, E., Nigro, A., Noris, P., Gangarossa, S., Rocca, B., Gresele, P., Bizzaro, N., Malatesta, P., Koivisto, P. A., Longo, I., Musso, R., Pecoraro, C., Iolascon, A., Magrini, U., Rodriguez Soriano, J., Renieri, A., Ghiggeri, G. M., Ravazzolo, R., Balduini, C. L., and Savoia, A. (2003). Myh9-related disease: May-hegglin anomaly, sebastian syndrome, fechtner syndrome, and epstein syndrome are not distinct entities but represent a variable expression of a single illness. *Medicine (Baltimore)*, 82(3):203–215.

Shirato, I. (2002). Podocyte process effacement in vivo. *Microsc Res Tech*, 57(4):241–246.

Shirato, I., Sakai, T., Kimura, K., Tomino, Y., and Kriz, W. (1996). Cytoskeletal changes in podocytes associated with foot process effacement in masugi nephritis. *Am J Pathol*, 148(4):1283–1296.

Shu, X., Lev-Ram, V., Deerinck, T. J., Qi, Y., Ramko, E. B., Davidson, M. W., Jin, Y., Ellisman, M. H., and Tsien, R. Y. (2011). A genetically encoded tag for correlated light and electron microscopy of intact cells, tissues, and organisms. *PLoS Biol*, 9(4):e1001041.

Simons, M., Schwarz, K., Kriz, W., Miettinen, A., Reiser, J., Mundel, P., and Holthöfer, H. (2001). Involvement of lipid rafts in nephrin phosphorylation and organization of the glomerular slit diaphragm. *Am J Pathol*, 159(3):1069–1077.

Smoyer, W. E. and Mundel, P. (1998). Regulation of podocyte structure during the development of nephrotic syndrome. *J Mol Med (Berl)*, 76(3-4):172–183.

Smoyer, W. E., Mundel, P., Gupta, A., and Welsh, M. J. (1997). Podocyte alpha-actinin induction precedes foot process effacement in experimental nephrotic syndrome. *Am J Physiol*, 273(1 Pt 2):F150–F157.

Somlo, S. and Mundel, P. (2000). Getting a foothold in nephrotic syndrome. *Nat Genet*, 24(4):333–335.

Stadler, C., Rexhepaj, E., Singan, V. R., Murphy, R. F., Pepperkok, R., Uhlén, M., Simpson, J. C., and Lundberg, E. (2013). Immunofluorescence and fluorescent-protein tagging show high correlation for protein localization in mammalian cells. *Nat Methods*, 10(4):315–323.

Stevens, G. R., Zhang, C., Berg, M. M., Lambert, M. P., Barber, K., Cantallops, I., Routtenberg, A., and Klein, W. L. (1996). Cns neuronal focal adhesion kinase forms clusters that co-localize with vinculin. *J Neurosci Res*, 46(4):445–455.

Stricker, J., Falzone, T., and Gardel, M. L. (2010). Mechanics of the f-actin cytoskeleton. *J Biomech*, 43(1):9–14.

Suleiman, H., Heudobler, D., Raschta, A. S., Zhao, Y., Zhao, Q., Hertting, I., Vitzthum, H., Moeller, M. J., Holzman, L. B., Rachel, R., Johnson, R., Westphal, H., Rascle, A., and Witzgall, R. (2007). The podocyte-specific inactivation of lmx1b, ldb1 and e2a yields new insight into a transcriptional network in podocytes. *Dev Biol*, 304(2):701–712.

Sweeney, E., Fryer, A., Mountford, R., Green, A., and McIntosh, I. (2003). Nail patella syndrome: a review of the phenotype aided by developmental biology. *J Med Genet*, 40(3):153–162.

Takano, K., Kawasaki, Y., Imaizumi, T., Matsuura, H., Nozawa, R., Tannji, M., Suyama, K., Isome, M., Suzuki, H., and Hosoya, M. (2007). Development of glomerular endothelial cells, podocytes and mesangial cells in the human fetus and infant. *Tohoku J Exp Med*, 212(1):81–90.

Takeda, T., McQuistan, T., Orlando, R. A., and Farquhar, M. G. (2001). Loss of glomerular foot processes is associated with uncoupling of podocalyxin from the actin cytoskeleton. *J Clin Invest*, 108(2):289–301.

Testagrossa, L., Azevedo Neto, R., Resende, A., Woronik, V., and Malheiros, D. (2013). Immunohistochemical expression of podocyte markers in the variants of focal segmental glomerulosclerosis. *Nephrol Dial Transplant*, 28(1):91–98.

Tian, X., Kim, J. J., Monkley, S. M., Gotoh, N., Nandez, R., Soda, K., Inoue, K., Balkin, D. M., Hassan, H., Son, S. H., Lee, Y., Moeckel, G., Calderwood, D. A., Holzman, L. B., Critchley, D. R., Zent, R., Reiser, J., and Ishibe, S. (2014). Podocyte-associated talin1 is critical for glomerular filtration barrier maintenance. *J Clin Invest*, 124(3):1098–1113.

Torii, T., Miyamoto, Y., Sanbe, A., Nishimura, K., Yamauchi, J., and Tanoue, A. (2010). Cytohesin-2/arno, through its interaction with focal adhesion adaptor protein paxillin, regulates preadipocyte migration via the downstream activation of arf6. *J Biol Chem*, 285(31):24270–24781.

Troidl, K., Rüding, I., Cai, W. J., Mücke, Y., Grossekettler, L., Piotrowska, I., Apfelbeck, H., Schierling, W., Volger, O. L., Horrevoets, A. J., Grote, K., Schmitz-Rixen, T., Schaper, W., and Troidl, C. (2009). Actin-binding rho activating protein (abra) is essential for fluid shear stress-induced arteriogenesis. *Arterioscler Thromb Vasc Biol*, 29(12):2093–2101.

Turner, C. E., Glenney, J. R., and Burridge, K. (1990). Paxillin: a new vinculin-binding protein present in focal adhesions. *J Cell Biol*, 111(3):1059–1068.

Turner, J. W. (1933). An hereditary arthrodysplasia associated with hereditary dystrophy of the nails. *JAMA*, 100(12):882–884.

Verma, R., Kovari, I., Soofi, A., Nihalani, D., Patrie, K., and Holzman, L. B. (2006). Nephrin ectodomain engagement results in src kinase activation, nephrin phosphorylation, nck recruitment, and actin polymerization. *J Clin Invest*, 116(5):1346–1359.

Verma, R., Wharram, B., Kovari, I., Kunkel, R., Nihalani, D., Wary, K. K., Wiggins, R. C., Killen, P., and Holzman, L. B. (2003). Fyn binds to and phosphorylates the kidney slit diaphragm component nephrin. *J Biol Chem*, 278(23):20716–20723.

Vollrath, D., Jaramillo-Babb, V. L., Clough, M. V., McIntosh, I., Scott, K. M., Lichter, P. R., and Richards, J. E. (1998). Loss-of-function mutations in the lim-homeodomain gene, lmx1b, in nail-patella syndrome. *Hum Mol Genet*, 7(7):1091–1098.

Wang, L., Ellis, M. J., Gomez, J. A., Eisner, W., Fennell, W., Howell, D. N., Ruiz, P., Fields, T. A., and Spurney, R. F. (2012). Mechanisms of the proteinuria induced by rho gtpases. *Kidney Int*, 81(11):1075–1085.

Wang, Y. L. (1985). Exchange of actin subunits at the leading edge of living fibroblasts: possible role of treadmilling. *J Cell Biol*, 101(2):597–602.

Wei, S. M., Xie, C. G., Abe, Y., and Cai, J. T. (2009). Adp-ribosylation factor like 7 (arl7) interacts with alpha-tubulin and modulates intracellular vesicular transport. *Biochem Biophys Res Commun*, 384(3):352–356.

Welsh, G. I. and Saleem, M. A. (2011). The podocyte cytoskeleton–key to a functioning glomerulus in health and disease. *Nat Rev Nephrol*, 8(1):14–21.

Whiteside, C., Prutis, K., Cameron, R., and Thompson, J. (1989). Glomerular epithelial detachment, not reduced charge density, correlates with proteinuria in adriamycin and puromycin nephrosis. *Lab Invest*, 61(6):650–660.

Whiteside, C. I., Cameron, R., Munk, S., and Levy, J. (1993). Podocytic cytoskeletal disaggregation and basement-membrane detachment in puromycin aminonucleoside nephrosis. *Am J Pathol*, 142(5):1641–1653.

Witzgall, R. (2007). Nail-patella syndrome. *Molecular and Genetic Basis of Renal Disease*, 1st ed.:Chapter 11.

Witzgall, R. (2008). How are podocytes affected in nail-patella syndrome? *Pediatr Nephrol*, 23(7):1017–1020.

Xu, W., Baribault, H., and Adamson, E. D. (1998). Vinculin knockout results in heart and brain defects during embryonic development. *Development*, 125(2):327–337.

Yamamoto, S., Tsuda, H., Honda, K., Kita, T., Takano, M., Tamai, S., Inazawa, J., Yamada, T., and Matsubara, O. (2007). Actinin-4 expression in ovarian cancer: a novel prognostic indicator independent of clinical stage and histological type. *Mod Pathol*, 20(12):1278–1285.

Zaidel-Bar, R., Itzkovitz, S., Ma'ayan, A., Iyengar, R., and Geiger, B. (2007). Functional atlas of the integrin adhesome. *Nat Cell Biol*, 9(8):858–867.

Zhang, A. and Huang, S. (2012). Progress in pathogenesis of proteinuria. *Int J Nephrol*, 2012:314251.

Zhang, W., Huang, Y., and Gunst, S. J. (2012). The small gtpase rhoa regulates the contraction of smooth muscle tissues by catalyzing the assembly of cytoskeletal signaling complexes at membrane adhesion sites. *J Biol Chem*, 287(41):33996–34008.

Zhu, L., Jiang, R., Aoudjit, L., Jones, N., and Takano, T. (2011). Activation of rhoa in podocytes induces focal segmental glomerulosclerosis. *J Am Soc Nephrol*, 22(9):1621–1630.

Ziegler, W. H., Gingras, A. R., Critchley, D. R., and Emsley, J. (2008). Integrin connections to the cytoskeleton through talin and vinculin. *Biochem Soc Trans*, 36(Pt 2):235–239.

Glossary

A

A – Adenine or adenosine
A_{260} – Absorbance at 260 nm
aa – Amino acid
ABD – Actin binding domain
ABLIM – Actin binding LIM domain protein
ABRA – Actin-binding Rho activating protein
Amp – Ampicillin
APS – Ammonium persulfate
ARF6 – ADP-ribosylation factor 6
ARL4C – ADP-Ribosylation Factor-Like 4C
ARNO – Arf nucleotide-binding site opener
ATP – Adenosine 5'-triphosphate

B

BAP – Bacterial alkaline phosphatase
bp – Base pair
BSA – Bovine serum albumin

C

C – Cytosine or cytidine
$CaCl_2$ – Calcium chloride
CBP – Cyclic AMP-responsive element binding protein [(CREB)-binding protein]
CD31 – cluster of differentiation 31
cDNA – Complementary deoxyribonucleic acid
CD2AP – CD2-associated protein
ChIP – Chromatin immunoprecipitation
CNBr – Cyanogen bromide
CRCT1 – Cysteine-rich C-terminal 1
Cre – Cre recombinase
C-Terminus – Carboxy-terminus

D

DEAE – Diethylaminoethyl
DF – Dilution factor

DMEM – Dulbecco's modified Eagle (or minimum essential) medium
DMSO – Dimethyl sulfoxide
DNA – Deoxyribonucleic acid
DNase – Deoxyribonuclease
Dox – Doxycycline
DRP – Dystrophin-related protein
DTT – Dithiothreitol
dNTP – Deoxynucleotide triphosphate

E

ECL – Enhanced chemiluminescence
EDTA – Ethylenediaminetetraacetic acid
EGF – Epidermal growth factor
EGFR – Epidermal growth factor receptor
EGTA – Ethylene glycol-bis(2-aminoethylether)-N,N,N',N'-tetraacetic acid
et al. (lat. "*et alia*") – and others
e.g. (lat. "*exempli gratia*") – for example

F

Fab – Fragment antigen-binding
FAK – Focal adhesion kinase
FACS – Fluorescence-activated cell sorting
FP – Foot process
FCS – Fetal calf serum
FITC – Fluorescein isothiocyanate
FLAT – Far-linked adenine and thymine-rich
FRAP – Fluorescence recovery after photobleaching
FSGS – Focal segmental glomerulosclerosis

G

G – Guanine or guanosine
GAP – GTPase-activating protein
GAPDH – Glyceraldehyde-3-phosphate dehydrogenase
GBM – Glomerular basement membrane
GDP – Guanosine diphosphate
GEF – Guanine nucleotide exchange factor
GTE – Glucose, Tris base and EDTA containing buffer
GTP – Guanosine-5'-triphosphate

H

H_2O – Water
HCl – Hydrochloric acid
HEPES – (4-(2-hydroxyethyl)-1-piperazineethanesulfonic acid
His – Histidine

HRP – Horseradish peroxidase

I

i.e. (lat. "*id est*") – that is
IF – Immunofluorescence
IgG – Immunoglobulin G
IPTG – Isopropyl-1-thio-β-D-galactosidase

K

Kan – Kanamycin
kb – Kilobase
KCl – Potassium chloride
kDa – Kilodalton
K_2PO_4 – Dipotassium phosphate

L

LB Medium – Lysogeny broth medium
LMX1B – LIM homeobox transcription factor 1 beta

M

mAb – Monoclonal antibody
MAPK – Mitogen activated protein kinase
$MgCl_2$ – Magnesium chloride
mRNA – Messenger RNA
MTRF – Myocardin-related transcription factor

N

NaAc – Sodium acetate
$NaHCO_3$ – Sodium bicarbonate
NaCl – Sodium chloride
NaF – Sodium fluoride
NaOH – Sodium hydroxide
NMMHC-IIA – Non-muscle myosin heavy chain IIA
NPS – Nail-patella syndrome
nt –Nucleotide
N-Terminus – Amino-terminus

O

OD_{550} – Optical density at 550 nm
Oligo(dT) – Oligodeoxythymidylic acid

P

PAGE – Polyacrylamide gel electrophoresis
PBS – Phosphate-buffered saline
PCR – Polymerase chain reaction
PEI – Polyethylenimine
PMSF – Phenylmethanesulfonyl fluoride
PTK2 – Protein tyrosine kinase 2

Q

qPCR – Quantitative polymerase chain reaction

R

Rac1 – Ras-related C3 botulinum toxin substrate 1
RhoA – Ras homolog gene family, member A
RNA – Ribonucleic acid
RNase – Ribonuclease
ROI – Region of interest
RPMI – Roswell Park Memorial Institute
rpm – Revolutions per minute
RT-PCR – Reverse transcriptase polymerase chain reaction

S

SD – Standard deviation
SDS – Sodium dodecyl sulphate
SRF – Serum response factor
STARS – Striated muscle activator of Rho signalling
ss – Single stranded

T

T – Thymine or thymidine
TAE – Tris/acetate/EDTA (buffer)
Tcf4 –T-cell factor 4
TE – Tris/EDTA (buffer)
TEMED – N,N,N',N'-Tetramethylethylenediamine
Tet – Tetracycline
tetO – Tetracycline-Operator
$\mathbf{T}_m$ – Melting temperature
Tris – Tris(hydroxymethyl)aminomethane

U

U – Unit
UV – Ultraviolet
UTR – Untranslated region

V

V – Volt
VASP – Vasodilator stimulated phosphoprotein
vol – Volume

W

WB – Western Blot
WT-1 – Wilms tumor 1
Wnt3a – Wingless-type MMTV integration site family, member 3A

Acknowledgements

At the end of my thesis I would like to thank all those people who were supporting and encouraging me during my long doctoral journey.

Foremost, I would like to express my sincere gratitude to my advisor Prof. Dr. Ralph Witzgall for the patience, the support and confidence demonstrated during the last four years.

Besides my advisor, I am very grateful to my mentoring team: Prof. Dr. Matthias Mack and Prof. Dr. Michael Thomm for the advice provided during the evaluation of my research.

I acknowledge my gratitude to Dr. Tillmann Burghardt, who taught me "how to get my foot in the door" for professional advice and support.

I want to express my gratitude to Larissa Osten who gave me technical and "maternal" support during the last years. I would like to thank Cornelia Niemann who had patience in searching for miniSOG-transfected cells and for the electron microscopy studies she performed. Special thanks to Uwe de Vries for teaching me how to work with the LSM. Many thanks also to Olga Maier and Marion Kubitza who isolated primary podocytes.

My gratitude is also extended to all current and former members of Professor Witzgall's group for the wonderful atmosphere at work: Prof. Dr. Reinhard Rachel, Dr. Melanie Zaparty, Dr. Karin Babinger, Dr. Anya Krefft, Dr. Kerstin Schmidt, Dr. Melanie Grosch, Anita Hecht, Ton Maurer, Antje Zenker, Jenny Fletcher, Markus Setzer, Edeltraud Lautenschlager, Carina Mirbeth, Kerstin Herrmann, Christine Meese, Helga Othmen, Karin Schadendorf, Yulia Zaytseva, Ludwig Utz, Cäcilia Vitzthum, Richard Niedermeier, Andreas Rieger, and Markus Schöpperl.

I would like to thank all the PhD students I met in the lab: the electron microscope expert Benjamin Salecker and the miRNA expert Susanne Baumgarten. I would like to thank my dear friend Denise Schmied for sharing the good and bad moments we went through together. Many thanks to the friends from the "Italian group" who I had a pleasure to meet in Regensburg: Giada, Alessio, Paula, Salvatore, Yumi, Luca, Matthias, Thomas, David, Francesca, and Malte.

Of course no acknowledgments would be complete without giving thanks to my family: my parents, Antonina and Petro Stepanov, and my brother Alexandr, to whom I dedicated this work. Many thanks are addressed to my dear aunt Olga Horuzha, my cousin Juriy Horuzhi, my cousin's wife Ludmila Horuzha and my god-son Jarek Horuzhi. I would like to write words of gratitude to my no longer living grandmother Anela Horuzha.

Last, but not least, I would like to acknowledge with all my heart and soul my fiancé Dr. Nicola Paradiso for love, faith, support and everything he is doing for me.

Eidesstattliche Erklärung

Ich erkläre hiermit an Eides statt, dass ich die vorliegende Arbeit ohne unzulässige Hilfe Dritter und ohne Benutzung anderer als der angegebenen Hilfsmittel angefertigt habe; die aus anderen Quellen direkt oder indirekt übernommenen Daten und Konzepte sind unter Angabe des Literaturzitats gekennzeichnet.

Die Arbeit wurde bisher weder im In- noch im Ausland in gleicher oder ähnlicher Form einer anderen Prüfungsbehörde vorgelegt.

.....